POLITECNICO DI TORINO

Master's Degree in Aerospace Engineering

Master's Degree Thesis

Dynamic Characterization of Gas Turbine Blades During Validation Phase

Supervisors

Prof. Daniele BOTTO

Ing. Francesco BAGNERA

Ing. Sergei RIAZANTSEV

Candidate

Andrea TROGLIA GAMBA

December 2025

Summary

This Master's Degree Thesis focus is the Dynamic Characterization of a Gas Turbine Blade produced by Ansaldo Energia S.p.A in two different materials, in particular a first run of made of material **René 80** and one in **a Nickel Based Superalloy Directionally Solidified** material. The blade is part of a single stage of a complete gas turbine that is used for energy production. Due to the different properties of the aforementioned materials, the associated behaviour will be different, resulting in a different Modal Behaviour and a different vibrational pattern. The problem was accordingly studied by re-creating from the original model another FEM Model of the TB blade while at the same time assessing the differences and associated properties, simplifying the geometry and applying the needed modifications in order to investigate the discrepancies within the measured frequency. Different paths were investigated, considered and studied.

Acknowledgements

I would really like to express my deepest and most sincere gratitude to all the people who have supported, guided, and encouraged me throughout these past years at university. This journey would not have been possible without the constant presence and unwavering support of my family.

To my father Marco and my mother Luisella, thank you for always believing in me, for your endless patience, and for teaching me the value of perseverance and integrity, for allowing me to study all those years with your unconditioned support, for being the best parents everyone can dream of. To my sister Sofia, thank you for being supportive in the worst moments, for your advices, for always having my back and motivating me, I will always be more than grateful to have a sister like you and always will be proud of the person you are. To my grandmothers, Lucia and Natalina, whose affection, wisdom, and encouragement have been a constant source of comfort and motivation, especially when times were dark. To my girlfriend Chiara, thank you for standing by my side through every challenge, exam and stressful event, for your understanding during long nights of study, for your constant words of reassurance when things felt overwhelming, for being the human I am proud to have by my side in every situation. Each of you has played an irreplaceable role in helping me reach this point, and for that, I am deeply grateful, more than words will ever be able to express.

I would also like to extend my heartfelt thanks to the Ansaldo Team, whose guidance and professionalism have contributed immensely to both my academic and personal growth. Working with such talented and dedicated individuals has been more than a privilege. I am especially thankful to Francesco, my tutor and mentor during these past six months, for his invaluable support, patience, and insight. Beyond assisting me with my thesis work, he has helped me develop a deeper understanding of the professional environment, the importance of teamwork, and the skills needed to collaborate effectively within a group. His mentorship has not only enhanced my technical knowledge but also prepared me for the challenges of my future career.

To all those who, in one way or another, accompanied me throughout this journey - offering advice, encouragement, or simply a kind word when it was most needed

- thank you sincerely. Your support has made this experience both meaningful and unforgettable. Everyone of you has helped me more than imaginable. Every challenge in my future career and personal life will be much easier to bear with the support and knowledge that everyone of you has given me.

"Success is not final, failure is not fatal:
it is the courage to continue that counts."
Wiston Churchill

Table of Contents

List of Tables

List of Figures

Acronyms

DB
Database

AEN
Ansaldo Energia

TB
Turbine Blade

GT
Gas Turbine

IGT
Industrial Gas Turbine

JB
Joule Brayton

WB
Ansys Workbench

CAD
Computer Aided Design

FEM
Finite Element Model

SN
Serial Number

Chapter 1

Introduction

1.1 The Modern day Scenario

The intense and continuous drive to advance technologies and innovation - even more when amplified by external forces such as governing bodies, industrial competitors, and the introduction of new laws, standards, and regulatory frameworks - has greatly elevated the technological landscape to an entirely new dimension, previously considered impossible to reach. In this new environment, the pursuit of innovation is no longer optional or occasional for a company whose pursuit is to bring to the market state-of-the-art machines; it has become a structural and strategic imperative. Companies, research institutions, and development laboratories are required to operate in a state of perpetual and strenuous evolution, continuously refining, redesigning, and re-engineering components, processes, and entire systems or machines in order to keep pace with accelerating technological demands. This continuous cycle of improvement more often than not involves the integration of novel and up-to-standard materials, advanced manufacturing techniques, and cutting-edge digital tools and human engineering in order to to optimize both working conditions for the machine and functionality. The objective is not merely to enhance the performance or efficiency of individual components, but to achieve a complete and ever-lasting level of improvement across the entire system - ensuring higher reliability, reduced fuel consumption, and overall sustainability and future - proofing. Such an approach demands a deep understanding of multidisciplinary principles, from thermodynamics principles and materials science to system engineering and industrial management. Moreover, the convergence of innovation drivers - including stricter environmental policies, increased market expectations, and the push for digital transformation - compels organizations to rethink their traditional design philosophies. Incremental and non-consistent improvement is no longer sufficient; disruptive and forward-thinking strategies are

now essential to maintain competitiveness in rapidly evolving markets. In this context, innovation becomes a continuous process of learning, adaptation, and experimentation, where failure is treated not as a setback but as an integral step toward achieving excellence. Ultimately, this relentless pursuit of improvement fuels a virtuous cycle of technological progress that shapes the future of industry and redefines the boundaries of engineering capability.

The energy sector, and more in particular the segment associated with the development and production of gas turbines, electric power generation systems, and gas-fueled generators, represents one of the most dynamic, complex, and challenging industrial environments in existence today, since competitors, and as said before laws and regulation as well, always pose a threat for aging and non up to date or state-of-the-art machines. Constantly driven by the global demand for higher efficiency, lower emissions, and increased operational reliability, this field requires continuous innovation at both the technological and material-science levels. Companies, engineers, and research institutions are continuously engaged in the pursuit of new solutions that can enhance thermodynamic performance, improve combustion processes, and optimize energy conversion efficiency.

This continuous evolution is both fueled by a combination of external pressures and internal ambition. Gas turbine and generator manufacturers must therefore integrate cutting-edge technologies to refine their designs and achieve superior performance metrics. Furthermore, the increasing need for hybrid and flexible power systems capable of adapting to fluctuating energy demands reinforces the importance of multidisciplinary collaboration between mechanical, electrical, and control engineers.

In such a competitive and innovation-driven context, research facilities and industrial partners work hand in hand to explore new frontiers in efficiency, reliability, and environmental compatibility. The energy sector thus stands as both a technological and strategic frontier - one that continually challenges engineers to balance performance optimization with sustainability, economic viability, and compliance with ever-tightening global standards. It is within this demanding yet inspiring environment that the most significant advancements in energy generation technologies are conceived, developed, and brought to life. Following the aforementioned criteria, and thinking philosophy, **Ansaldo Energia S.p.A.** decided to embark on a path to modify the already proven and tested material of some turbine's blades[1] from a **Nichel-Based** isotropic superalloy called ***Renè 80*** to an ***Nickel Based DS Superalloy***, a directionally solidified anisotropic superalloy, to achieve better performances and real-world results without having to completely

[1]Those blades are part of the High Temperature (HT) stage of the turbine, taken from a new concept machine **from AEN**

redesign from scratch an already well-tested and proven design, thus allowing for a real, non biased comparison between the already proven alloy and the new one. In particular, this Master's Thesis's focus will be to evaluate Modal Behaviour, Dynamic Characterization and subsequent material modification, called **tuning**. From modifying the **FEM** design, assembling the parts and evaluation of the following results, the work was done in part by using Ansaldo Energia's own Data and Publicly-Available data, used for confrontation and tuning. In order to give a more in-depth understanding and a broader view of the results, some images of the turbines produced by the company AEN were provided. To better frame the up to date AEN machines as well, a series of images, showing state of the art complete assemblies and components during manufacturing process is provided [1].

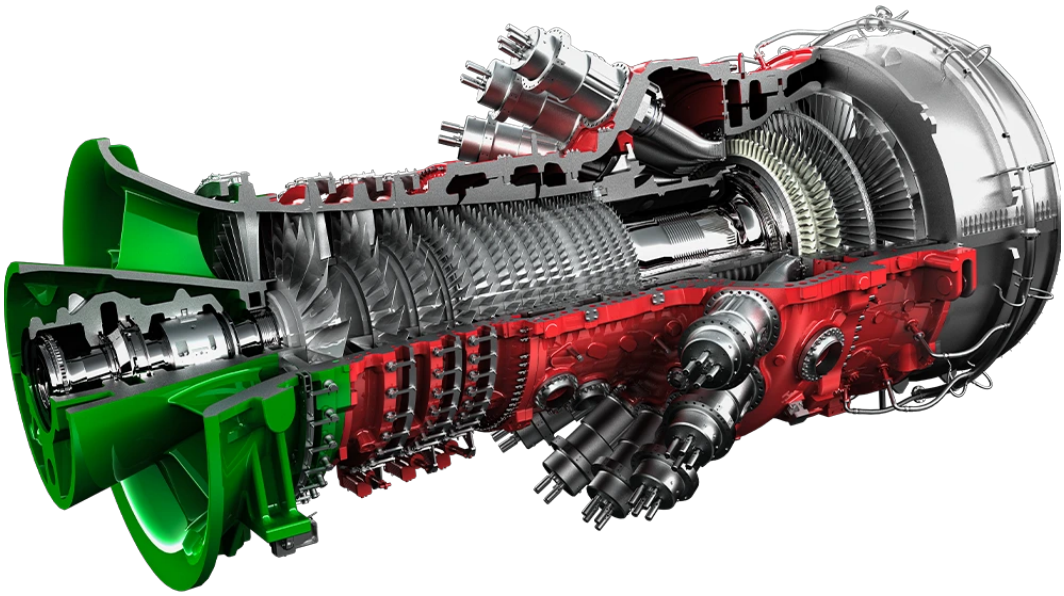

Figure 1.1: GT36 Turbine [1]

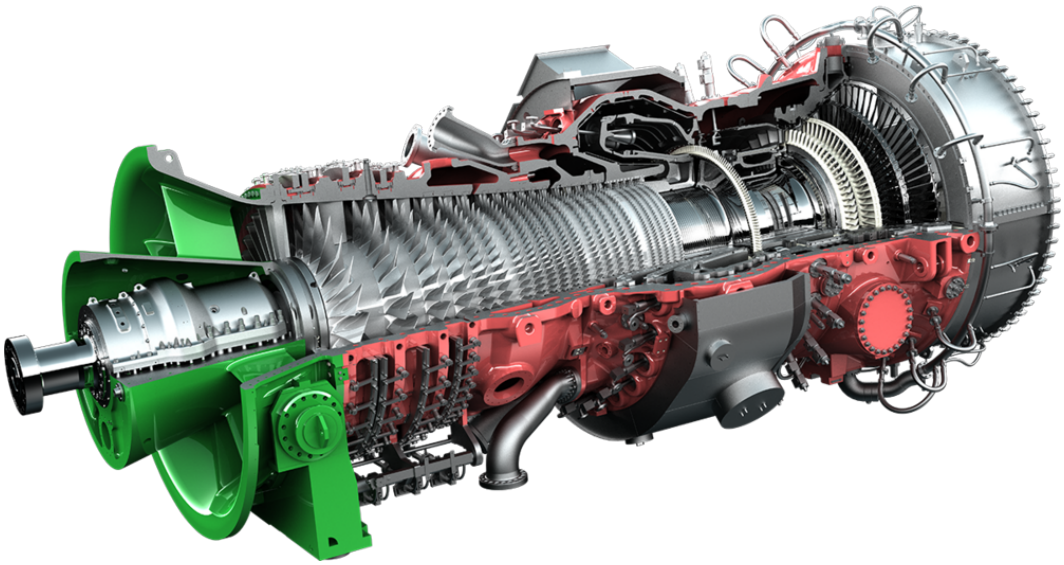

Figure 1.2: GT26 Turbine [1]

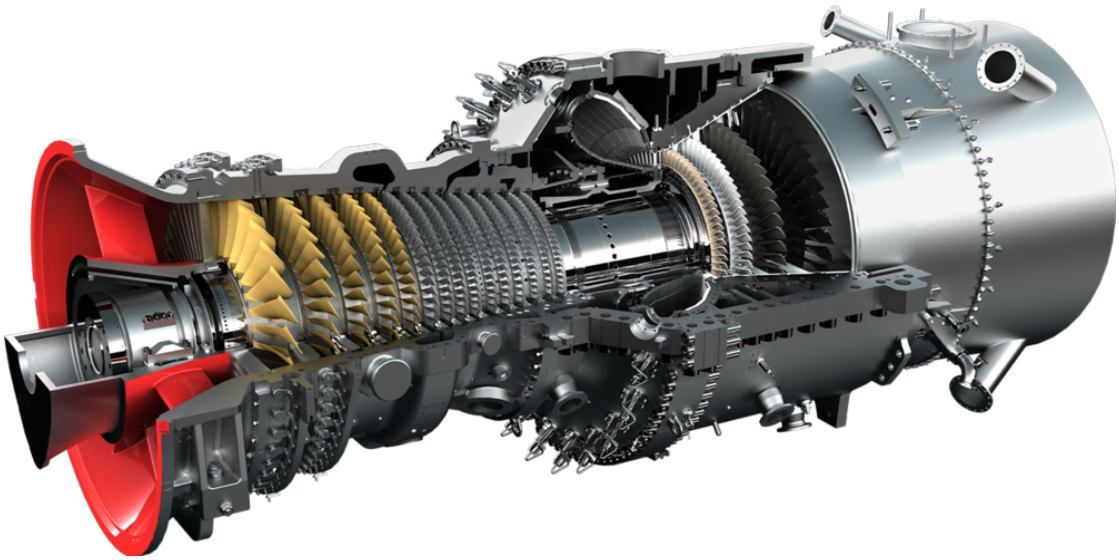

Figure 1.3: The Full View of the AE94.3A Turbine [1]

Figure 1.4: Compressor Stage during Assembly process [1]

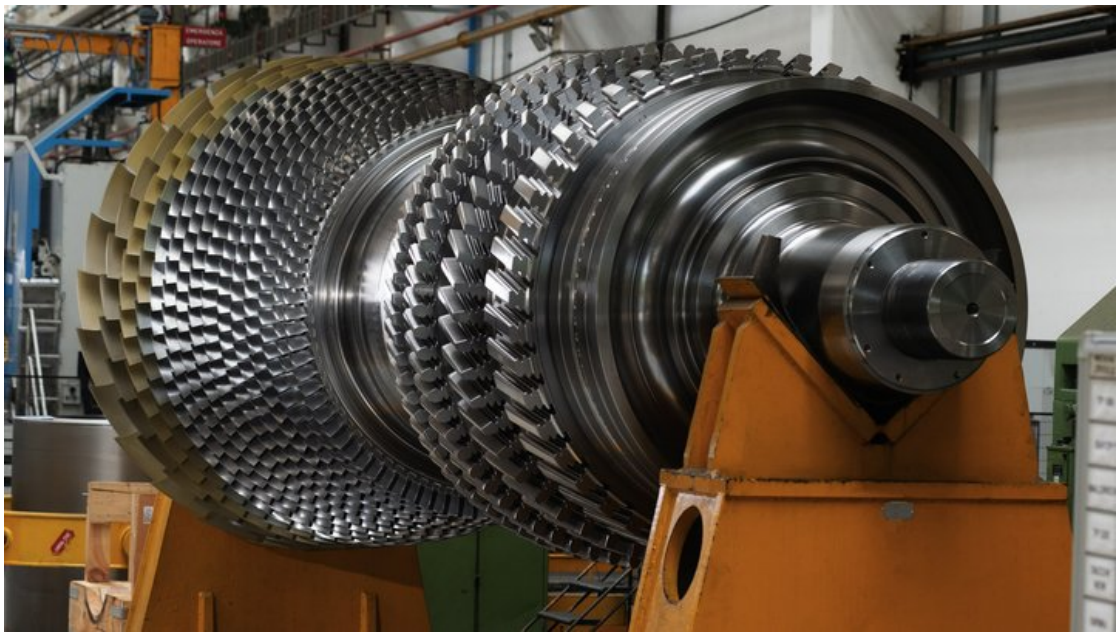

Figure 1.5: The Rotor during the assembly process [1]

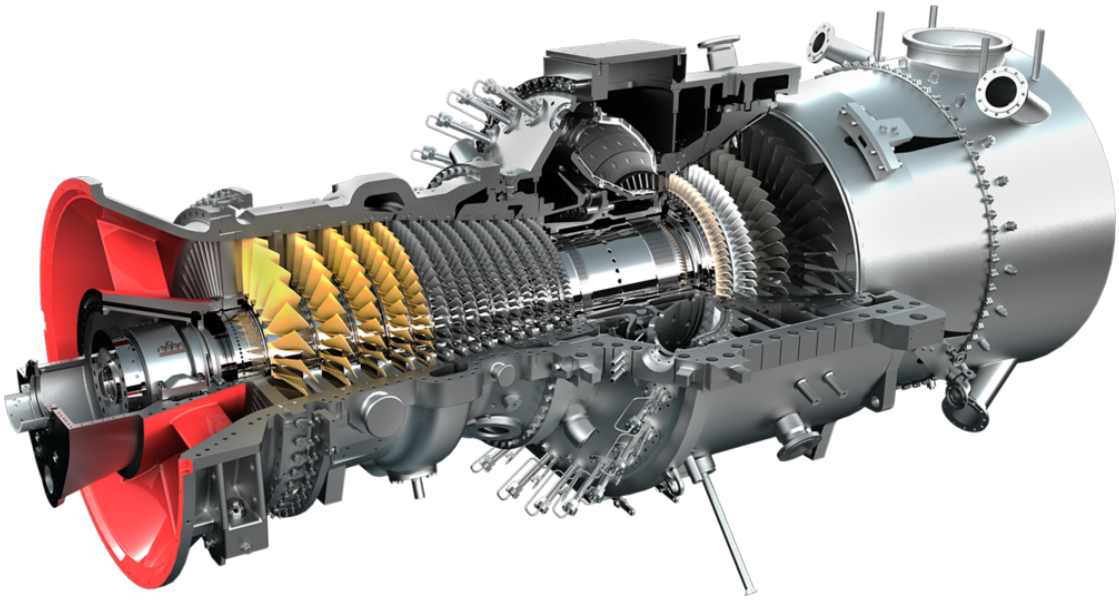

Figure 1.6: AE64.3A Turbine [1]

1.2 The Thermodynamics behind innovation

Since Gas-Powered Turbine Blades are based on the **Joule - Brayton** thermodynamic cycle, a brief description of the cycle's parts is necessary. In this section only a brief description of the **ideal cycle** and the **real cycle** will be provided, since both of them are needed for theorethical purposes and problem framing purposes. As shown in the image 1.7[2], where both the ideal (black line) and real (blue) cycle there are some important parameters to investigate. Beginning with the **Ideal** cycle (Black line):

- **Phase 1 → Phase 2**: isentropic compression, where W_c thermodynamic work (compression) needs to be performed;
- **Phase 2 → Phase 3**: isobaric combustion, where heat value Q_1 enters the cycle;
- **Phase 3 → Phase 4**: isentropic expansion, where W_t is obtained (expansion);
- **Phase 4 → Phase 1**: exhaust gas is released (with Q_2 **exiting the cycle)**;

And similarily for the **Real** cycle:

- **Phase 1 → Phase 2'**: Polythropic (non isentropic due to losses) compression, where W_c thermodynamic work (compression) needs to be performed. The component responsible for this in the machine is the compressor;
- **Phase 2 → Phase 3**: combustion, where heat value Q_1 enters the cycle, but accompanied with a slight pressure drop. This, in the real machine, takes place in the combustor;
- **Phase 3 → Phase 4**: polythropic expansion, where W_t is obtained from the cycle. The component that extracts work from the gas in the machine is the turbine;
- **Phase 4 → Phase 1**: exhaust gas is released (with Q_2 **exiting the cycle). Not that important, since exhaust gas is usually expelled**;

In our system, the W_c has to be done by the compressor stage, while W_t is obtained by the turbine,as said before. The values of the two Q_1 and Q_2 are the values of heat (measured in Joules) exchanged during the process. After having

[2]Image from Wikipedia, Public Domain

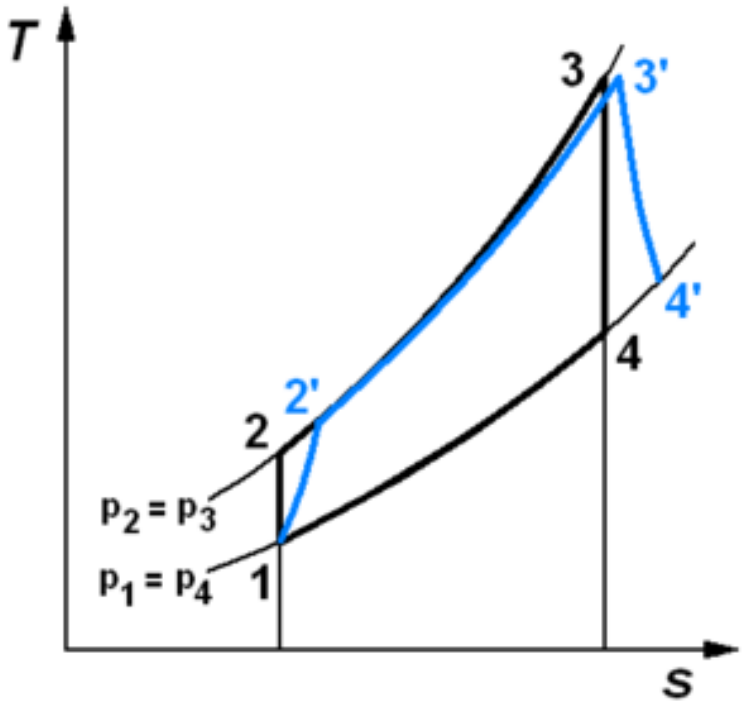

Figure 1.7: Ideal and Real Joule - Brayton Cycle on T-s diagram

defined those parameters, we can introduce the definition of **thermodynamic efficiency**. Thermodinamic efficiency is defined as follows [2]:

$$\eta_{th,id} = \frac{W_t - W_c}{Q_1} = \frac{Q_1 - Q_2}{Q_1} = 1 - \frac{Q_2}{Q_1} = 1 - \frac{\cancel{C_p}(T_4 - T_1)}{\cancel{C_p}(T_3 - T_2)} = 1 - \frac{T_4 - T_1}{T_3 - T_2} \quad (1.1)$$

Since the thermal efficiency can be summarized as:

$$\eta = \frac{W}{Q} \quad (1.2)$$

And we can define the Carnot Thermal Efficiency as

$$\eta_{Carnot,id} = 1 - \frac{T_{cold}}{T_{hot}} \quad (1.3)$$

Where T_{Hot} and T_{Cold} are respectively the higher and lower temperature of the Carnot's Cycle [3], we know that the JB Cycle can only *tend* to Carnot's Efficiency, never one. Summarized in formulas:

$$\eta_{JB,id} = 1 - \frac{T_{Cold}}{T_{EndCompression}} < \eta_{Carnot,id} < 1 \quad (1.4)$$

Chapter 2

CAD and FEM Software Modeling and Mesh

In preparation for the subsequent analysis, it was no less than essential to first establish a solid foundation to ensure the **reliability, accuracy, and overall robustness** of the numerical simulations that would have come later. This required a preliminary yet fundamental phase dedicated to the verification, validation and subsequent refinement of the computational model provided. Such a step is not only crucial for the results, but also to familiarize with the model itself, as the validity of any simulation-based investigation inherently depends on the fidelity of the geometric representation and the precision of the boundary conditions applied. Therefore, before proceeding with the main campaign of calculations, particular attention was devoted to realize the FEM model with sufficient quality and overall refinement in order to minimize potential numerical inaccuracies and ensure, at least for the FEM section, a good level of accuracy.

A three-dimension computer-aided design (CAD) model (geometry) of the TB turbine blade was already available, serving as the first initial basis for the creation of the FEM Model. However, the original geometry required some initial modification in order to ease the realization of the model for the problem it was decided to investigate. This was made possible with the methodology described below.

2.1 The Initial Problem

The previous analysis showed there were present some discrepancies with the measured results that were shown to come out of the tested blades (real world testing). Due to this aforementioned discrepancy, it was decided to investigate further the reason behind those, and this was the task of this Master Theisis. The task was studied analysing some of the possible sources of inaccuracy, such as checking the influence of the geometrical tolerancies, repeating different analysis variating boundaries conditions and constraints, testing conditions, and lastly attributing to material properties what we could not explain differently. In order to remove the eventual problems or hidden issues that could have originated as far back as the FEM Model, the idea was to start back from the design itself, studying it, familiarizing with it, assessing the geometry, being careful not to modify it, and then meshing it and only as the last step launching the simulations. For this reason, it was decided to start directly from the unmodified original piece, applying some degree of modification (turbolators, geometry fixing if needed[1]) to ensure no mistakes rendered the future simulations useless. This was performed following the procedure subsequently described.

2.2 ANSYS SpaceClaim

Using the commercially available software ***Ansys Mechanical Suite*** the design was modified directly from the original source file (but originally the model was designed using another commercially available software, using **SpaceClaim** (2.1), that provides a flexible and user-friendly interface for modifying and repairing CAD models prior to using them in simulations[2]. The ease of use and compatibility was the main reason for the decision of using SpaceClaim instead of another CAD software in this first part.

2.2.1 Alterations Effected upon the Component: Turbolators Removal

In the original component several internal features known as ***turbolators*** (as illustrated in Fig. 2.1) were present. All of these small-scale elements inherently introduced a significant level of complexity into the meshing process. Due to

[1]Sometimes the software can modify the model inadvertedly without notifying the user. In order to avoid this, a geometry check was performed

[2]The turbolators were removed one by one, checking after every removal that the geometry was still unmodified

their dimensions (considerably smaller than the characteristic length of the overall blade) the internal geometry became particularly difficult to discretize accurately, since in order to capture the fine geometrical details of the turbolators within the computational domain, the mesh elements would have to be smaller than the smallest characteristic dimension of these features. Consequently, generating a mesh capable of adequately and correctly resolving the turbolators would result in an exceptionally dense grid and, therefore, a considerable increase in computational cost and processing time. This trade-off between geometric fidelity and numerical feasibility required careful consideration during the model refinement phase. This fact posed a significant challenge that didn't really have a mean to exist, at least in the initial part. Since calculations would have ended up being way more expensive (computationally) and slow, in the first phase, they were removed from the model[3]. Since the turbolators themselves do not give (or, as will be discussed in another chapter extremely limited, thus, at least for the first parts and first calculations, negligible) structural contribution, it was decided to remove them from the inner vanes of the blade and therefore not consider them since they are not structural parts (a more extensive discussion and explanation of turbulators will be given in the Appendix). Leaving the inner part of the component completely flat would be a disaster for thermal purposes and heat exchange, but for mechanical integrity in the beginning they can be removed. **Important note to sum the paragraph up:** the turbolators, in this initial section, were removed in order to **simplify** the model and assess results quickly and understand clearly how the model was influenced by factors (different material and deviations from nominal values for example). It is clear, of course, that this simplification would inherently make results **less accurate**. It was deemed acceptable when it came to the first part, but later they were added back as more accurate results were needed. The extent of the effect of the turbolators is discusses **in detail** in Chapter 6.

[3]The computational time required for turbolators' present model was around one to three days. The model without them, roughly took one day for calculation results to show

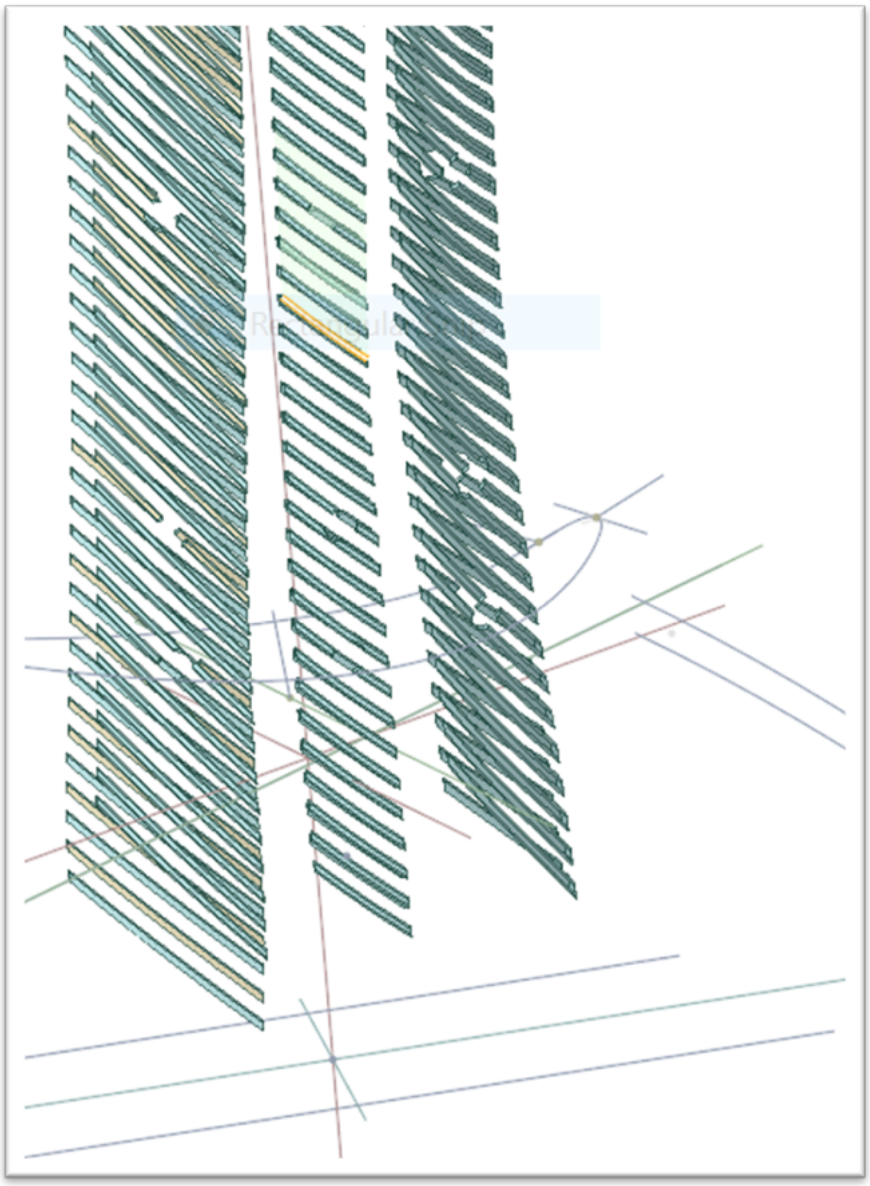

Figure 2.1: The removal process of turbolators with Ansys SpaceClaim

2.3 The Meshing Process

The meshing process is a fundamental process that has to occur in the a very controlled and precise way before calculation, in order to obtain the most accurate results possible. In particular, in this section only the method used for meshing is discussed, for a more refined explanation on mesh types and influence, it is best to

consult Chapter 5 Section 5.1. For now, it is important to remind only that the meshing process in this first section was conducted without turbolators. This made the work easier and more managable.

Chapter 3

Statistical Analysis

In order to have a deeper understanding of the effects of having some blades that during the production process end up having some points that could be over (or under) nominal technical drawing value, it was decided to use some statistic to display the given data and find eventual correlations.

3.1 Deviation From Nominal Values

Since it is not clear how many blades were actually in the acceptable Ansaldo range, and which blades on the other hand were not fitting into it, it was deemed useful to graph the value of the variation from the **nominal design value**, hence giving a quick visual confirmation of the values and giving a fast way to spot eventual non-compliant blades. In particular, it was decided to count per-single point variation, where the aforementioned points are listed in the figure below (Fig: 3.1 and Fig: 3.2). In particular, the blade has two sides, a *concave* and a *convex*, called respectively the **pressure side** and **suction side**, due to the difference in pressure of those two sides (where the pressure side has a greater pressure value). To give a brief sum up of the results of the results that were found, it is best to say that none of the analised blades had fallen outside of the Ansaldo's designated acceptable range. In addition to this, in the following graphs it was also decided to put a another line that represents the development of the normal distribution when overlapped with the diagram. As a quick reminder, the following list is given to have a faster understading of the meaning of the graphed lines:

- **Orange Line:** this line represents the normal distribution, useful to visualize where the values would mathematically need to be;
- **Blue Line:** the blue lines represent the values of the number of blades with that number of deviation for the considered point. For example, for the idea

of saying that seven blades were having a specific deviation out of the batch, the blue line would reach the value **seven** on the **y-axis**.

Important Note: The x-axis shows the value of the deviation, from left to right. Left is a smaller number (smaller deviation), while right means a bigger deviation The **Points** that are referenced in the graph are relative to the image 3.1 and image 3.2 respectively and refer to places both in suction side and in pressure side. The reason for this reference is that the operators that perform measures need to know exactly where to measure in order to obtain the values that are easy to confront with the reference in the technical specification.

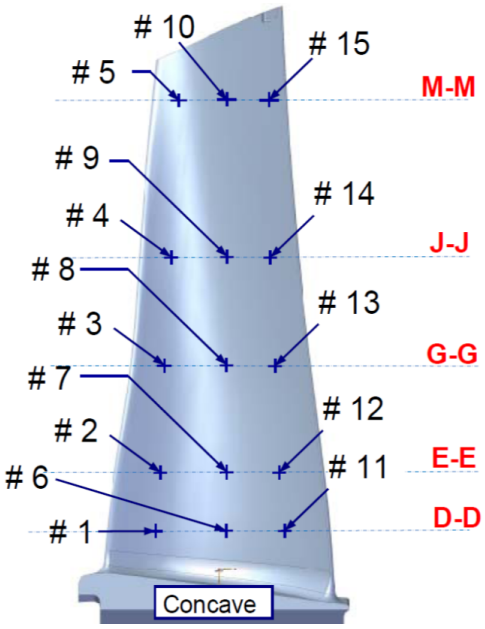

Figure 3.1: Concave Reference of Points for the Blade Element

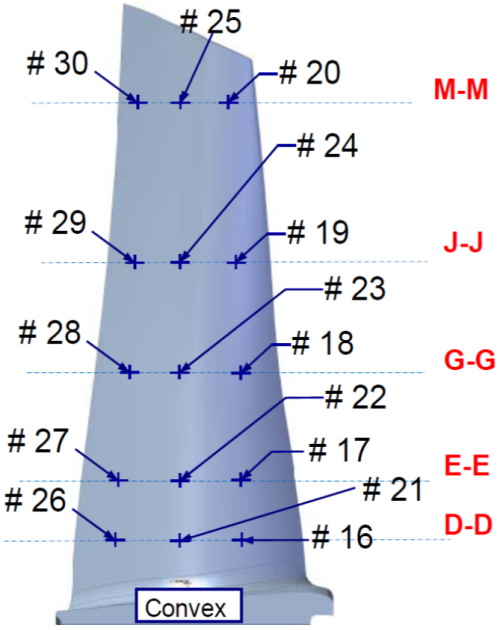

Figure 3.2: Convex Reference of Points for the Blade Element

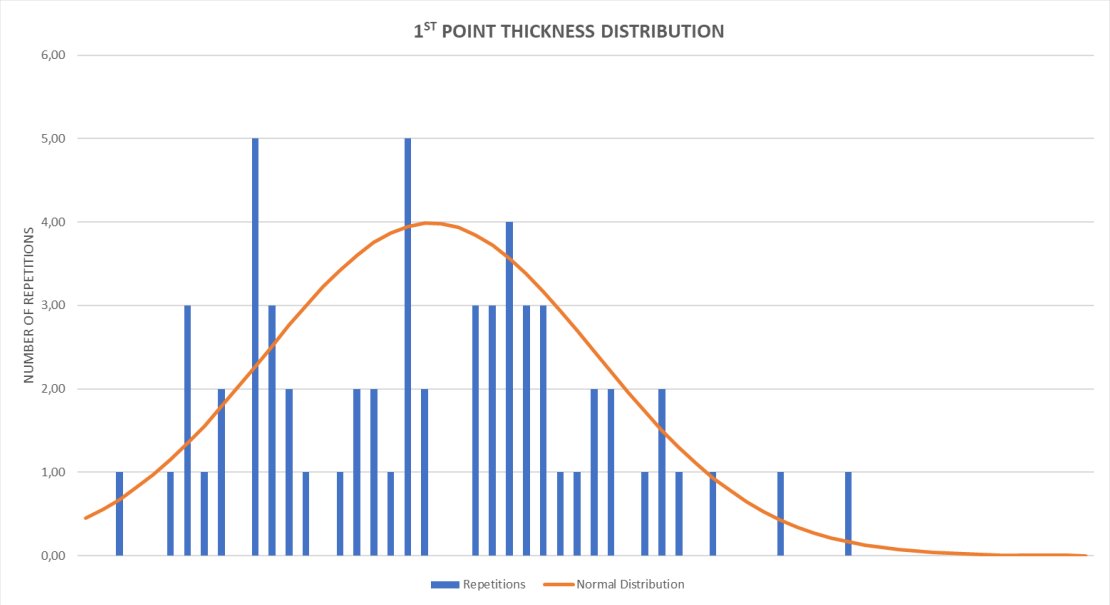

Figure 3.3: 1 Point Distribution Thickness

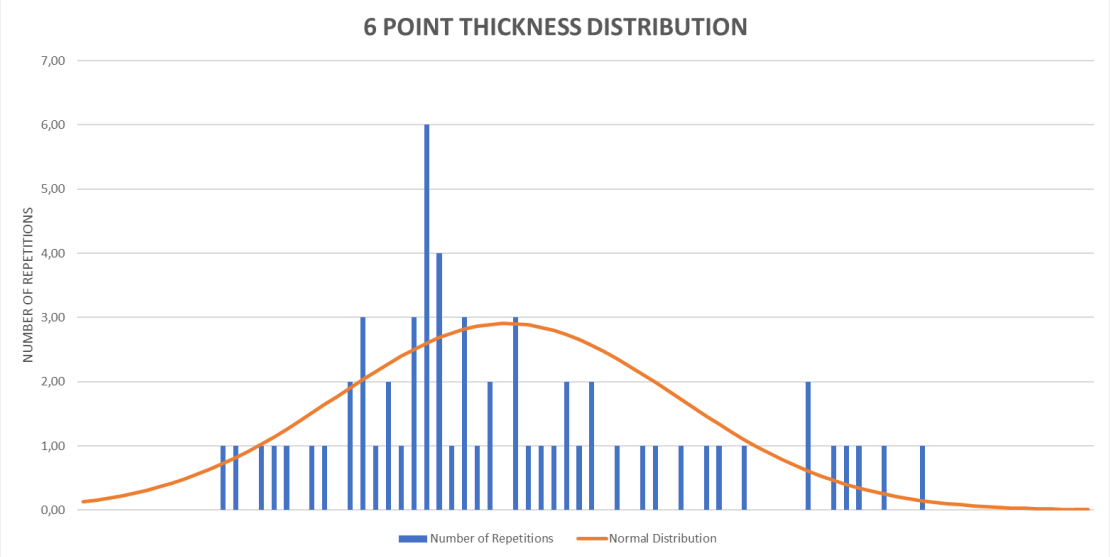

Figure 3.4: 6 Point Distribution Thickness

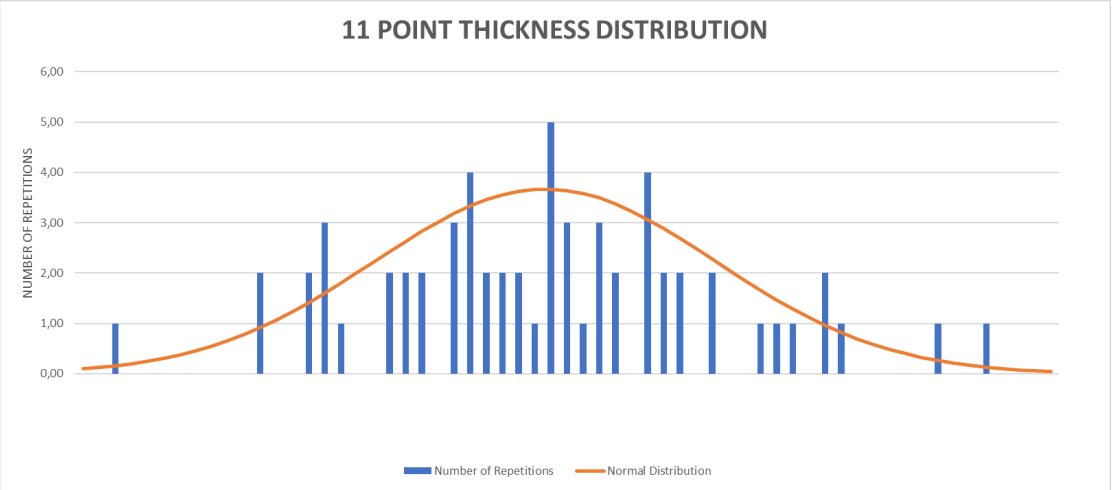

Figure 3.5: 11 Point Distribution Thickness

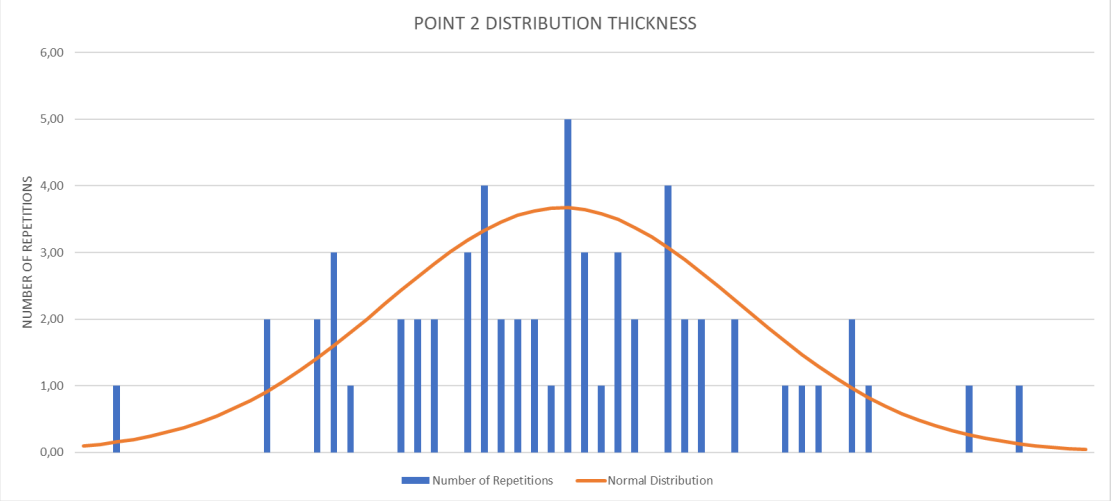

Figure 3.6: 2 Point Distribution Thickness

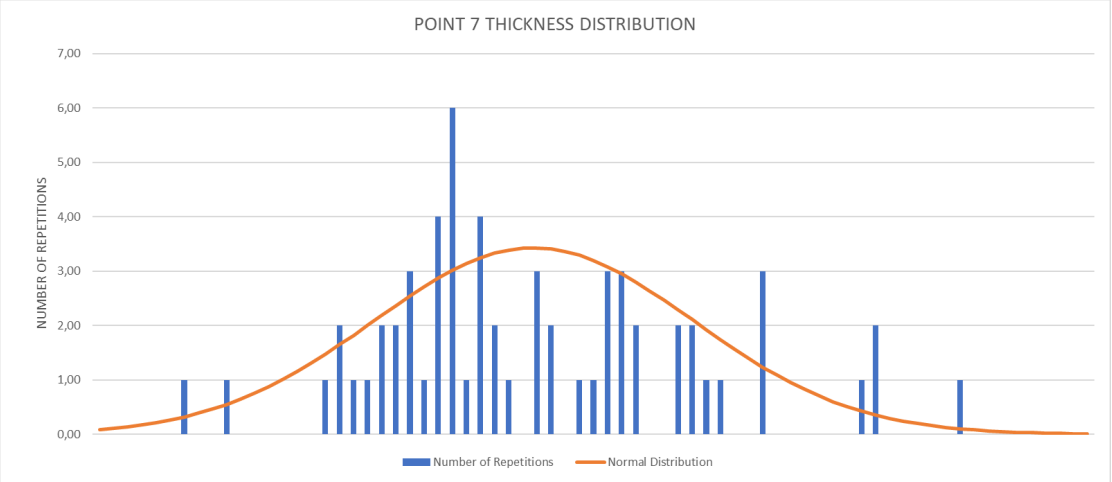

Figure 3.7: 7 Point Distribution Thickness

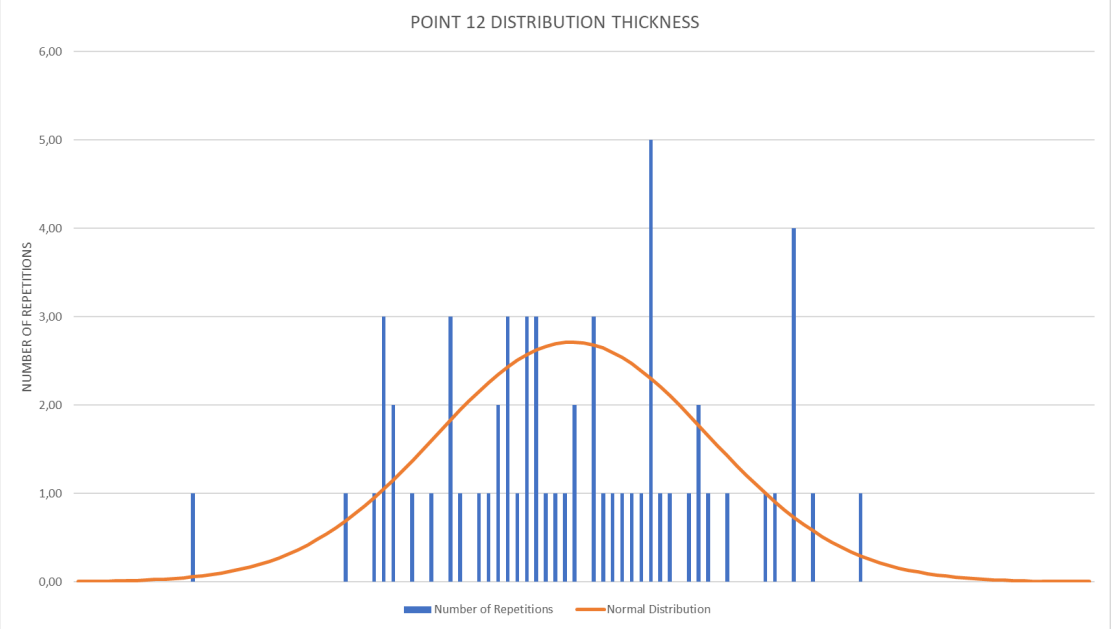

Figure 3.8: 12 Point Distribution Thickness

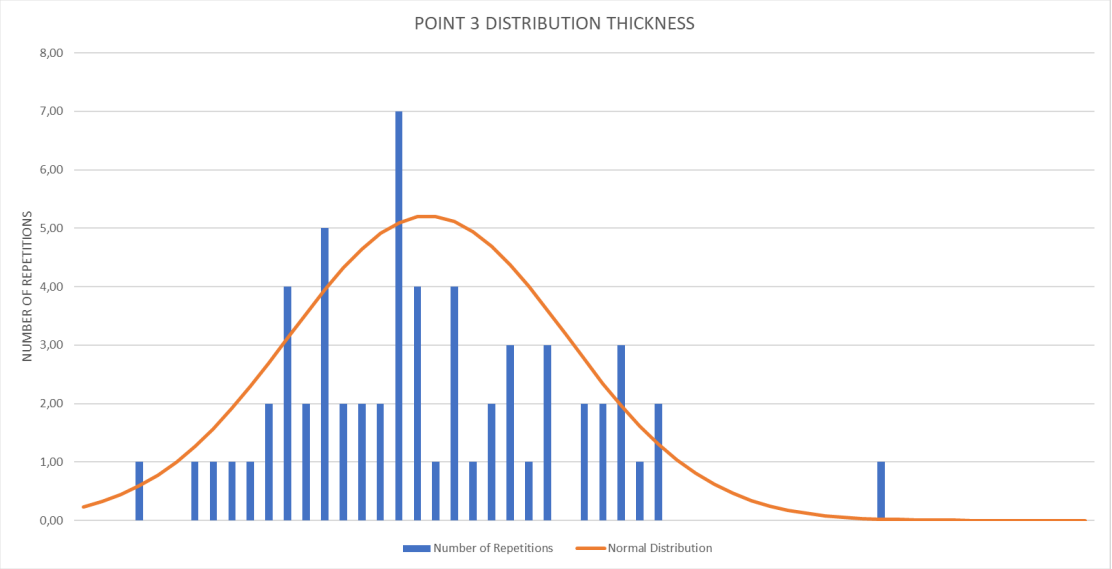

Figure 3.9: 3 Point Distribution Thickness

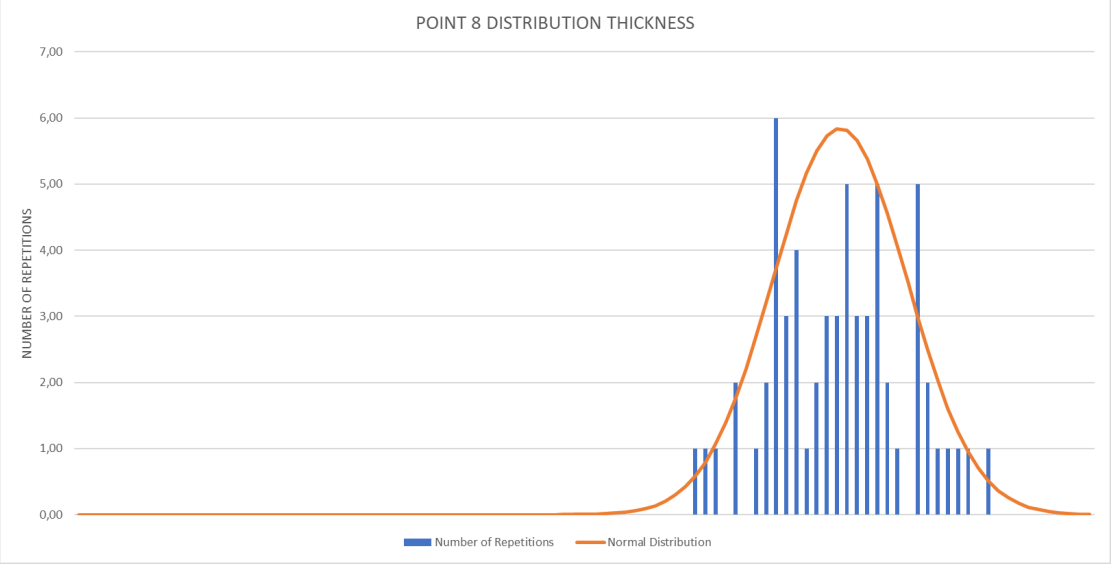

Figure 3.10: 8 Point Distribution Thickness

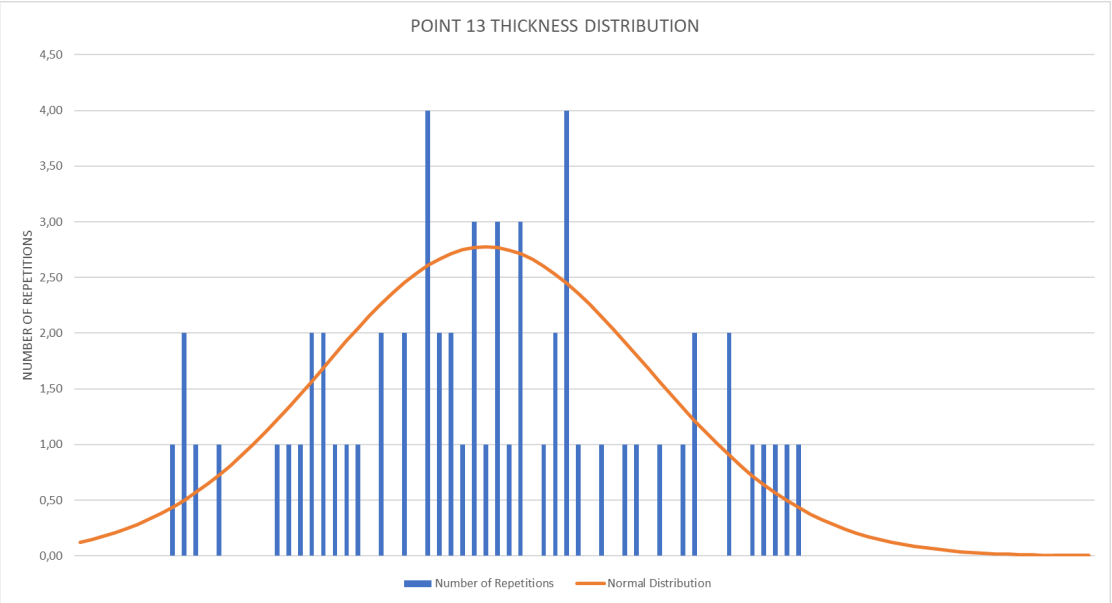

Figure 3.11: 13 Point Distribution Thickness

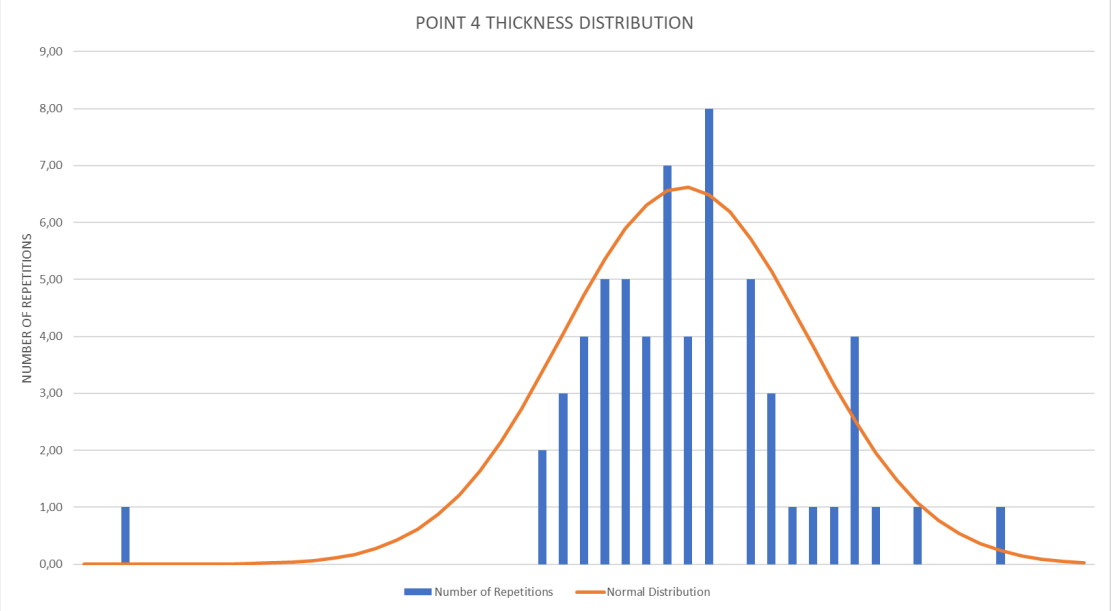

Figure 3.12: 4 Point Distribution Thickness

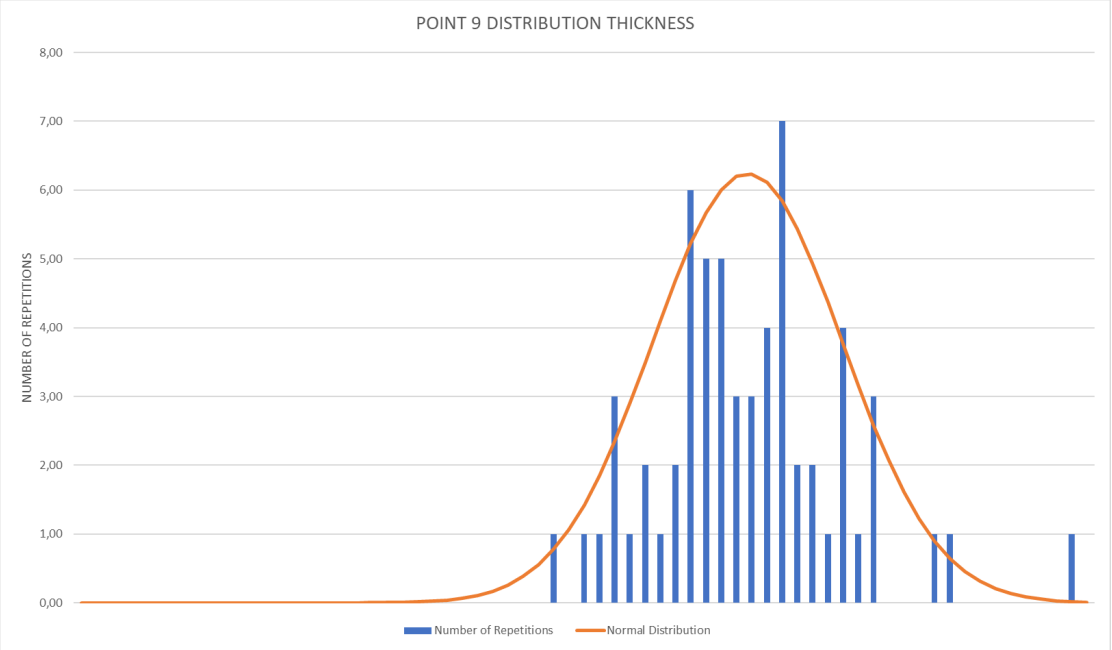

Figure 3.13: 9 Point Distribution Thickness

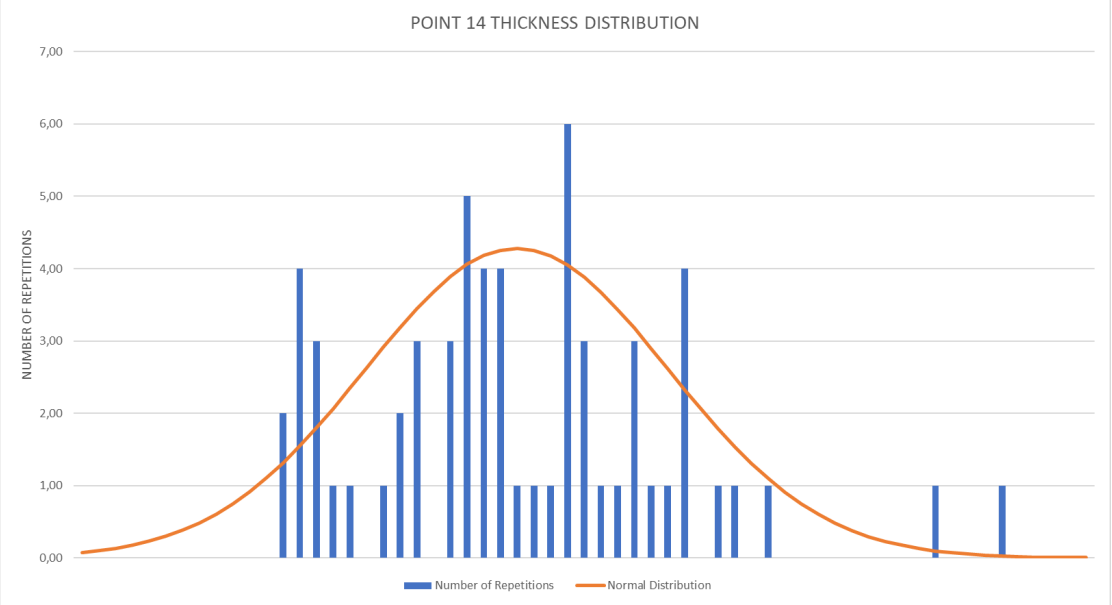

Figure 3.14: 14 Point Distribution Thickness

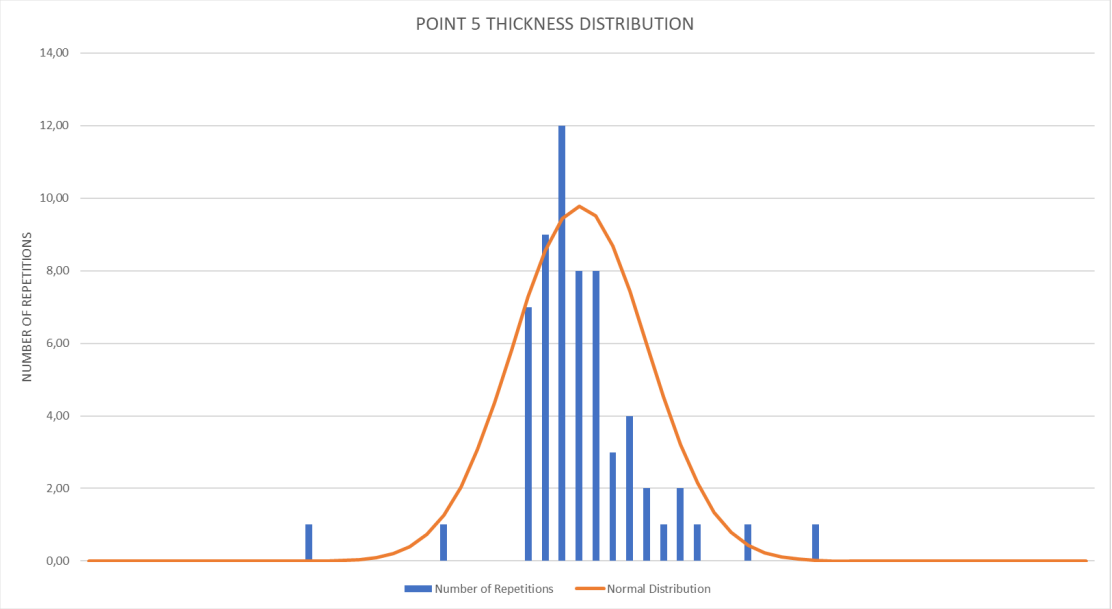

Figure 3.15: 5 Point Distribution Thickness

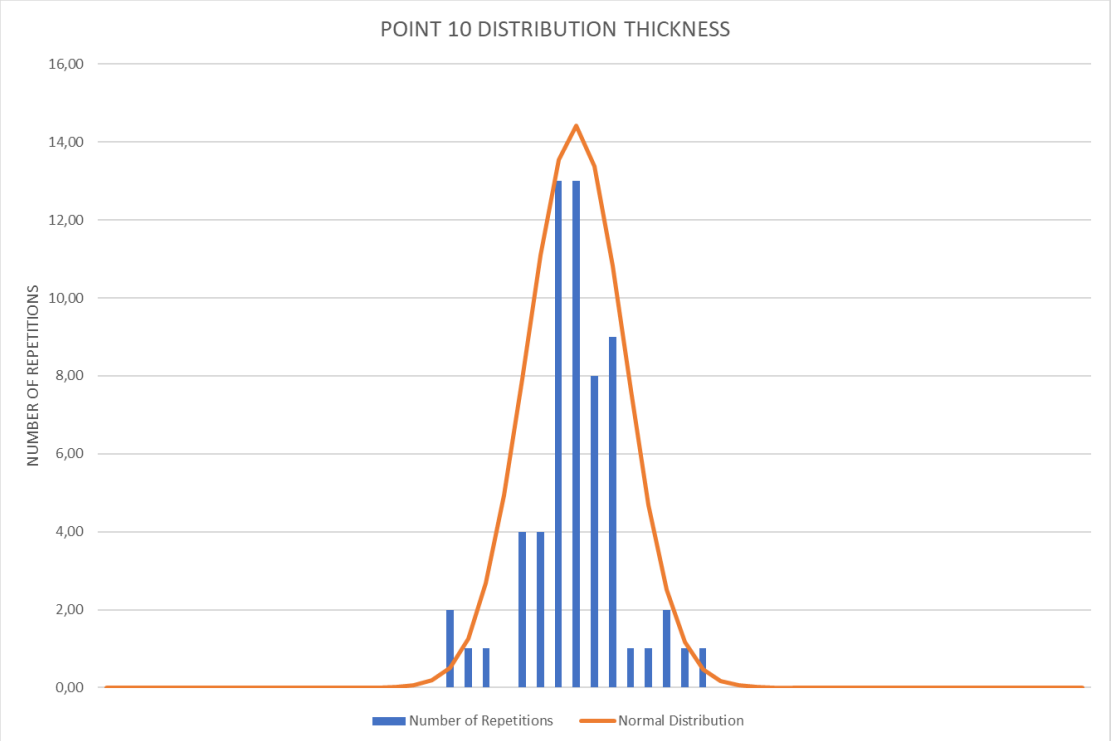

Figure 3.16: 10 Point Distribution Thickness

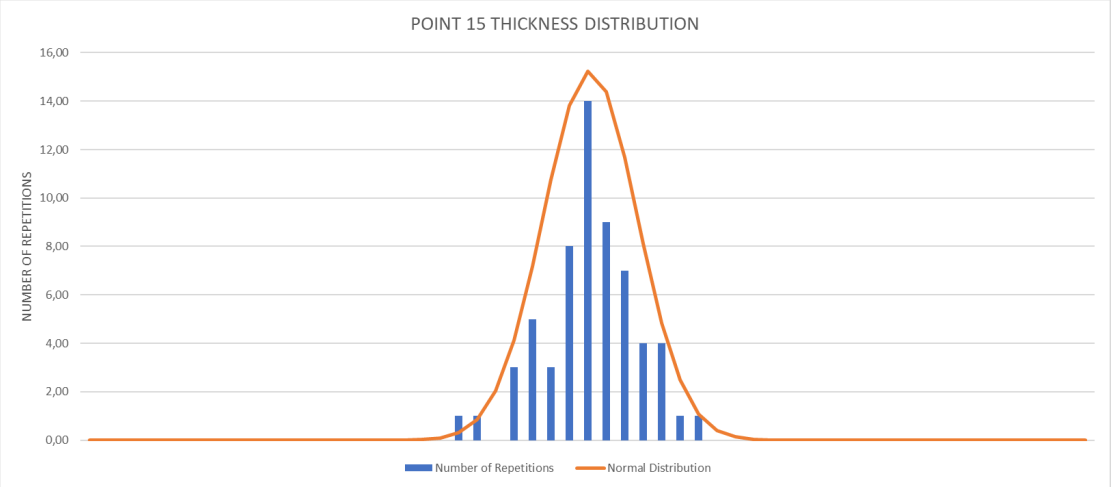

Figure 3.17: 15 Point Distribution Thickness

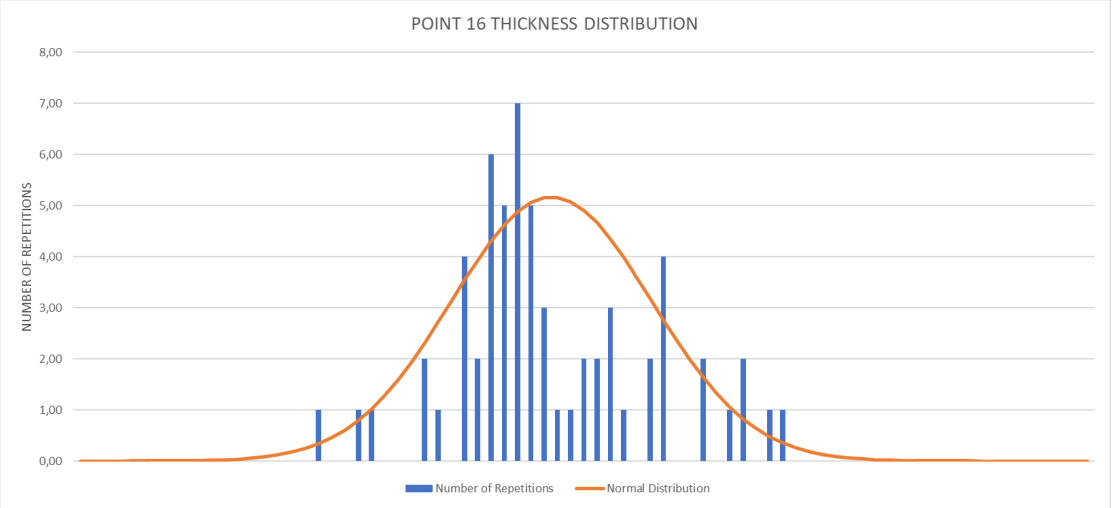

Figure 3.18: 16 Point Distribution Thickness

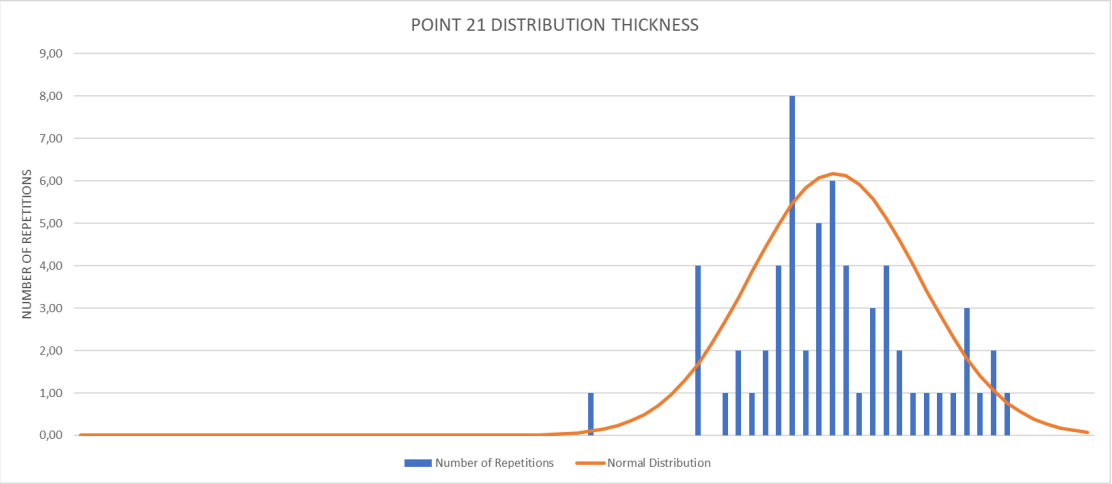

Figure 3.19: 21 Point Distribution Thickness

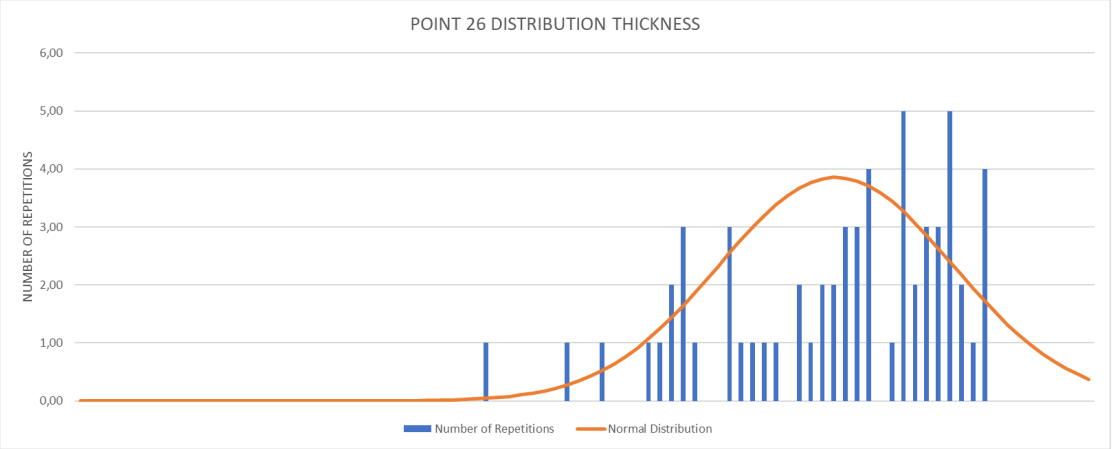

Figure 3.20: 26 Point Distribution Thickness

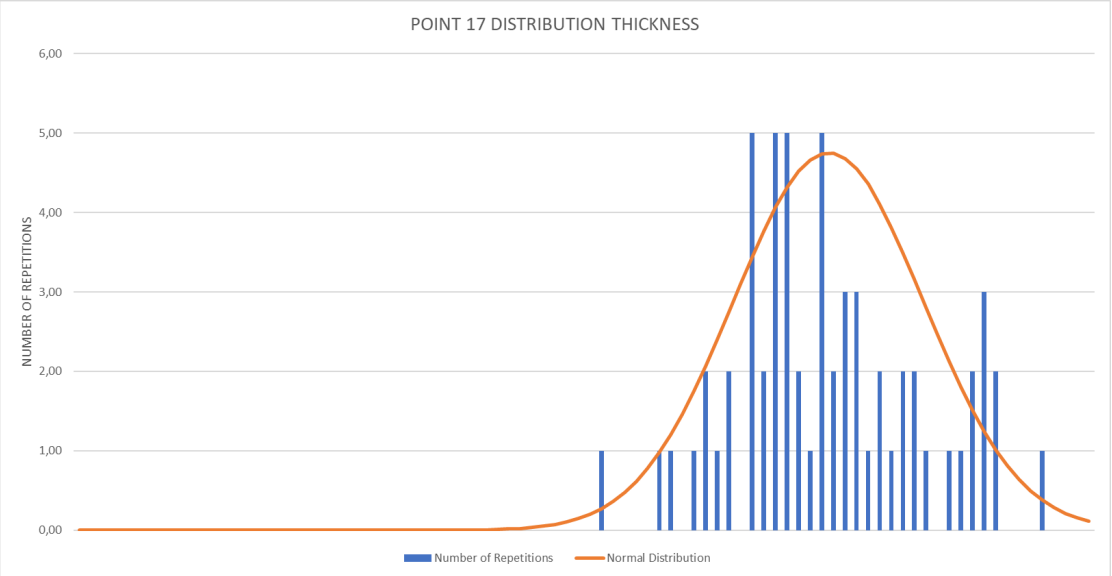

Figure 3.21: 17 Point Distribution Thickness

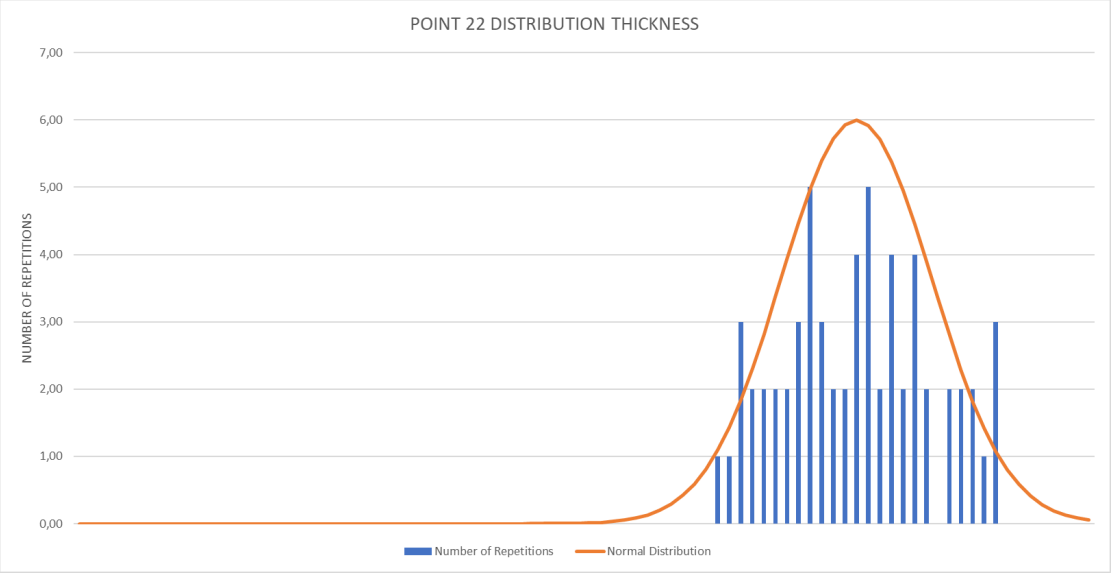

Figure 3.22: 22 Point Distribution Thickness

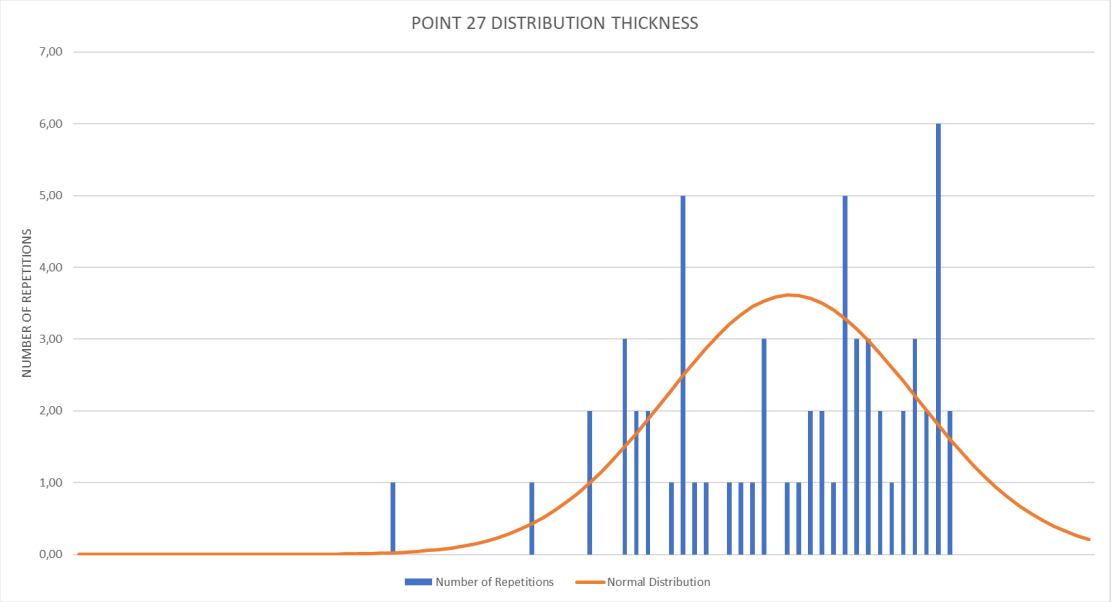

Figure 3.23: 27 Point Distribution Thickness

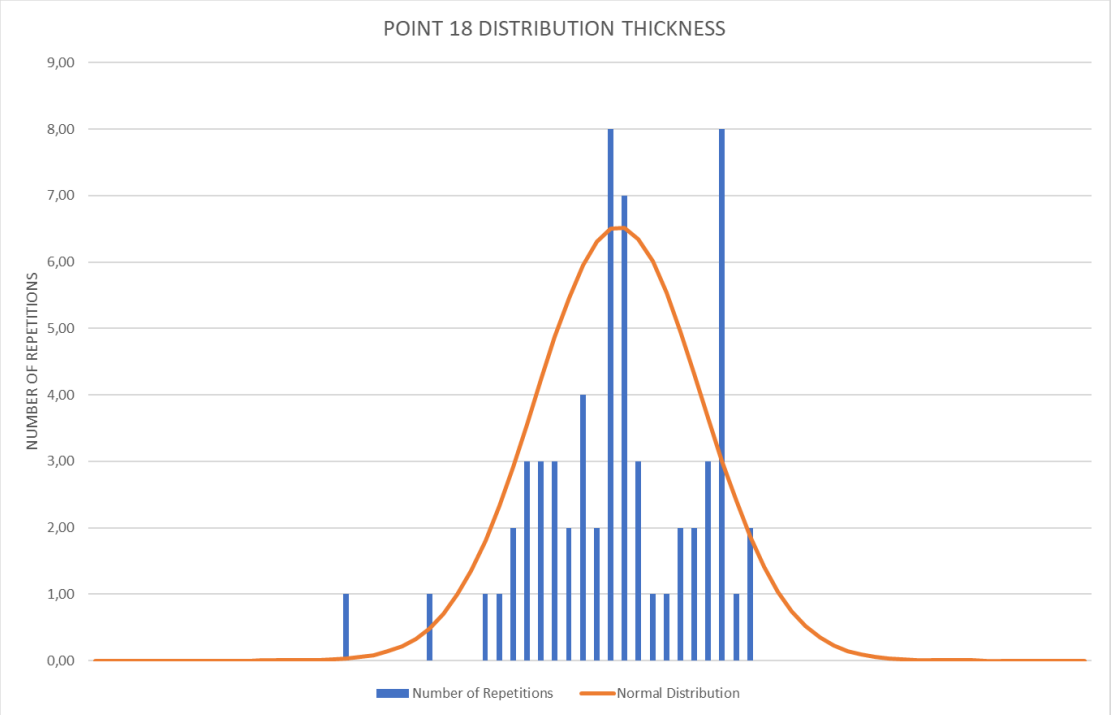

Figure 3.24: 18 Point Distribution Thickness

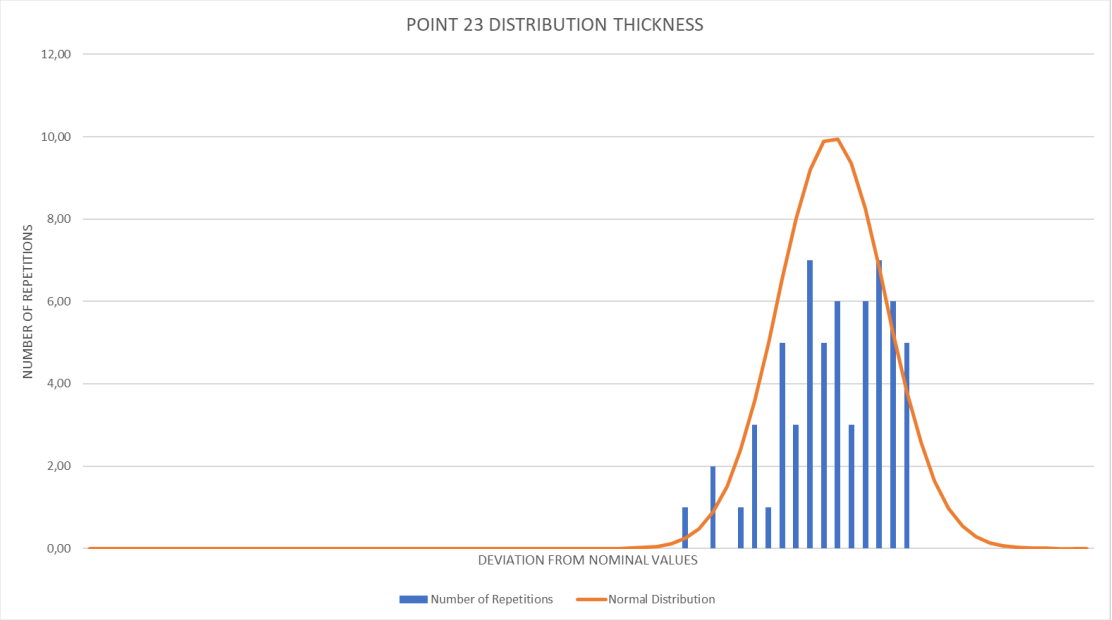

Figure 3.25: 23 Point Distribution Thickness

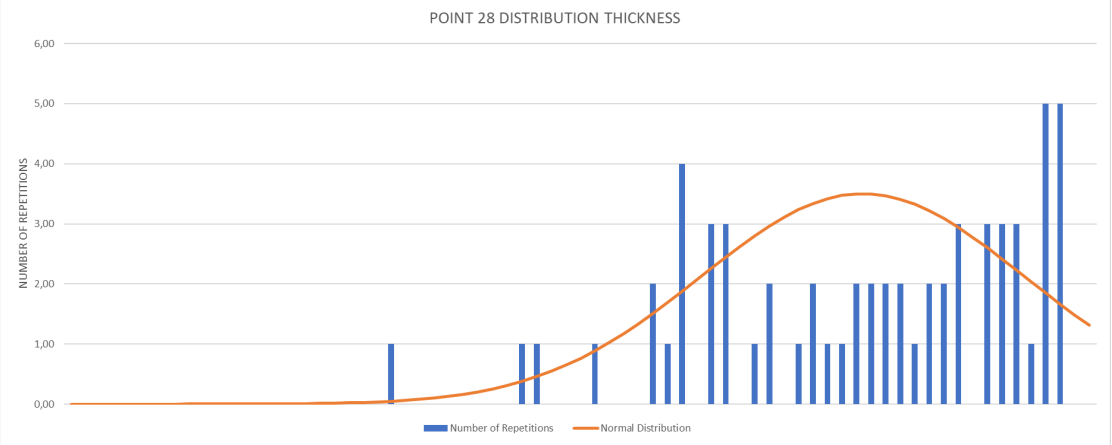

Figure 3.26: 28 Point Distribution Thickness

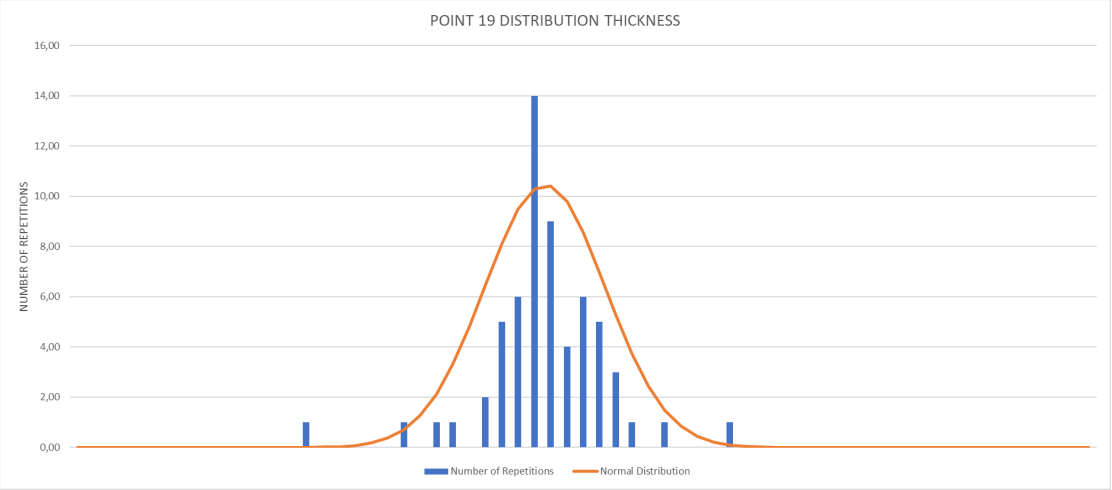

Figure 3.27: 19 Point Distribution Thickness

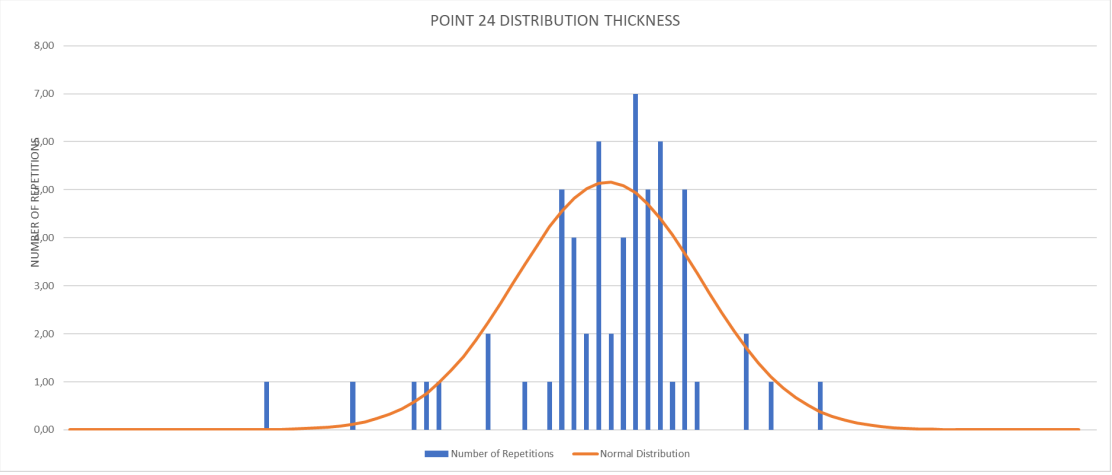

Figure 3.28: 24 Point Distribution Thickness

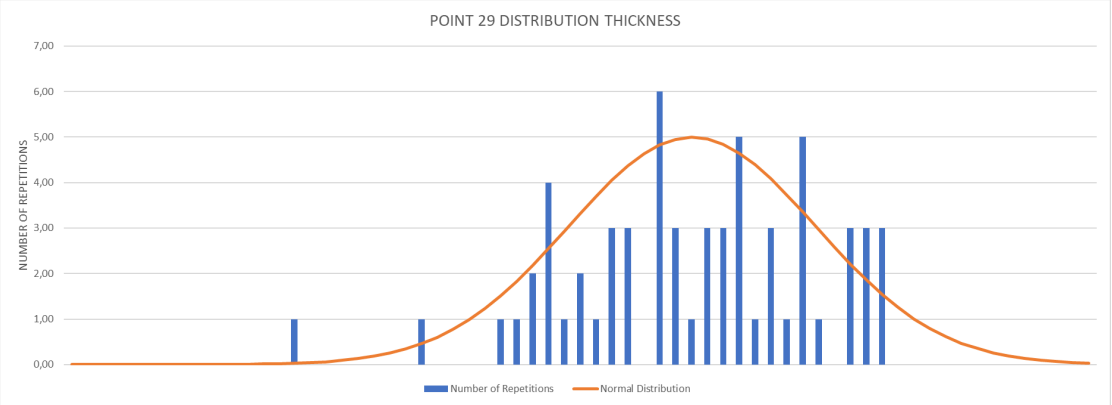

Figure 3.29: 29 Point Distribution Thickness

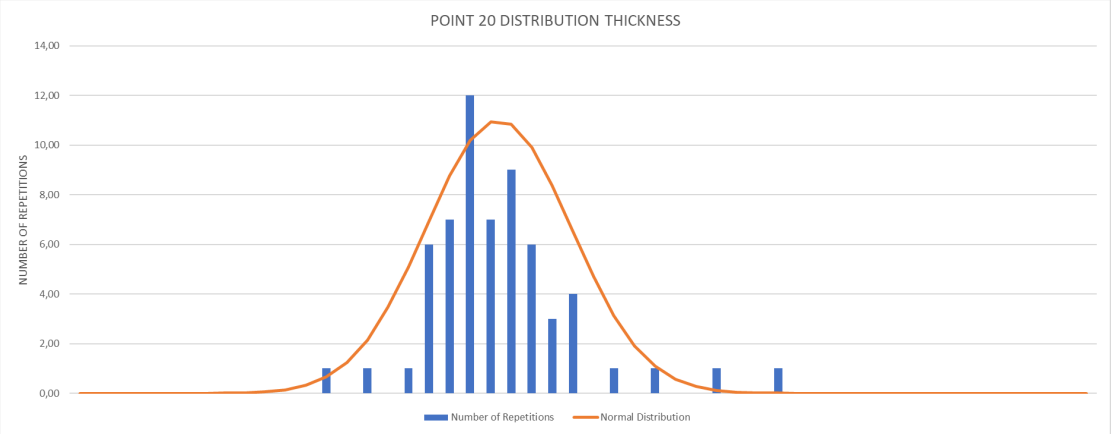

Figure 3.30: 20 Point Distribution Thickness

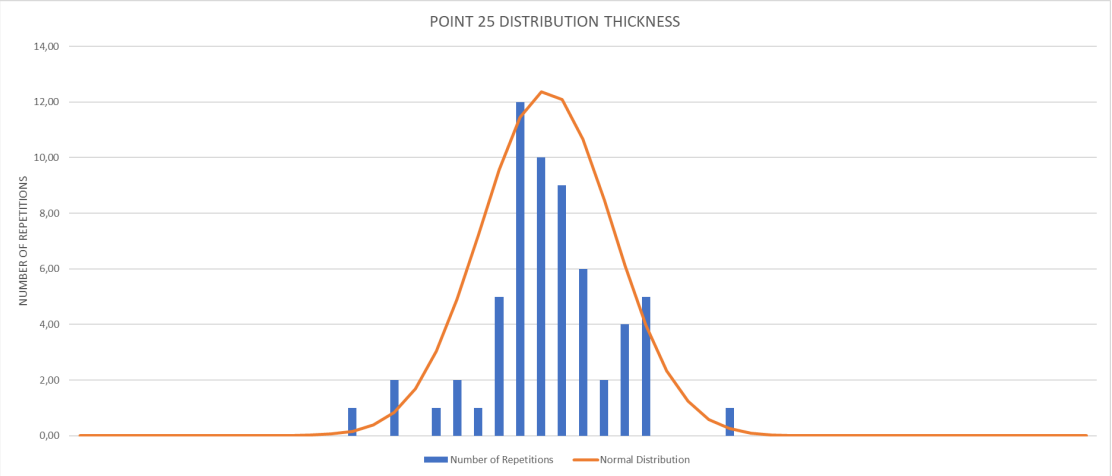

Figure 3.31: 25 Point Distribution Thickness

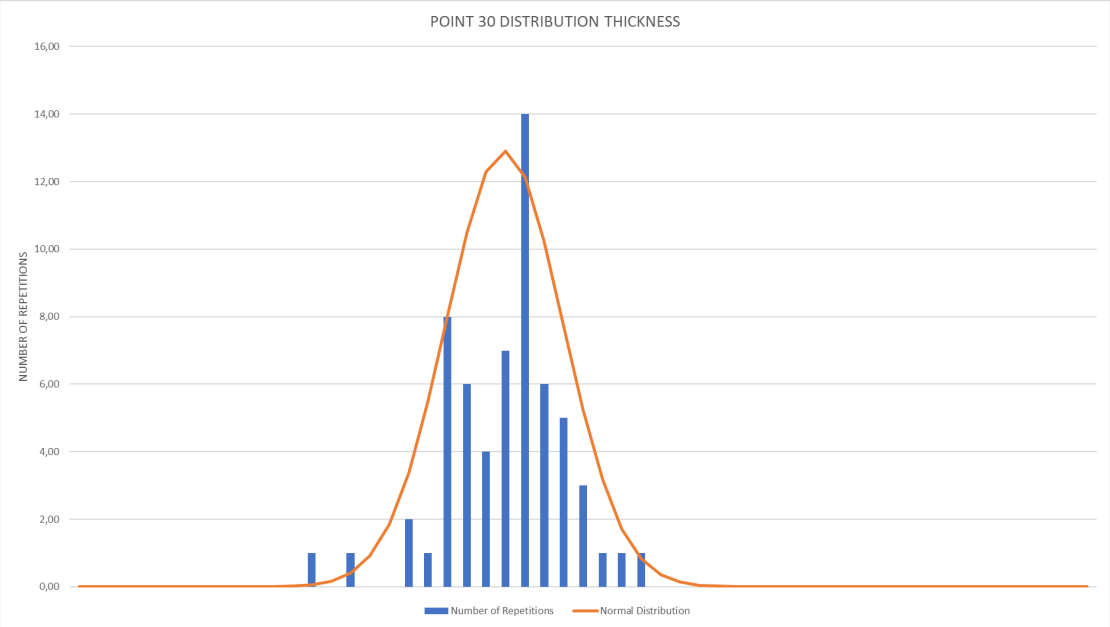

Figure 3.32: 30 Point Distribution Thickness

As it can be seen from the graphs, not a single blade happened to be outside of the AEN's Extremes. This shows that out of the measured blades, not a single one would have not been used in real world application. Since all blades were in the extremes, there was confidence that if there happened to be some kind of deviation, and that would have significantly impacted results, with the following case study that would have been highlighted. Thus it is clear at this point that something else has to be studied in order to find the source of discrepancy. The following section then will take into account every single blade mentioned above, since none of them is non-compliant. Having compliant to extremes blades was the first idea to investigate, because it wouldn't have made sense to continue with non-usable blades, since as said every blade could be used, the investigation continued.

3.2 Deviation Affection on Frequency

Another idea that was investigated was the possibility that certain deviations of certain points (or some grouping of points as well) would have negatively affected the measured frequency for the batch of tested blades. This was evaluated by using a batch of measured blades' frequencies that were provided. To understand more deeply the results, the simulations and investigations were conducted for both the directionally solidified Nickel-based New Superalloy (the new alloy used) and Renè 80 materials. The blades that were evaluated were part of a batch of previously measured blades as said before in both superalloys and subsequently frequency tested, in order to observe if there where any patters to recognize and investigate further. In particular, a diverse number or grouping patterns were investigated. In particular, the grouping schemes were the following:

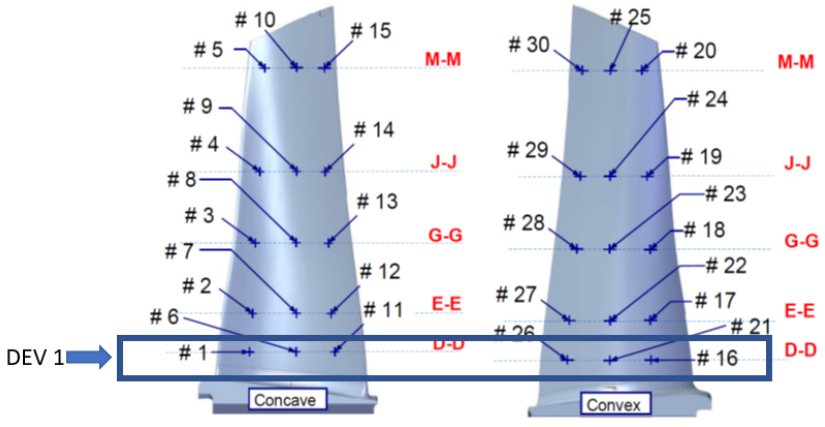

Figure 3.33: Point Grouping for Deviation 1

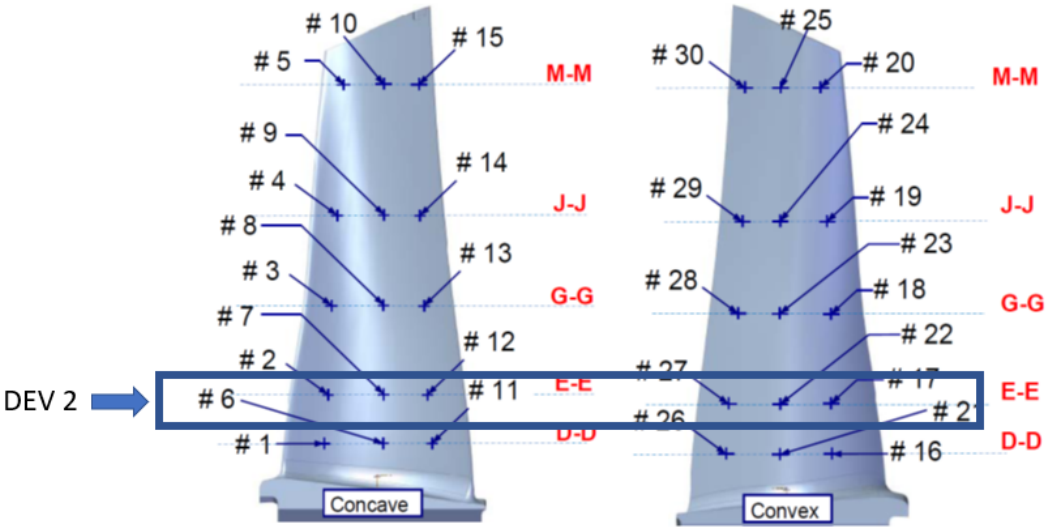

Figure 3.34: Point Grouping for Deviation 2

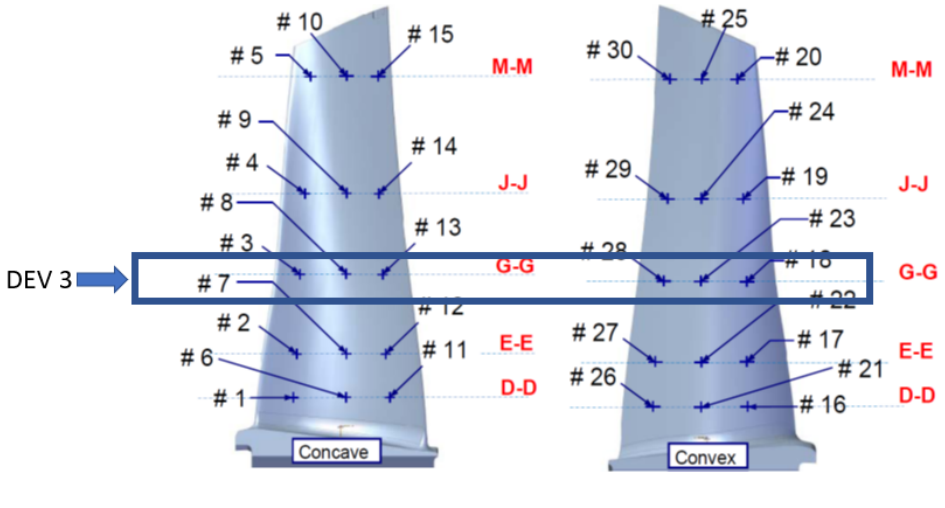

Figure 3.35: Point Grouping for Deviation 3

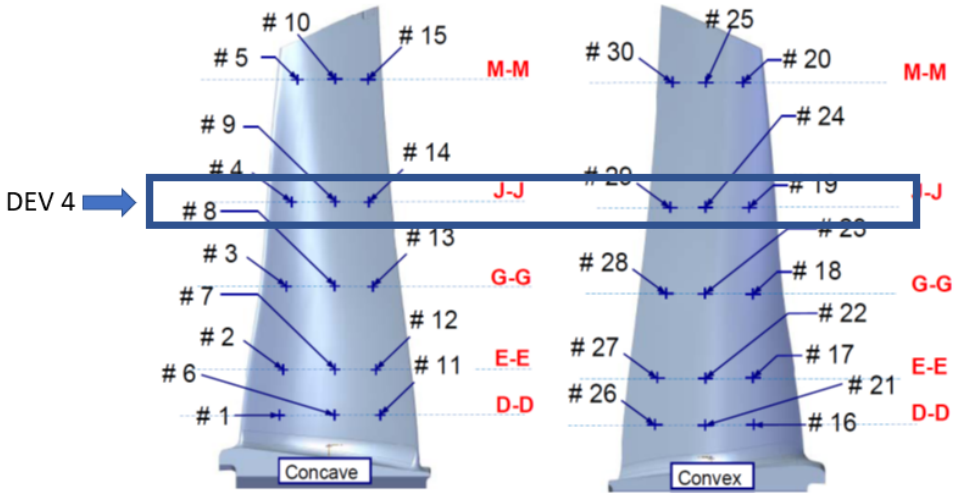

Figure 3.36: Point Grouping for Deviation 4

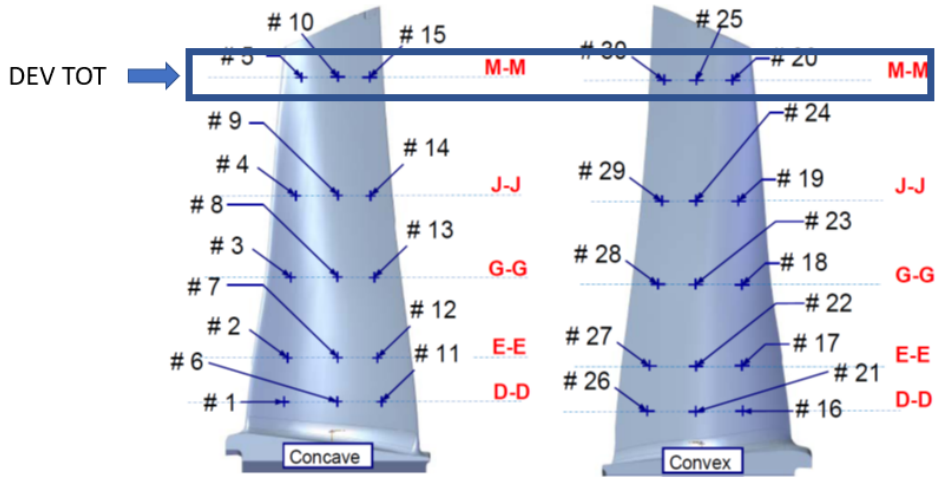

Figure 3.37: Point Grouping for Total Deviation

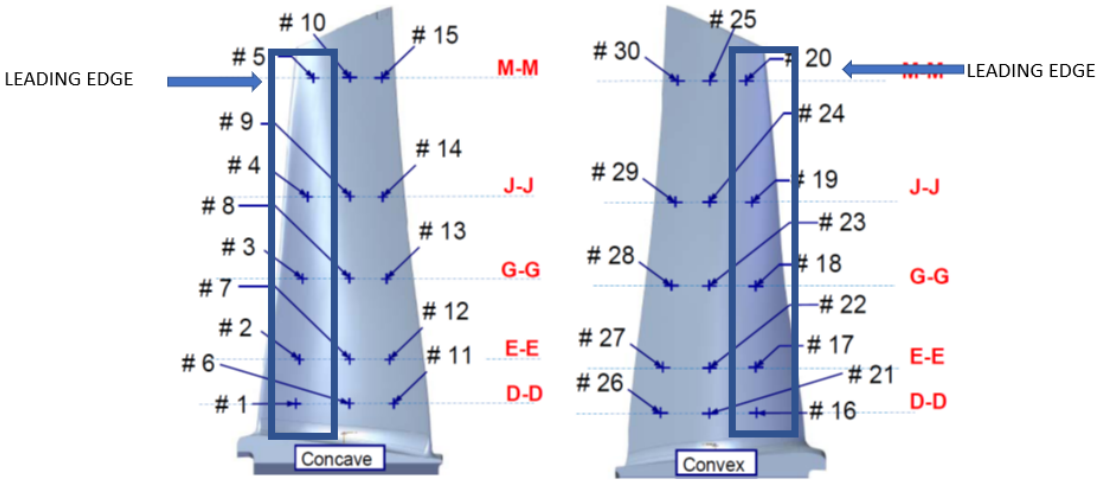

Figure 3.38: Point Grouping for Leading Edge

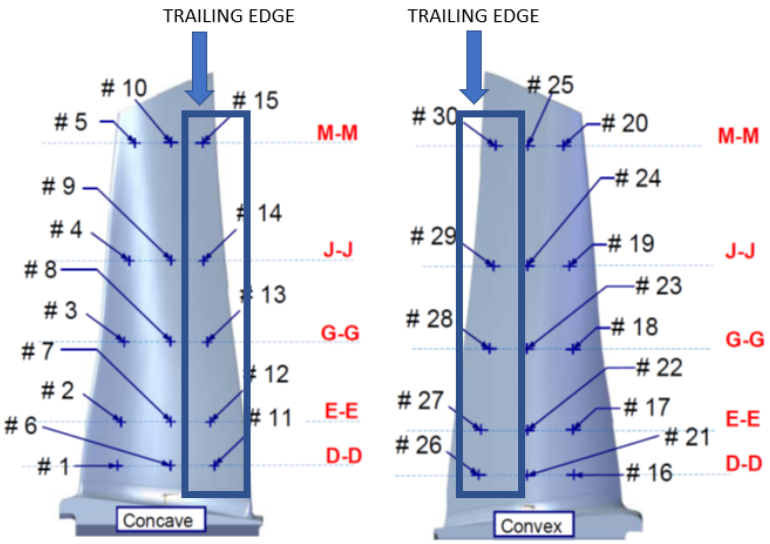

Figure 3.39: Point Grouping for Trailing Edge

After clearly stating what the grouping schemes were referencing to, there is still the need to describe how the deviation for the values was calculated. Deviation for the point's value:

$$\text{DEVIATION}_{Point} = \left(\frac{\text{Measured Value of Point}}{\text{Nominal Value}} - 1 \right) \cdot 100 \tag{3.1}$$

and for the sum of deviations (e.g. Trailing Edge):

$$\text{Deviation N} = \sum_{n=1}^{N} \text{Dev}_i \tag{3.2}$$

Where the sum is obtained by adding the points highlighted in the respective index (the images 3.33 to 3.39). This is the reason why sometimes the values will exceed 100%[1]. Frequency Percentage (showed on the **y axis**) was calculated with this formula;

$$\text{DEVIATION}_{Frequency} = \left(\frac{\text{Measured Value for Blade}}{\text{Average Frequency}} - 1 \right) \cdot 100 \tag{3.3}$$

[1]It is important to note that the sum was performed taking into account the sign of the value. Hence it also takes into account if a specific blade will either have for example a bigger deviation in postive or in negative values in different places.

3.2.1 René 80 Measurements

Single Point Deviation

Starting from single-point deviation for the first modes[2], the graphs are provided below:

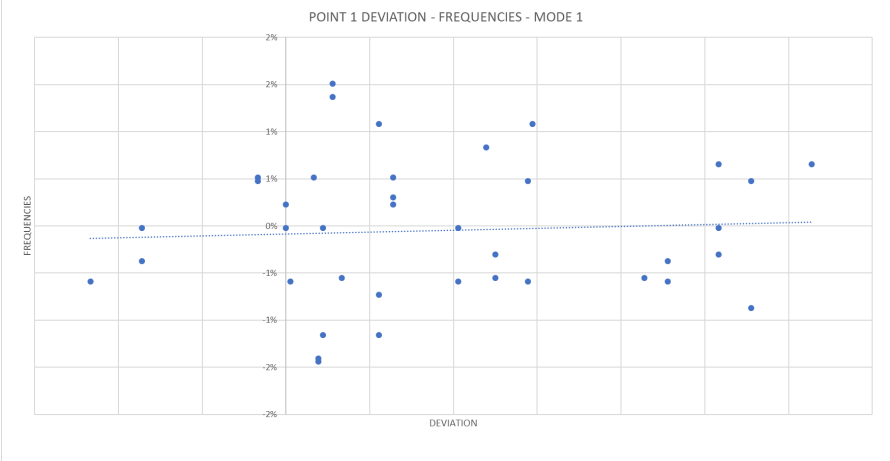

Figure 3.40: Point 1 - Mode 1 Frequency Deviation

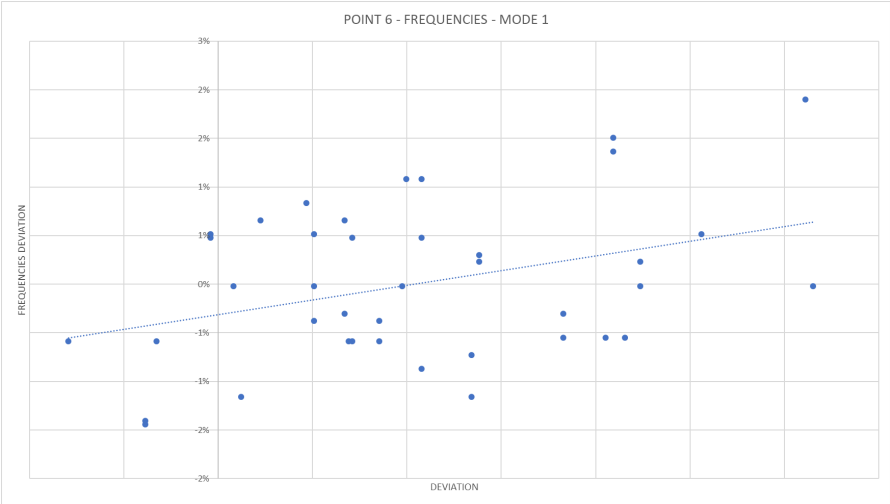

Figure 3.41: Point 6 - Mode 1 Frequency Deviation

[2]Since the interesting modes are the first ones, the evaluation was done up until the fourth mode.

Important Note: the x-axis cannot refer to specific values, but to be intended as going from smaller up to bigger values of deviation, from negative to positive.

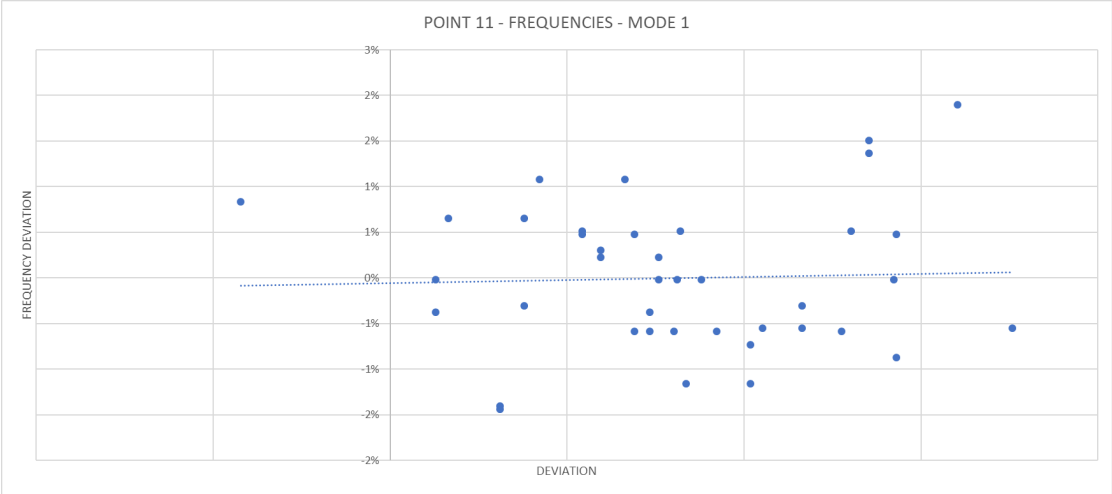

Figure 3.42: Point 11 - Mode 1 Frequency Deviation

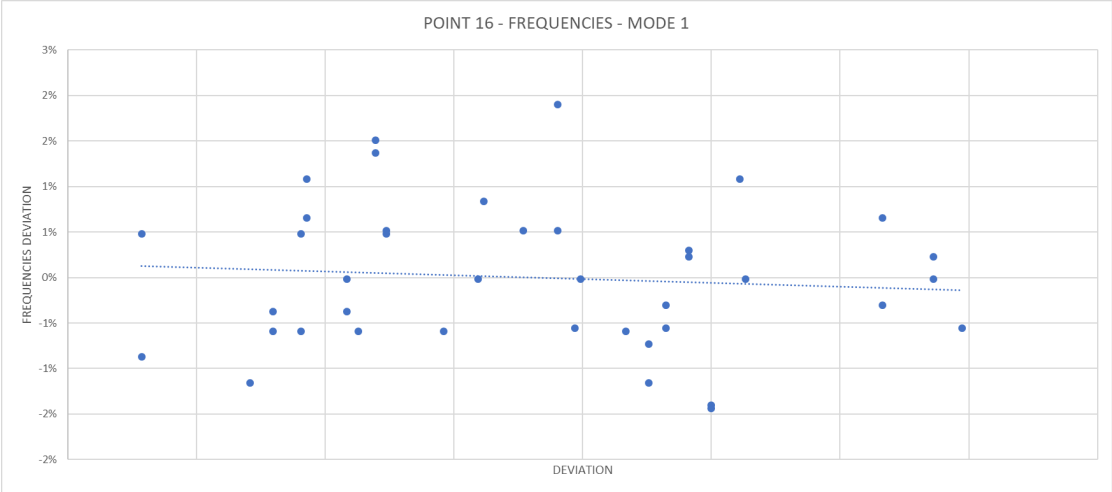

Figure 3.43: Point 16 - Mode 1 Frequency Deviation

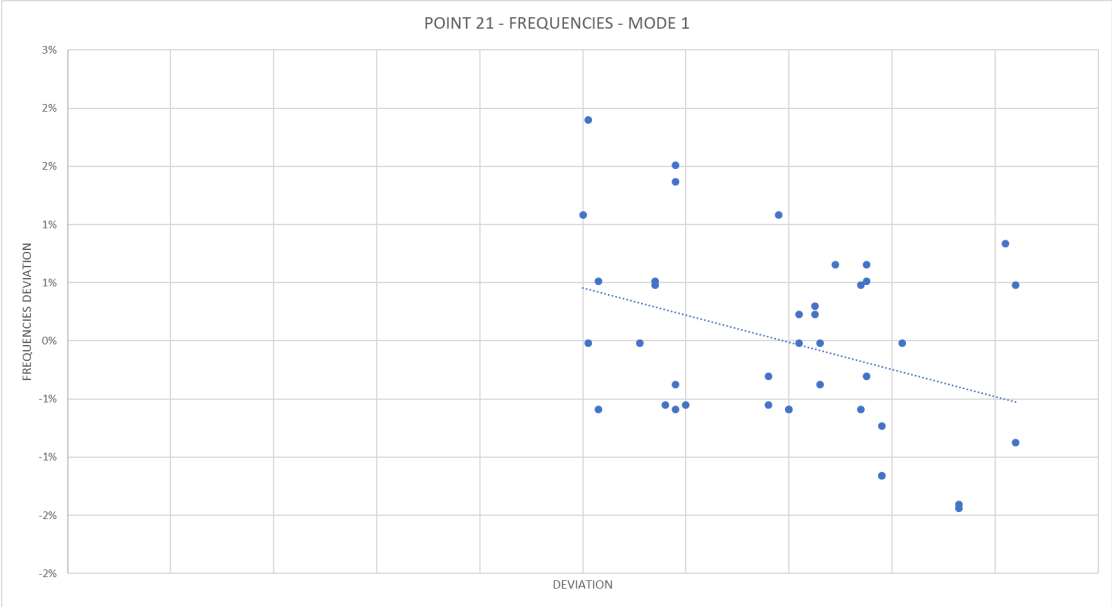

Figure 3.44: Point 21 - Mode 1 Frequency Deviation

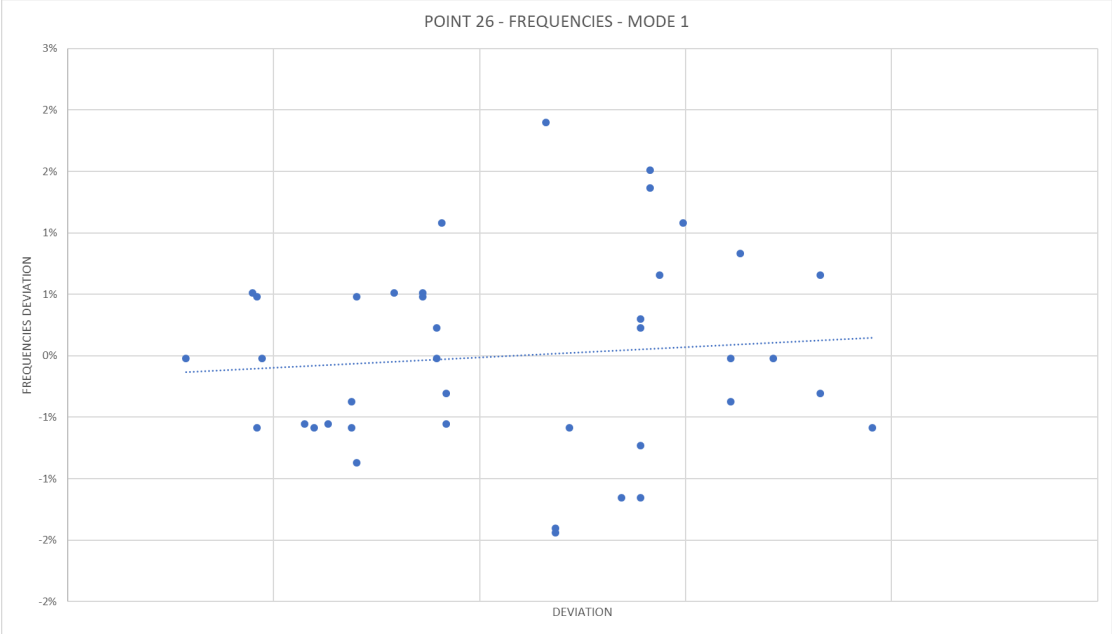

Figure 3.45: Point 26 - Mode 1 Frequency Deviation

At this point, from looking at the provided graphs, where every single point represents a blades' Serial Number and the dotted line represents the linear regression,

it can be concluded that there is no such influence from single point deviation to measured frequency. The reason of investigating the first six points from the base and the first mode is clear when observing the vibrational mode shape of Mode 1 3.46. The Mode 1 is a **flexional mode**, hence it was decided to test the influence of the base points to see if **individually** they had some significant effect. As said before, from the dotted lines trend in the graphs, there is no such effect. This possibility was ruled out, but the idea of grouping points, that will be present in the following graphs, is derived from the observation of the mode shape.

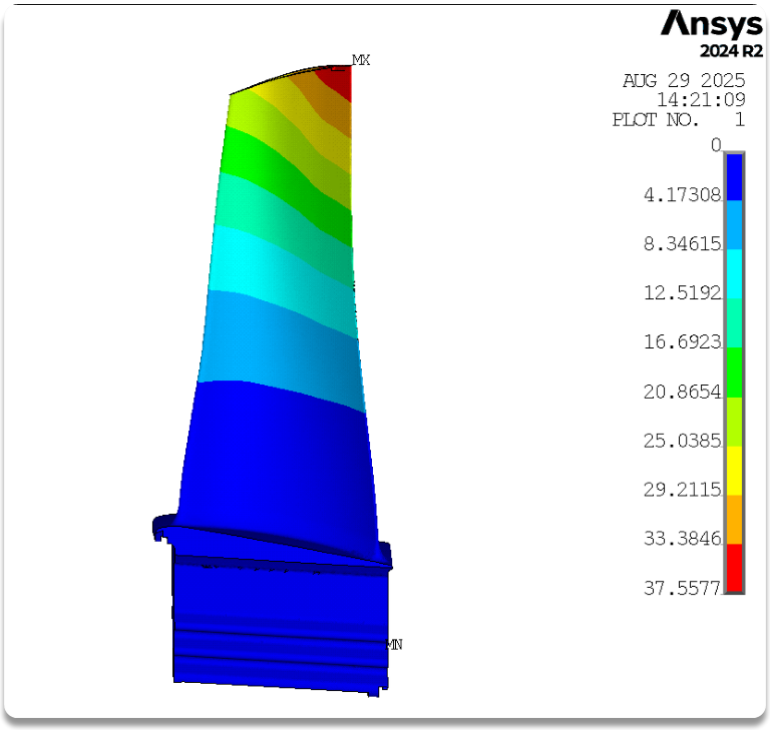

Figure 3.46: Vibrational Mode 1 Graphic Representation

Multiple Point Grouping

As mentioned, the idea of grouping points comes from observing the mode shape in order to assess the *most* effective way to evaluate the possibility of influence. As a result, in order to give a point of reference, a visualization of vibrational mode shape is given below:

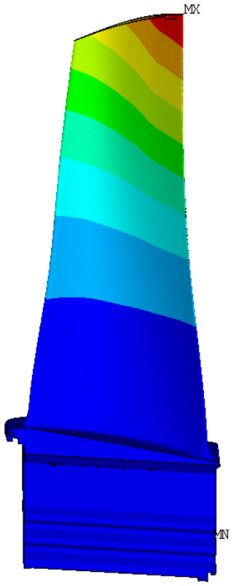

Figure 3.47: Vibrational Mode 1

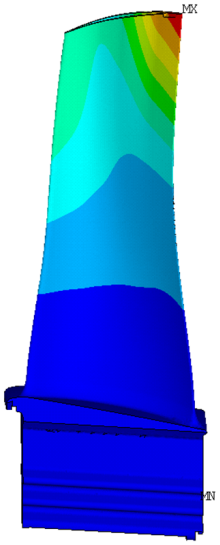

Figure 3.48: Vibrational Mode 2

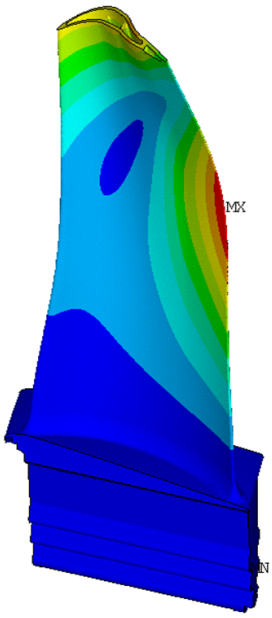

Figure 3.49: Vibrational Mode 3

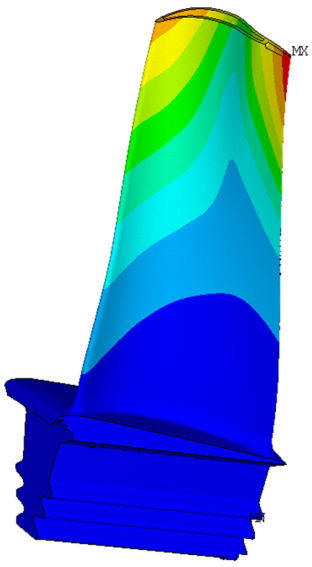

Figure 3.50: Vibrational Mode 4

After evaluating the mode shape correctly it was decided to analyse the values of the deviation for the **first four modes** shown before. As described, the grouping of points were chosen *after* checking the mode shapes.

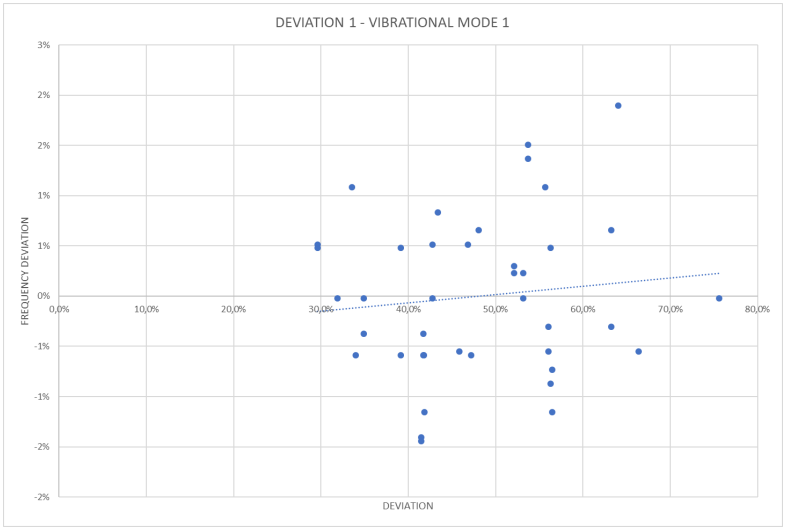

Figure 3.51: Sum of Deviations 1 for Mode 1

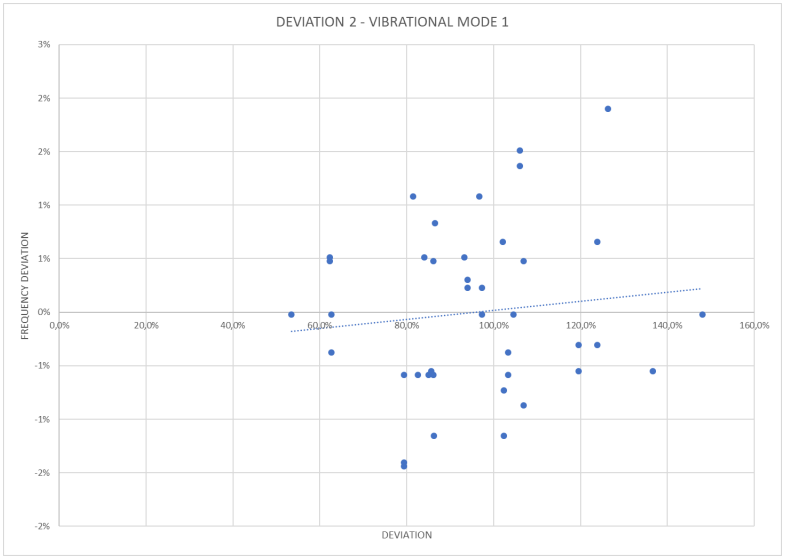

Figure 3.52: Sum of Deviations 2 for Mode 1

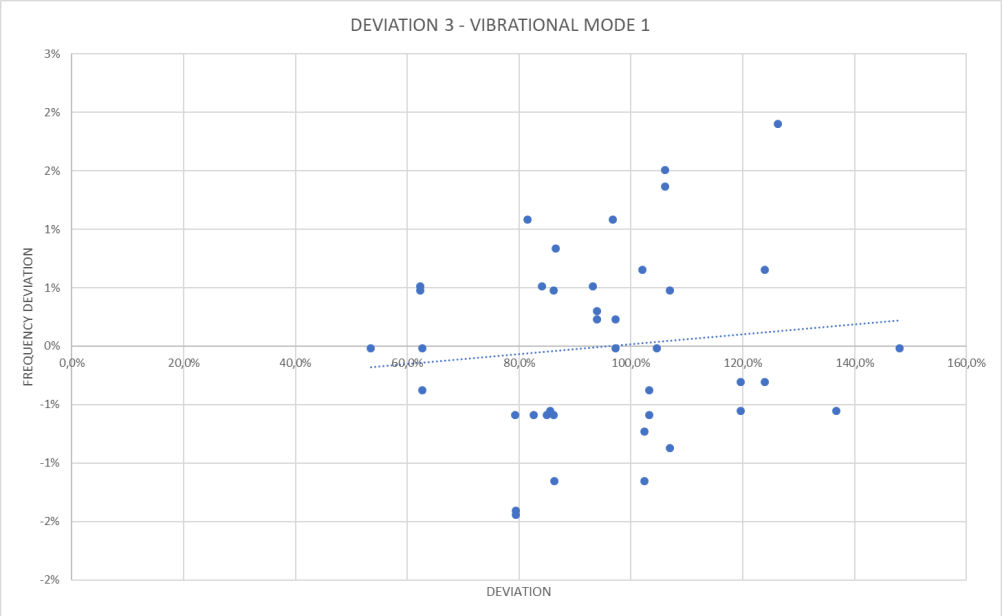

Figure 3.53: Sum of Deviations 3 for Mode 1

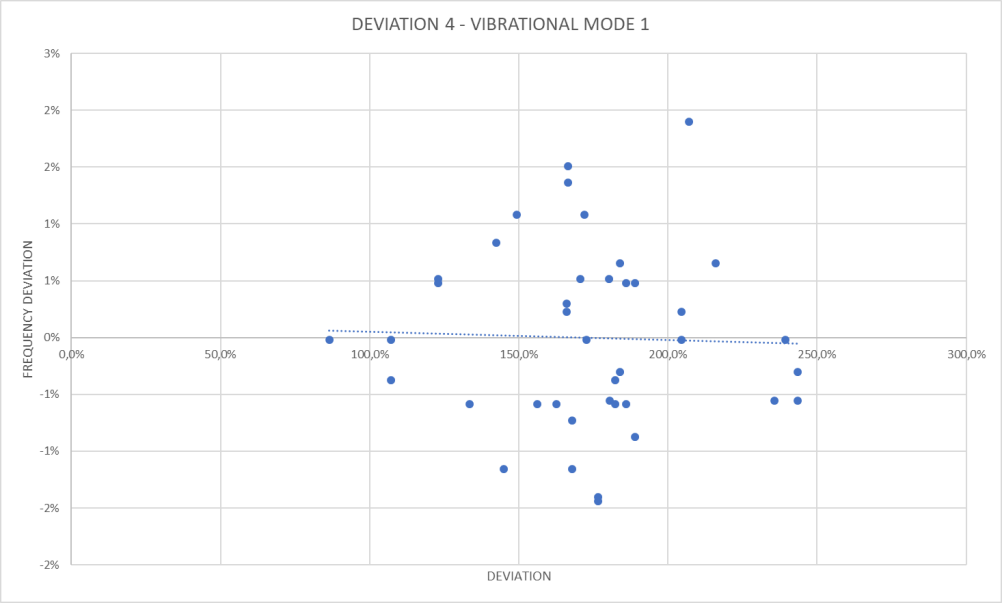

Figure 3.54: Sum of Deviations 4 for Mode 1

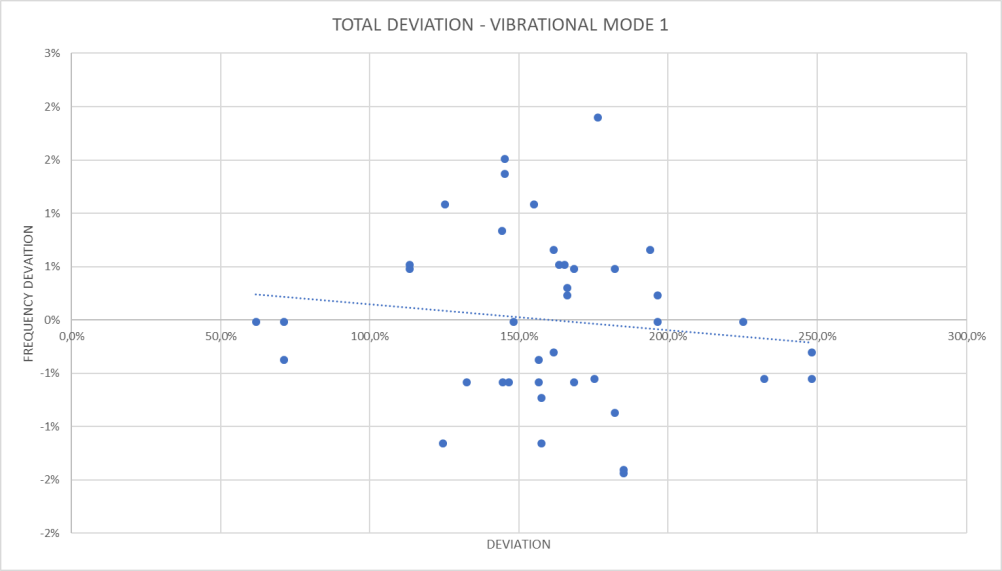

Figure 3.55: Sum of Total Deviation for Mode 1

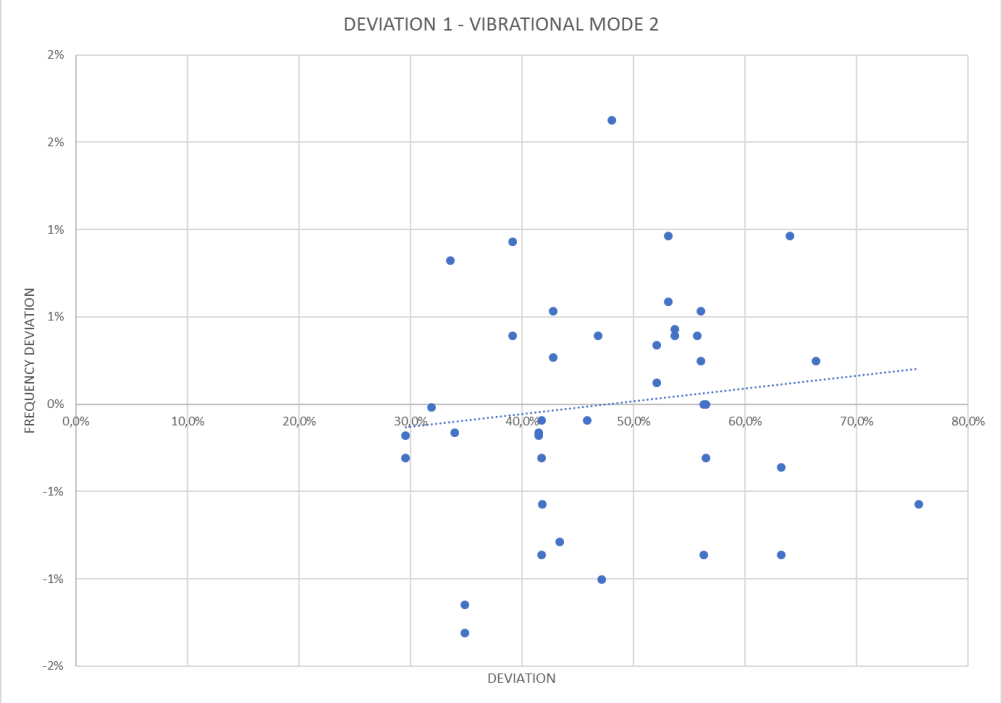

Figure 3.56: Sum of Deviations 1 for Mode 2

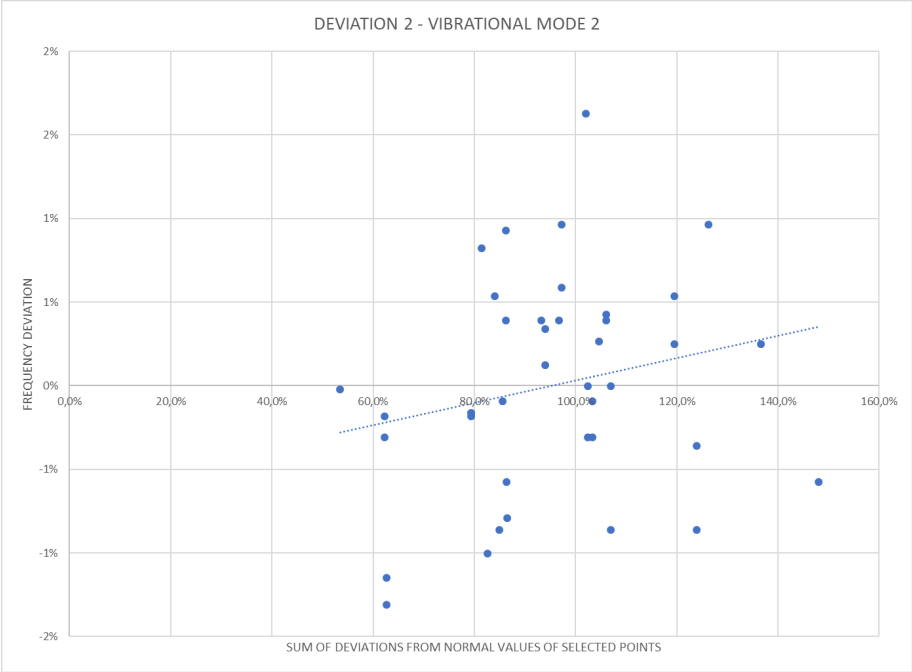

Figure 3.57: Sum of Deviations 2 for Mode 2

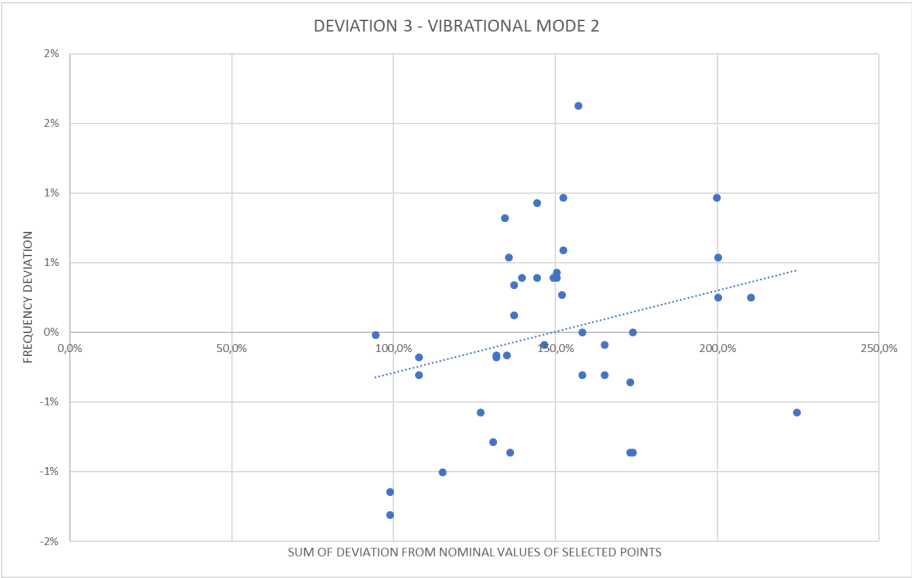

Figure 3.58: Sum of Deviations 3 for Mode 2

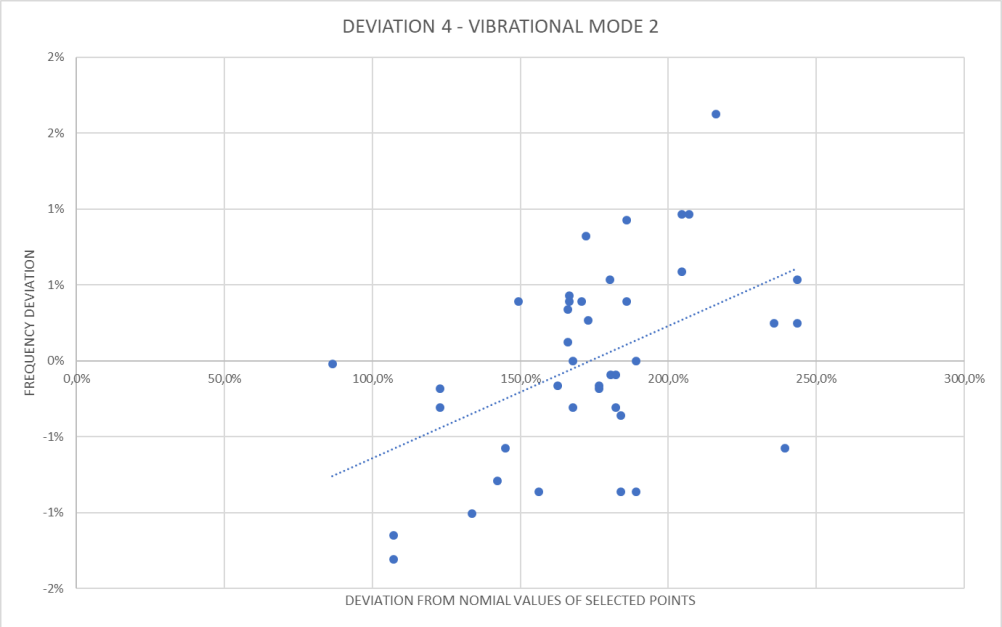

Figure 3.59: Sum of Deviations 4 for Mode 2

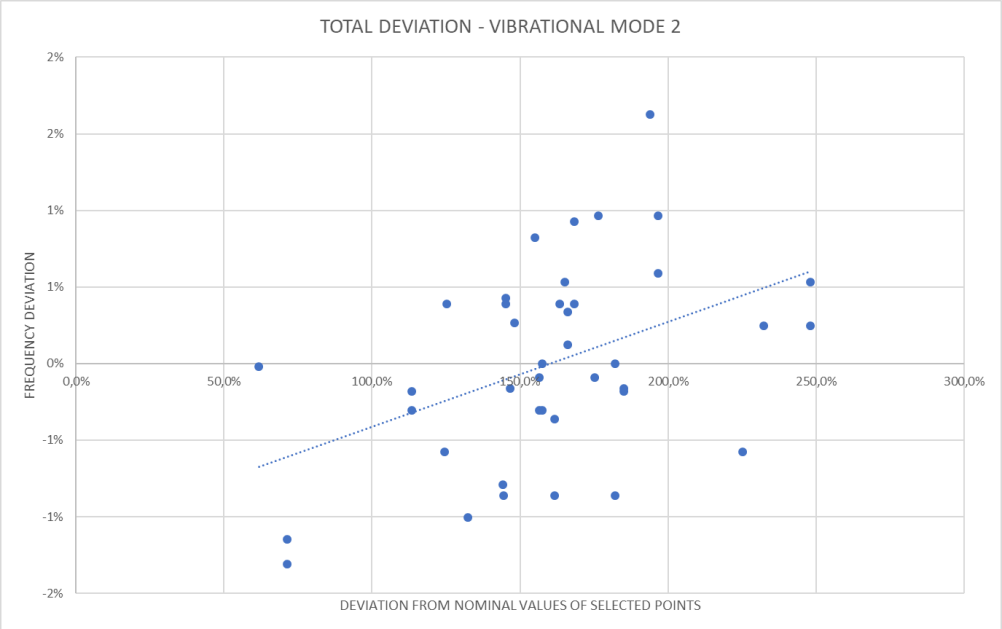

Figure 3.60: Sum of Total Deviations for Mode 2

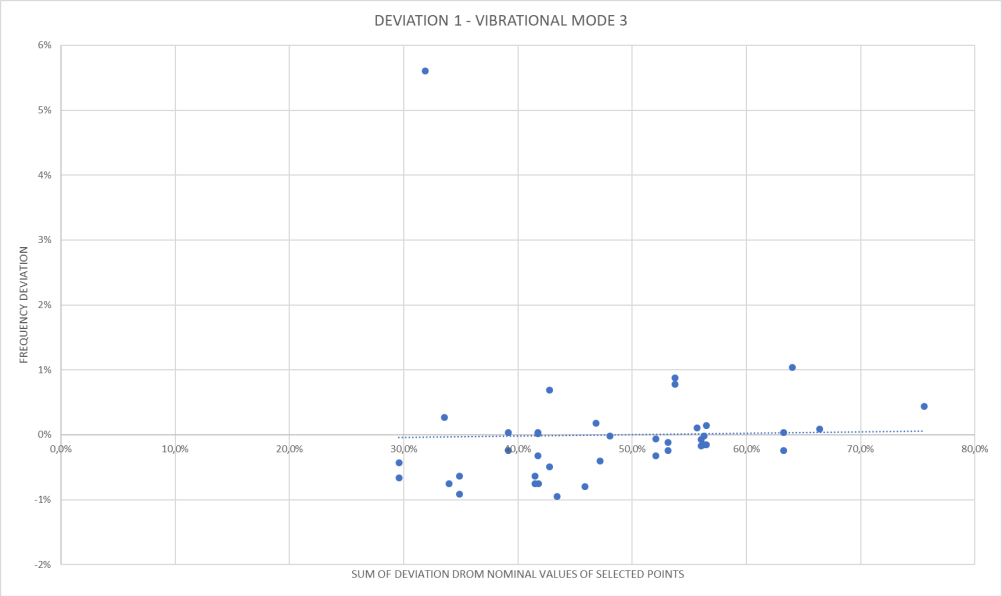

Figure 3.61: Sum of Deviations 1 for Mode 3

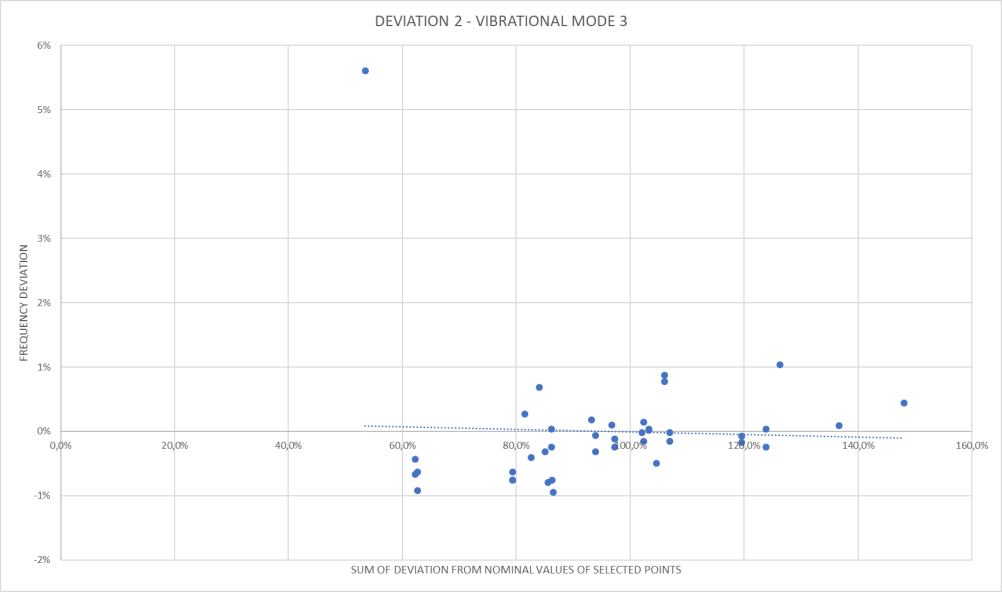

Figure 3.62: Sum of Deviations 2 for Mode 3

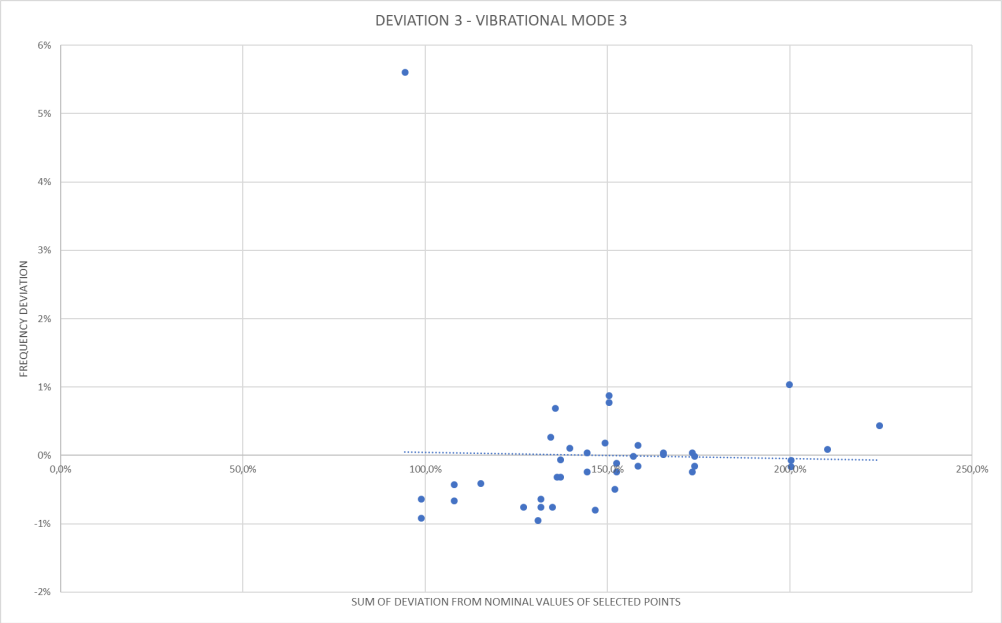

Figure 3.63: Sum of Deviations 3 for Mode 3

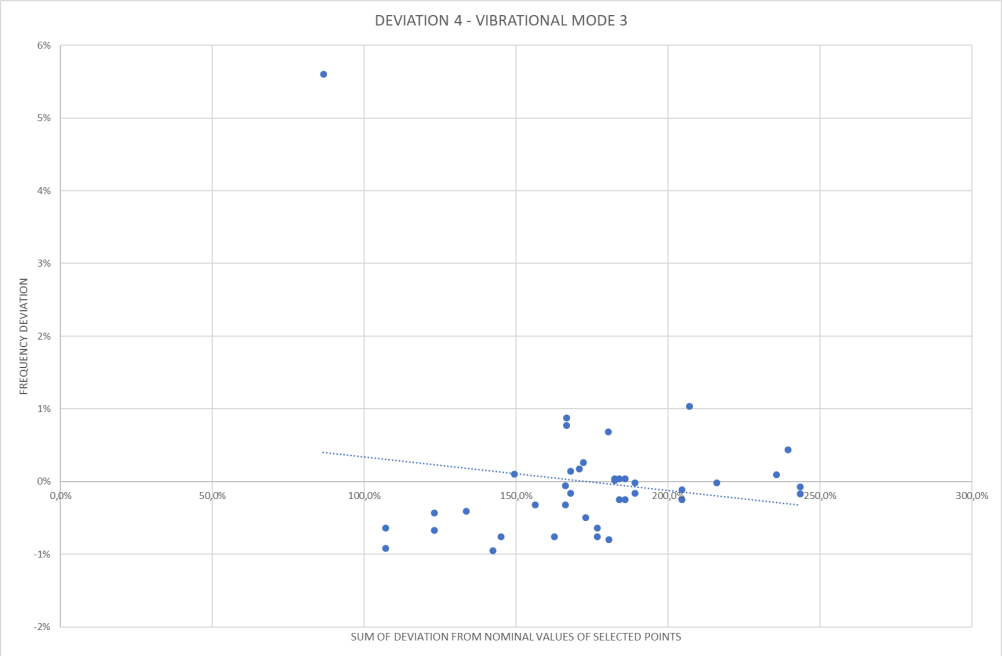

Figure 3.64: Sum of Deviation 4 for Mode 3

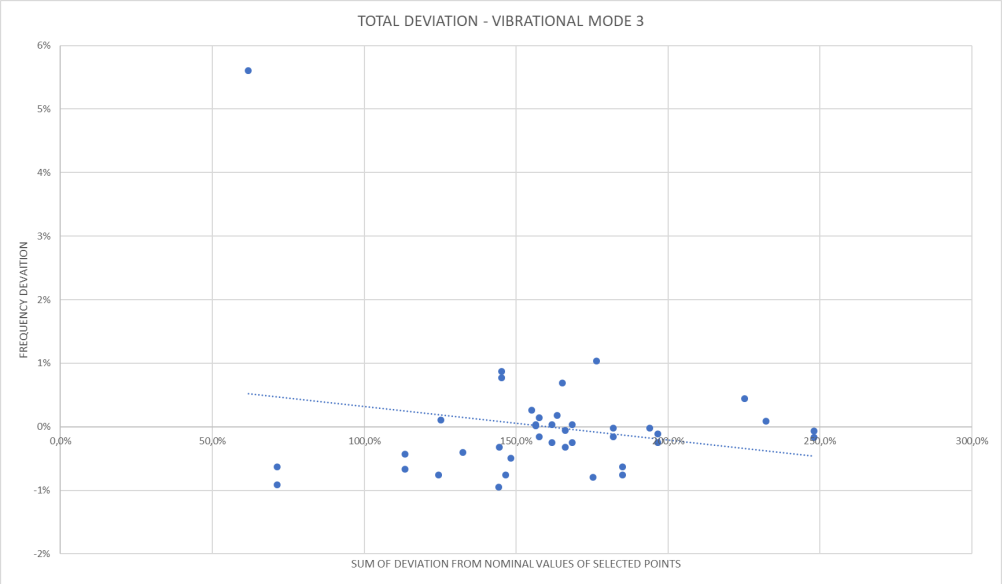

Figure 3.65: Sum of Total Deviation for Mode 3

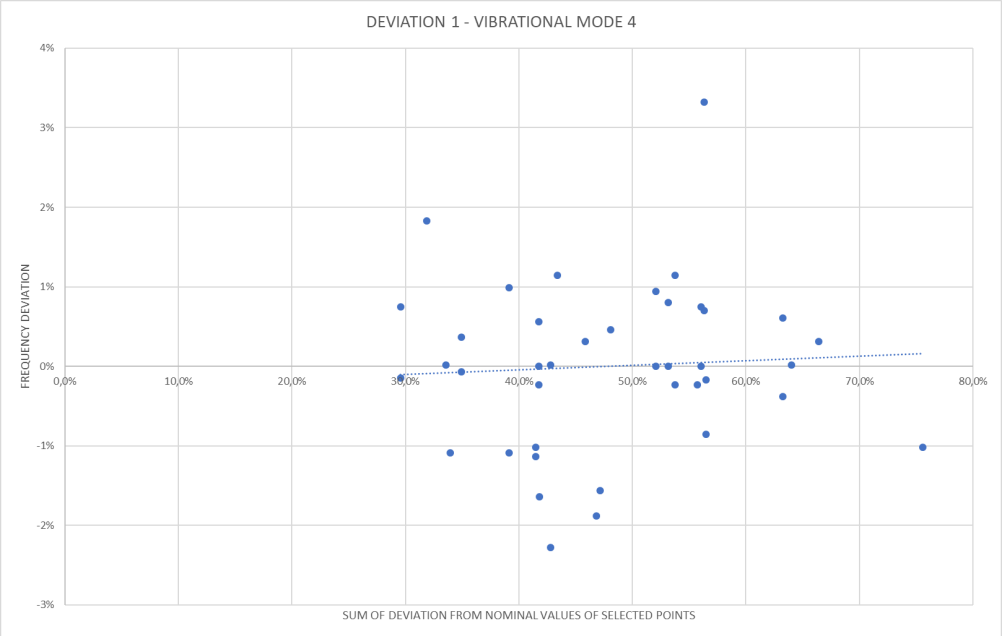

Figure 3.66: Sum of Deviation 1 for Mode 4

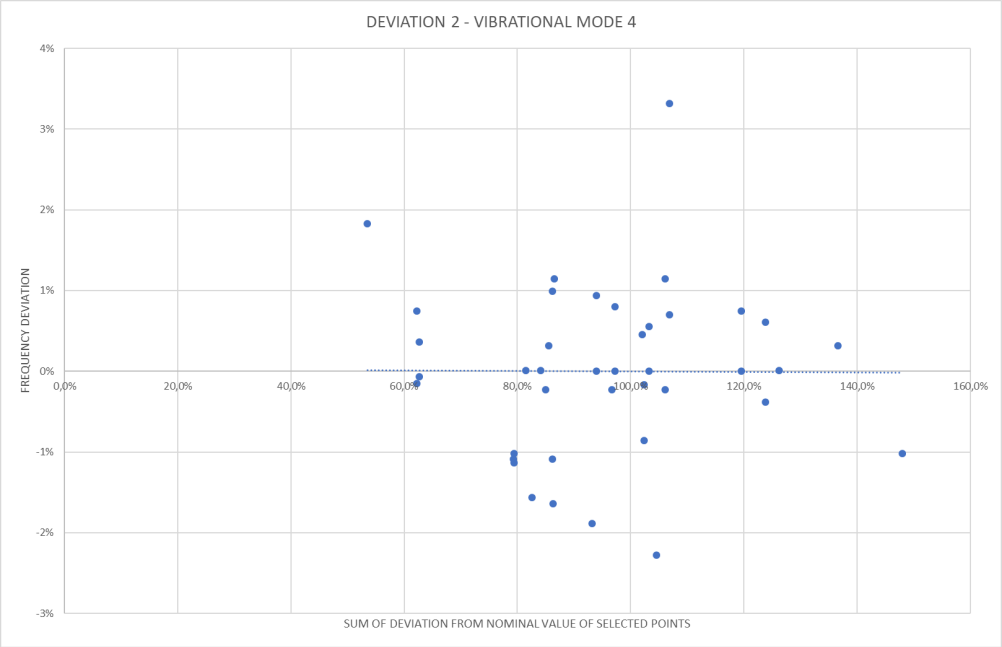

Figure 3.67: Sum of Deviations 2 for Mode 4

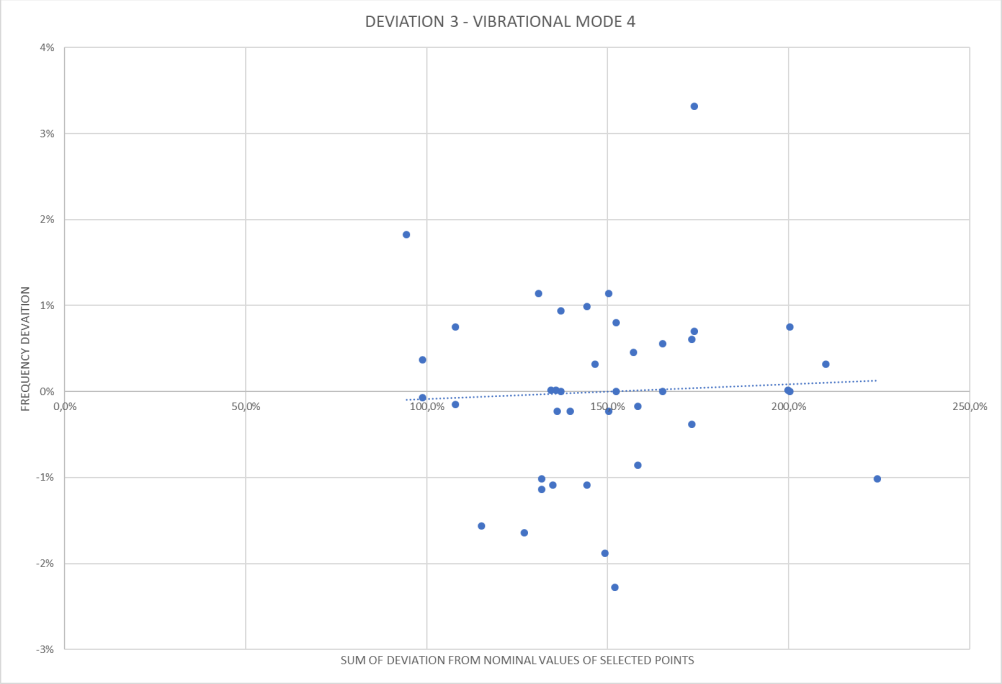

Figure 3.68: Sum of Deviations 3 for Mode 4

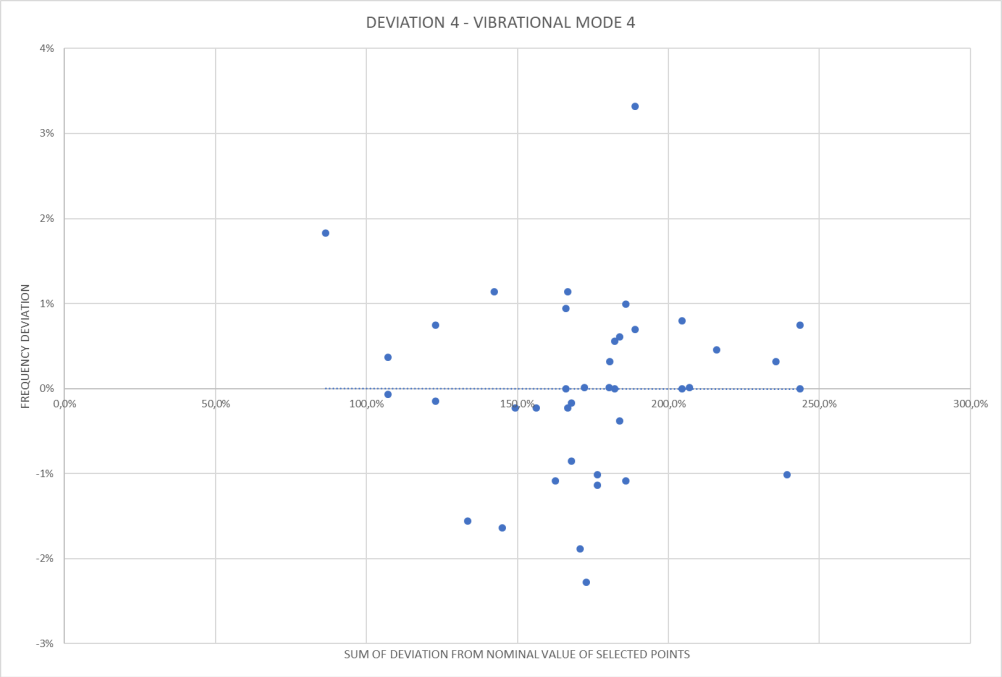

Figure 3.69: Sum of Deviations 4 for Mode 4

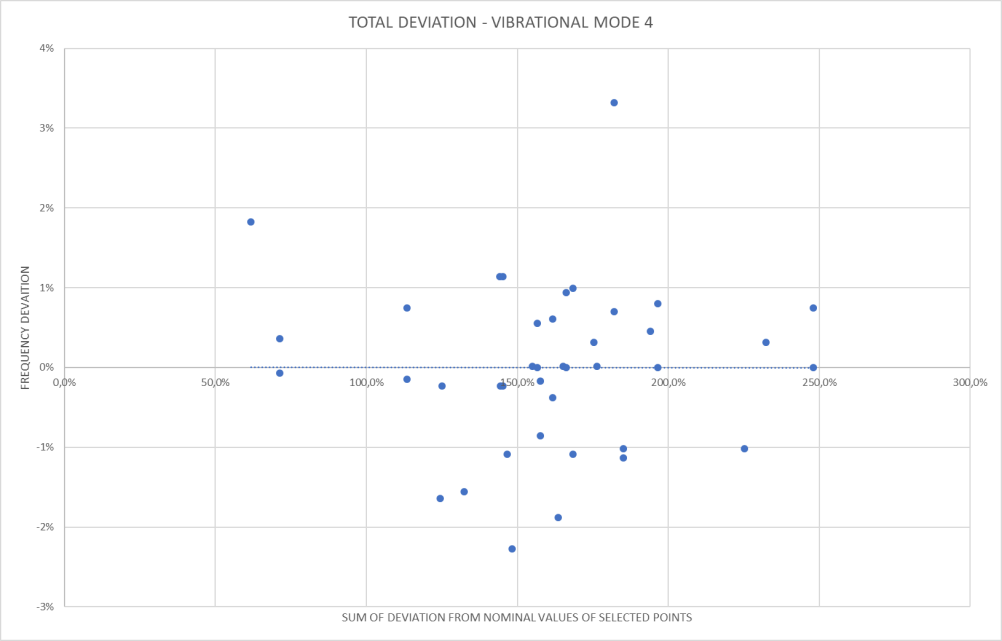

Figure 3.70: Sum of Total Deviations for Mode 4

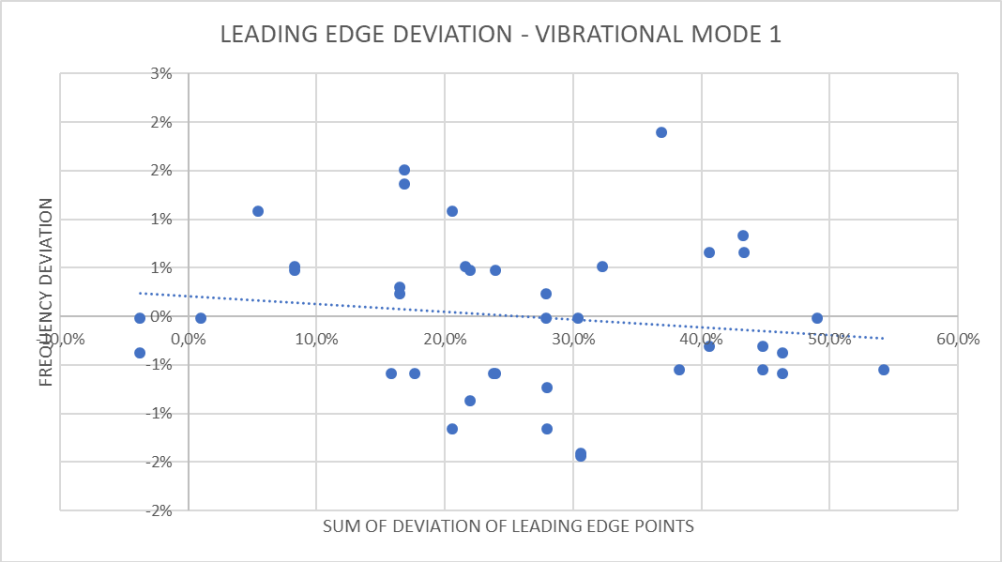

Figure 3.71: Sum of Deviation Leading Edge for Mode 1

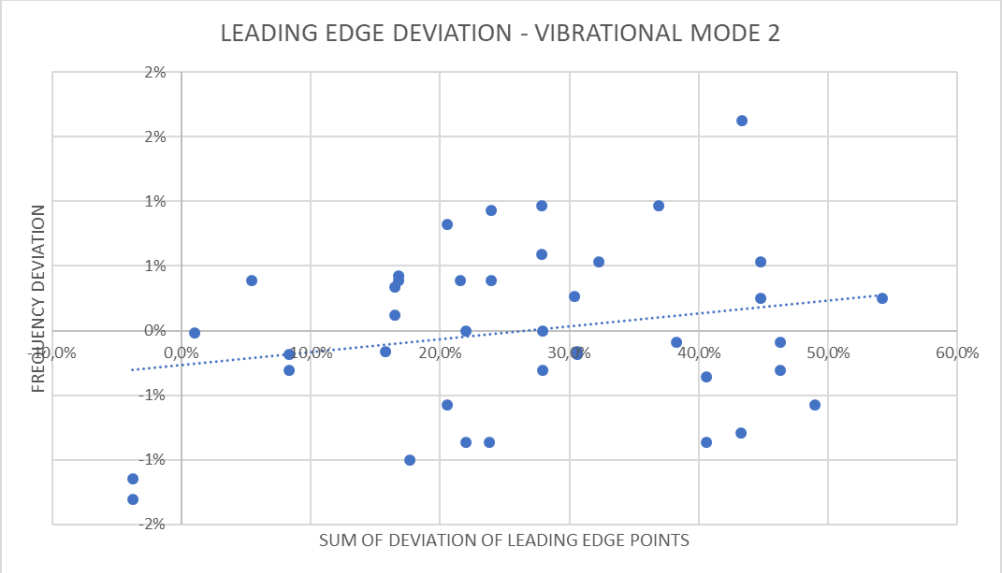

Figure 3.72: Sum of Deviation Leading Edge for Mode 2

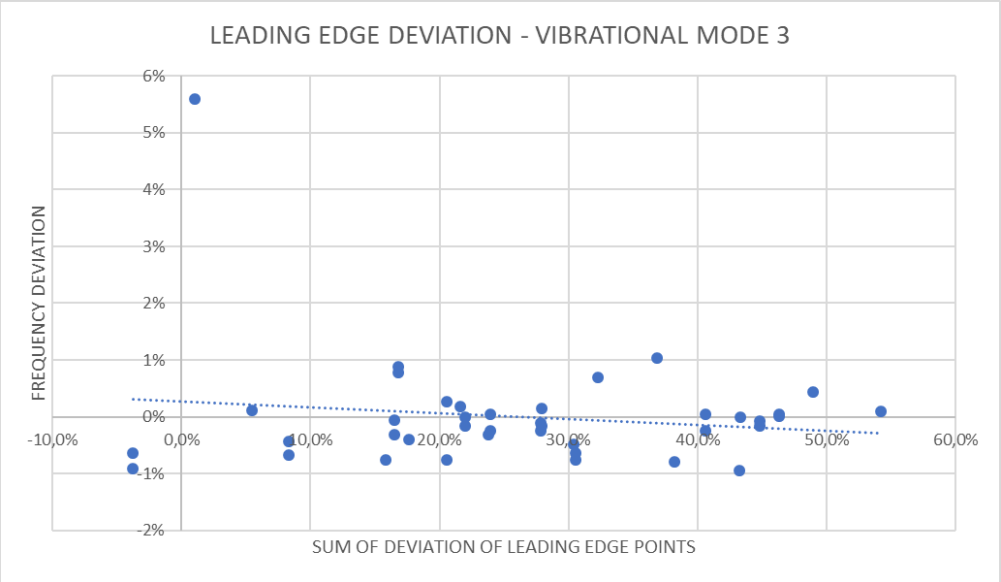

Figure 3.73: Sum of Leading Edge Deviation for Mode 3

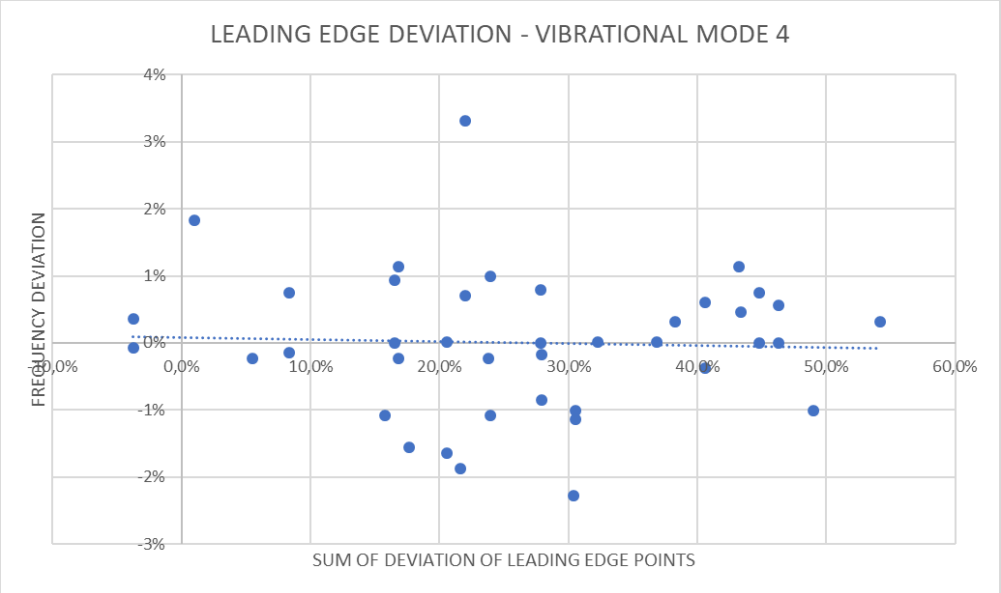

Figure 3.74: Sum of Leading Edge Deviation for Mode 4

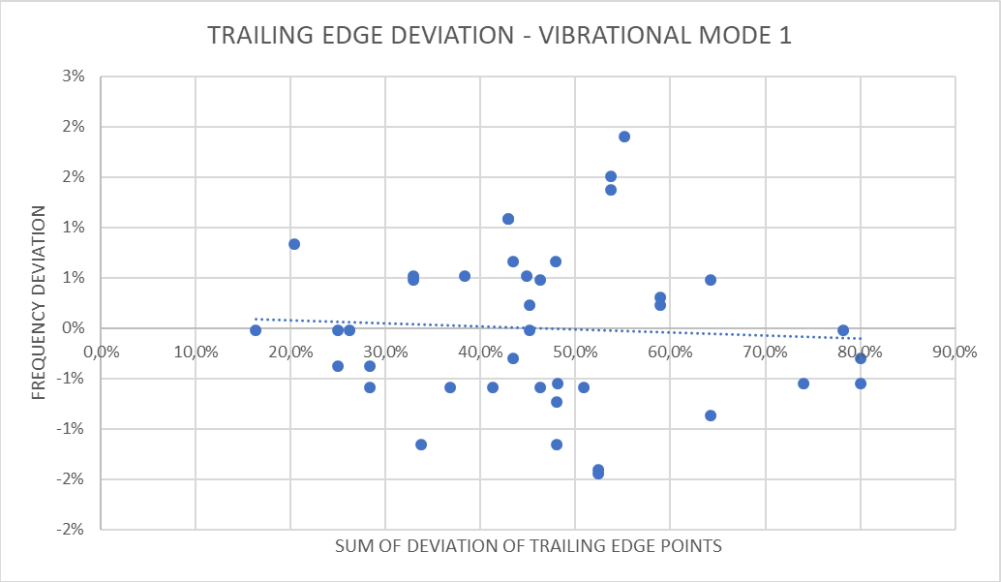

Figure 3.75: Sum of Trailing Edge Deviation for Mode 1

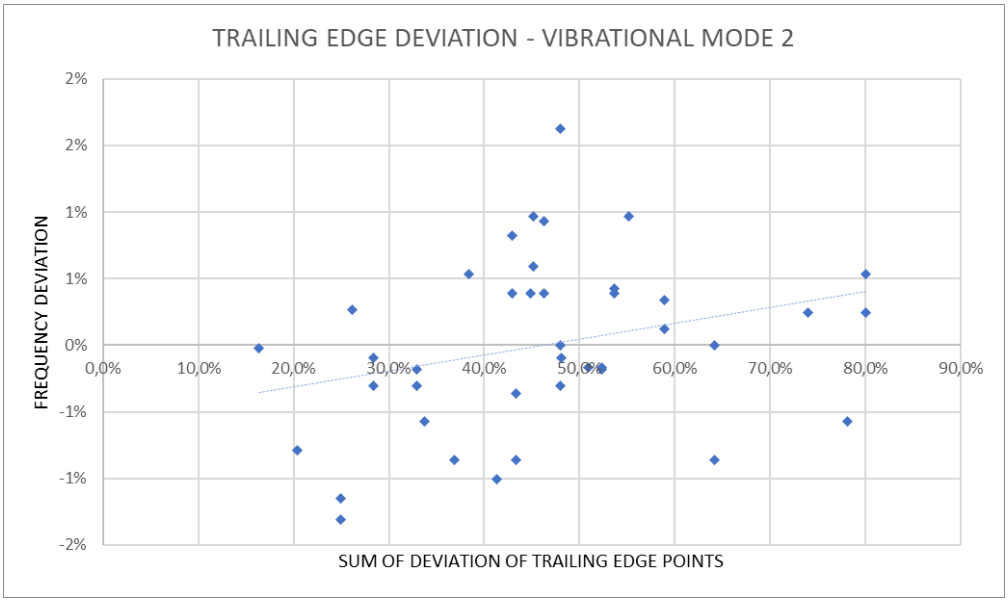

Figure 3.76: Sum of Trailing Edge Deviation for Mode 2

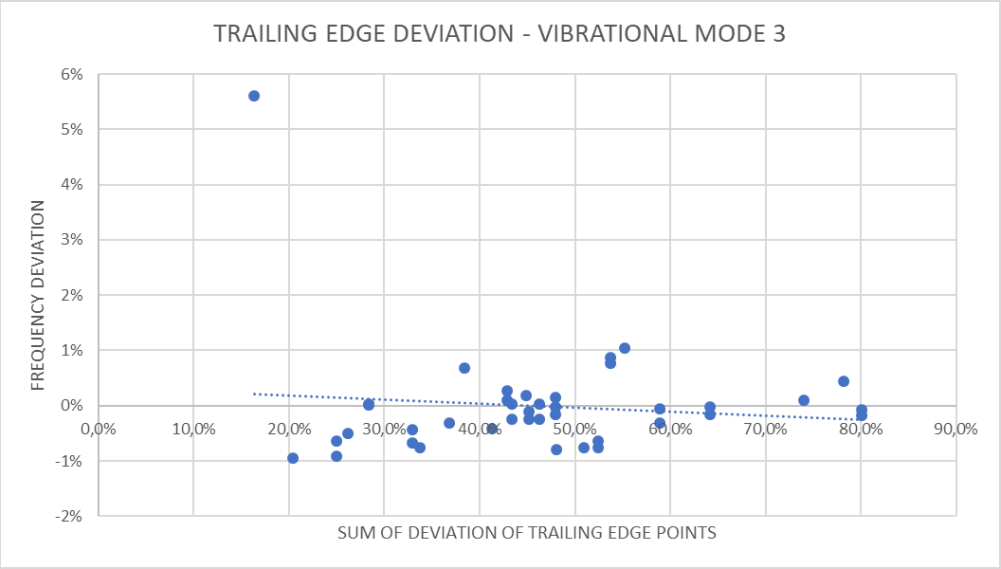

Figure 3.77: Sum of Trailing Edge Deviations for Mode 3

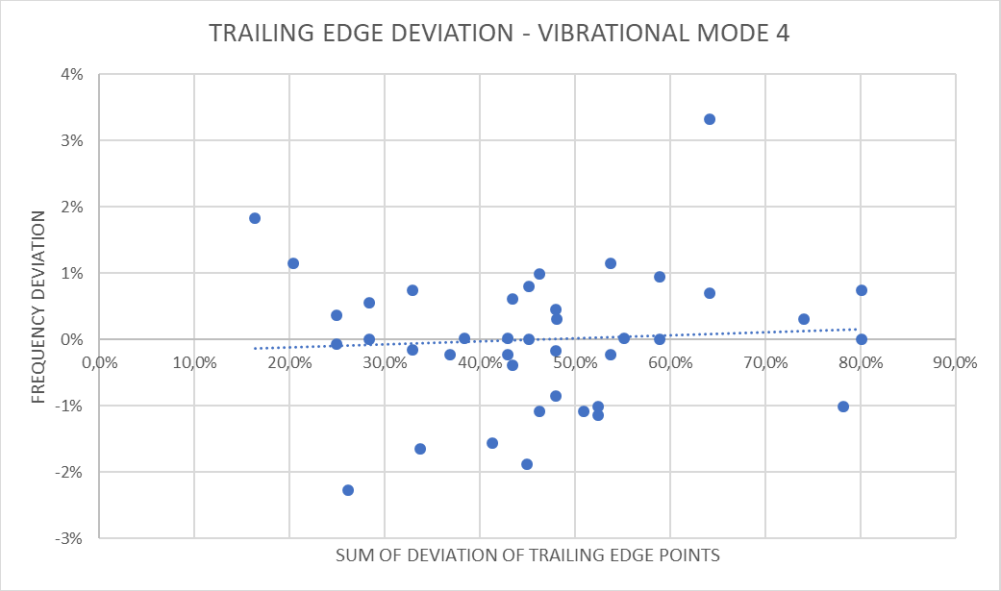

Figure 3.78: Sum of Trailing Edge Deviation for Mode 4

3.2.2 Nickel Based DS Superalloy Measurements

Exactly as Before, first a batch of single point measures and then different grouping of frequencies was analysed.

Single Point Measurements

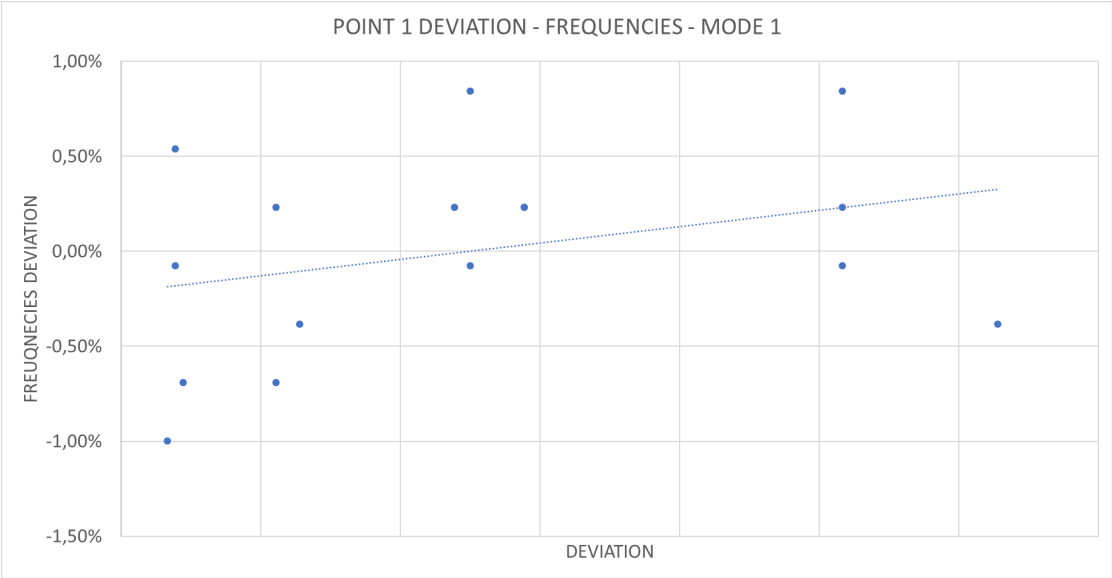

Figure 3.79: Point 1 - Mode 1 Nickel Based DS Superalloy

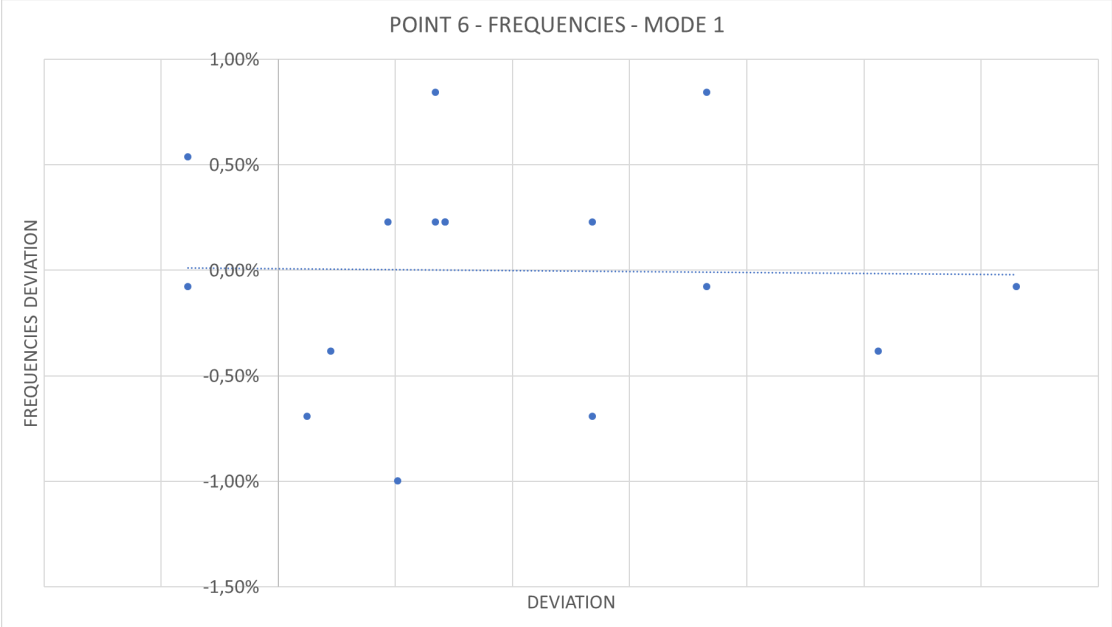

Figure 3.80: Point 6 - Mode 1 Nickel Based DS Superalloy

Important Note: the x-axis cannot refer to specific values, but to be intended as going from smaller up to bigger values of deviation, from negative to positive.

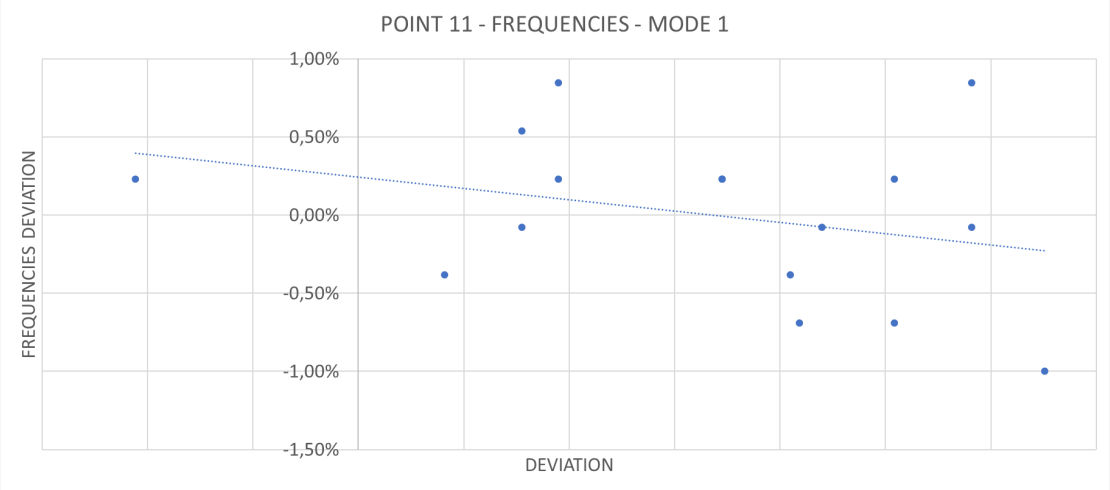

Figure 3.81: Point 11 - Mode 1 Nickel Based DS Superalloy

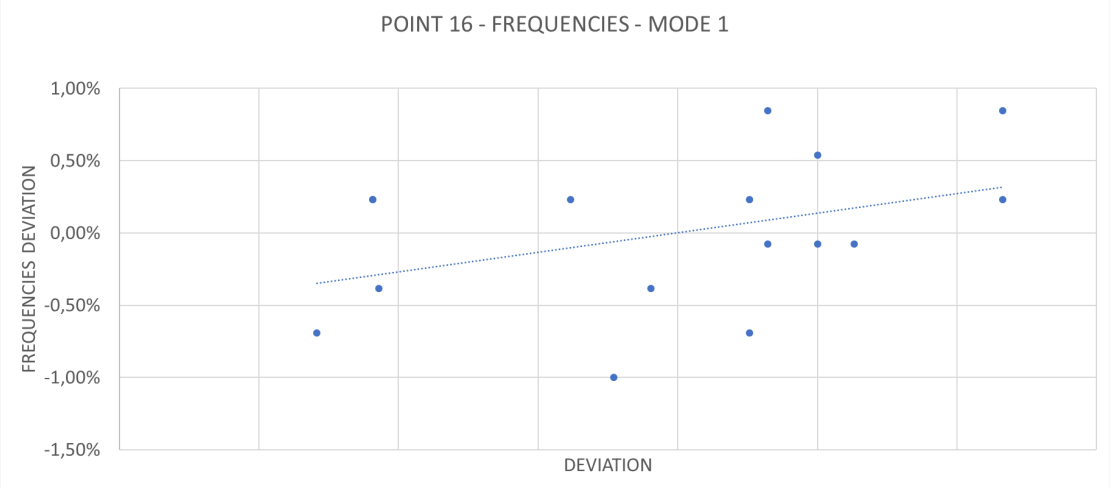

Figure 3.82: Point 16 - Mode 1 Nickel Based DS Superalloy

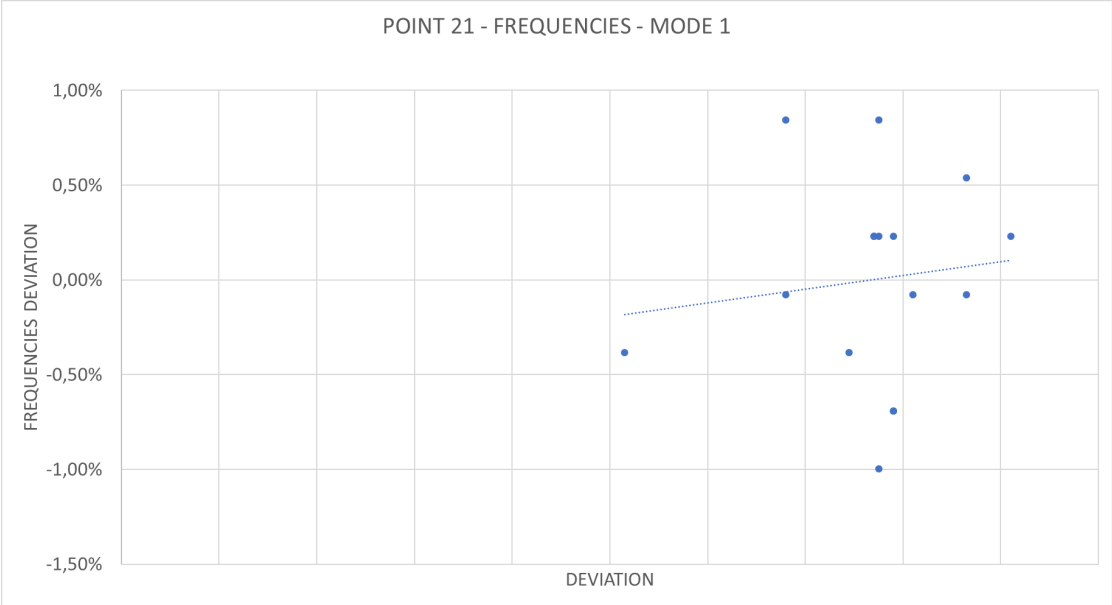

Figure 3.83: Point 21 - Mode 1 Nickel Based DS Superalloy

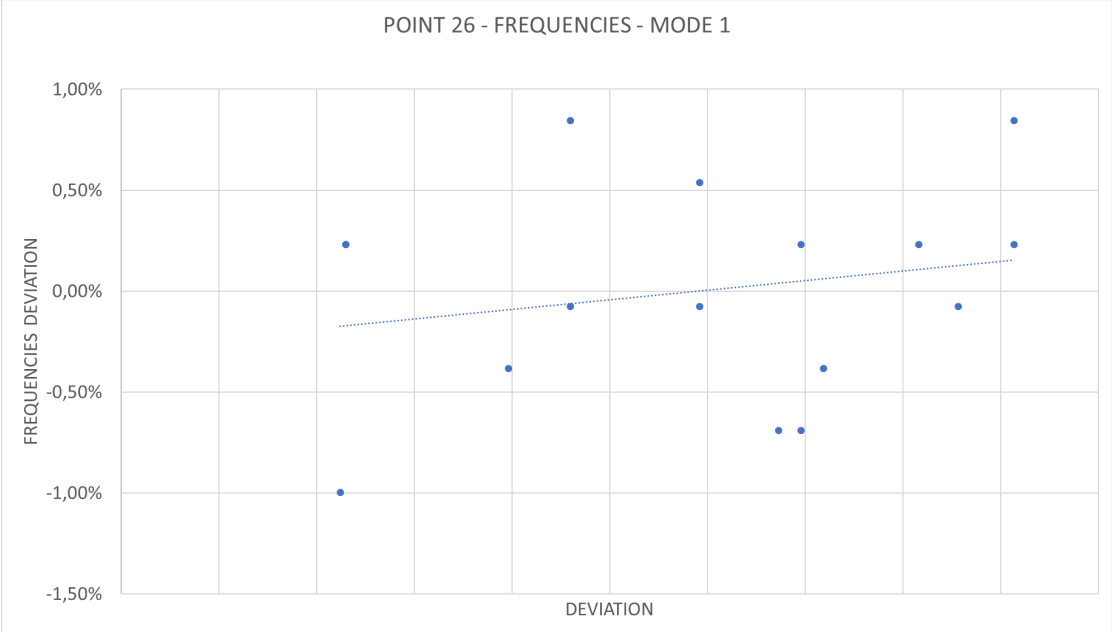

Figure 3.84: Point 26 - Mode 1 Nickel Based DS Superalloy

Multiple Point Grouping

Exactly in the same way as René 80, using the same patterns for grouping, IN792DS was investigated.

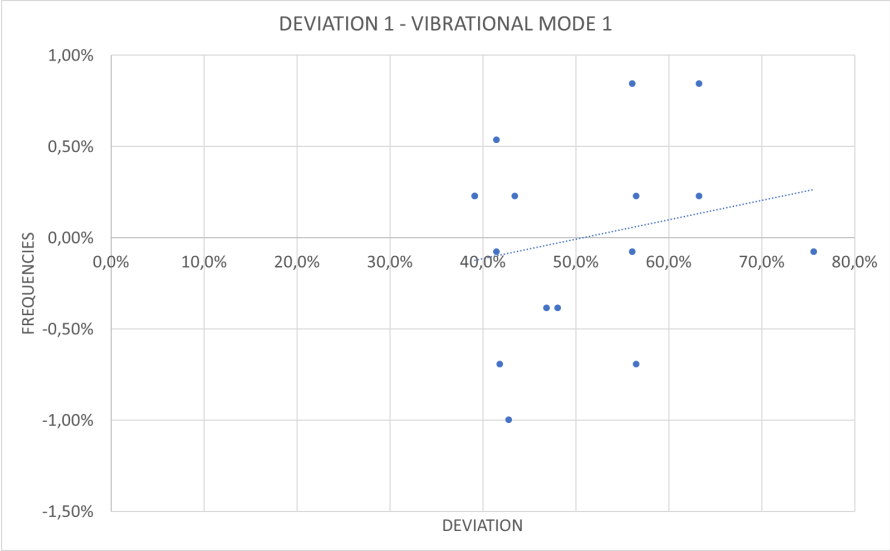

Figure 3.85: Sum of Deviation 1 for Mode 1 - Nickel Based DS Superalloy

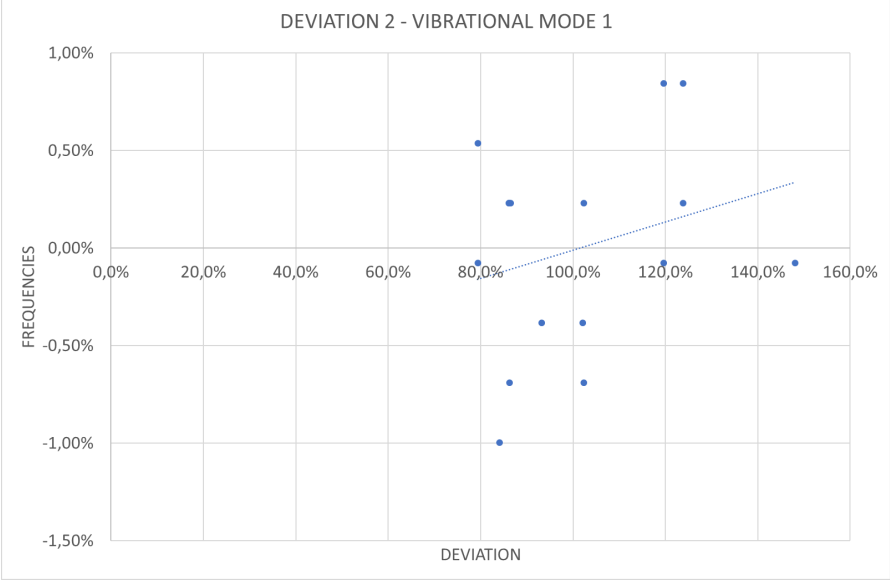

Figure 3.86: Sum of Deviation 2 for Mode 1 - Nickel Based DS Superalloy

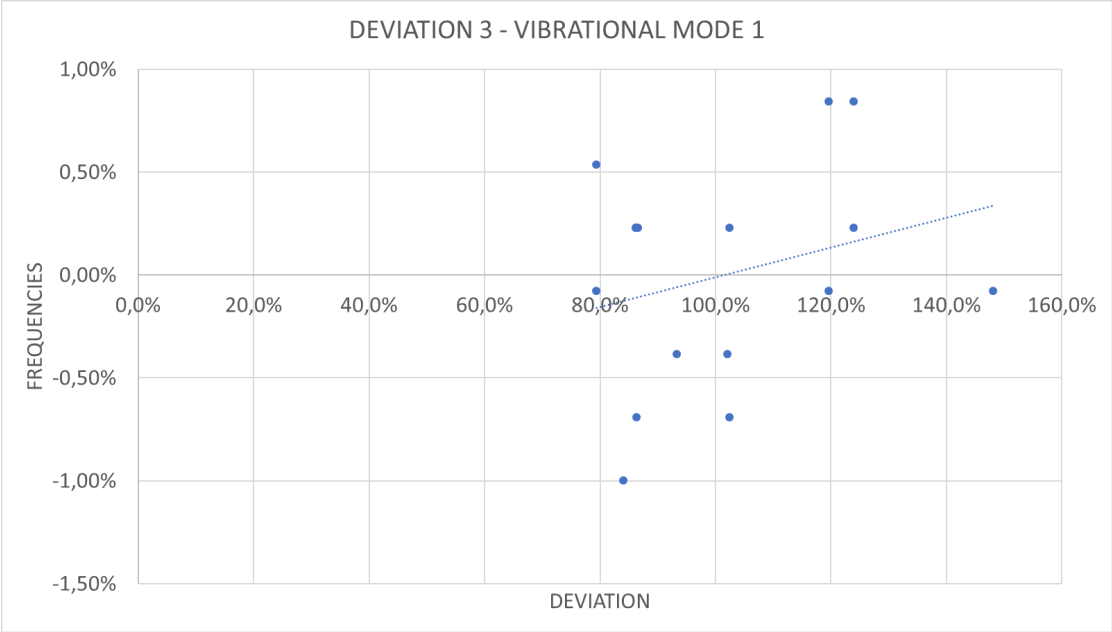

Figure 3.87: Sum of Deviation 3 for Mode 1 - Nickel Based DS Superalloy

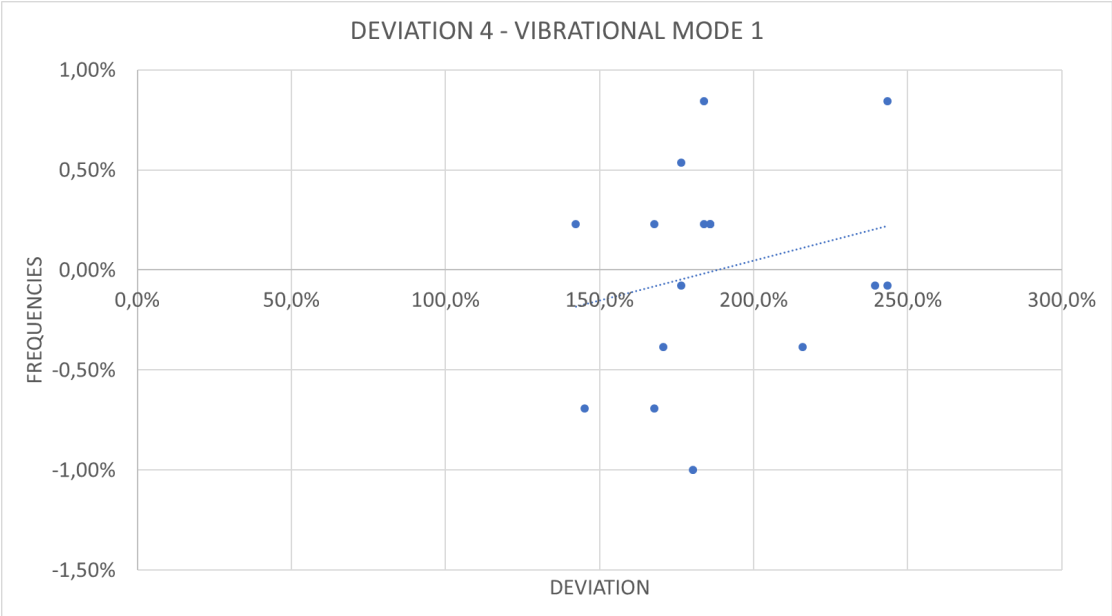

Figure 3.88: Sum of Deviation 4 for Mode 1 - Nickel Based DS Superalloy

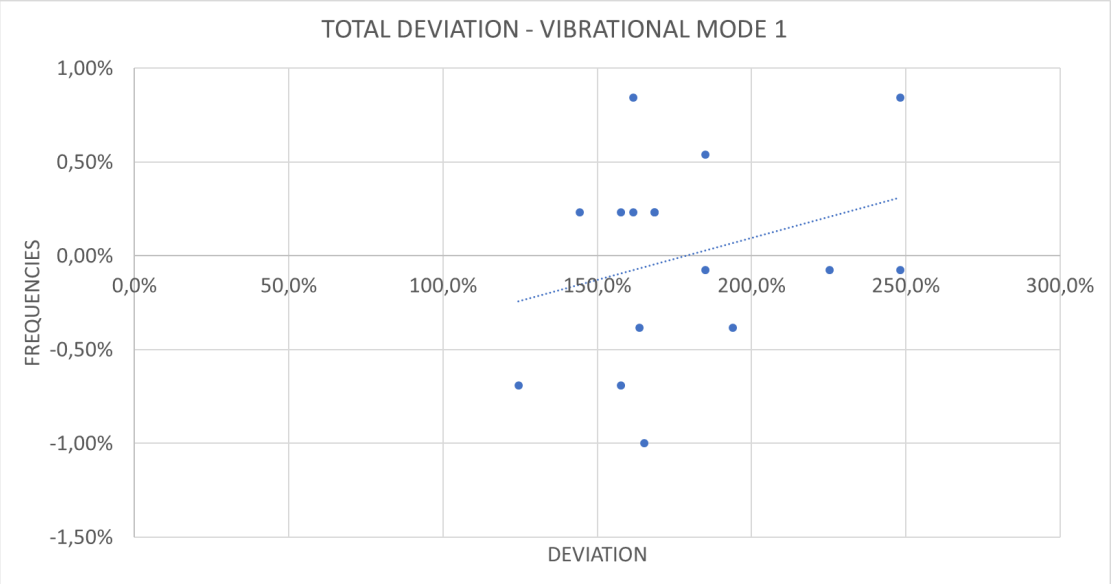

Figure 3.89: Sum of Total Deviation for Mode 1 - Nickel Based DS Superalloy

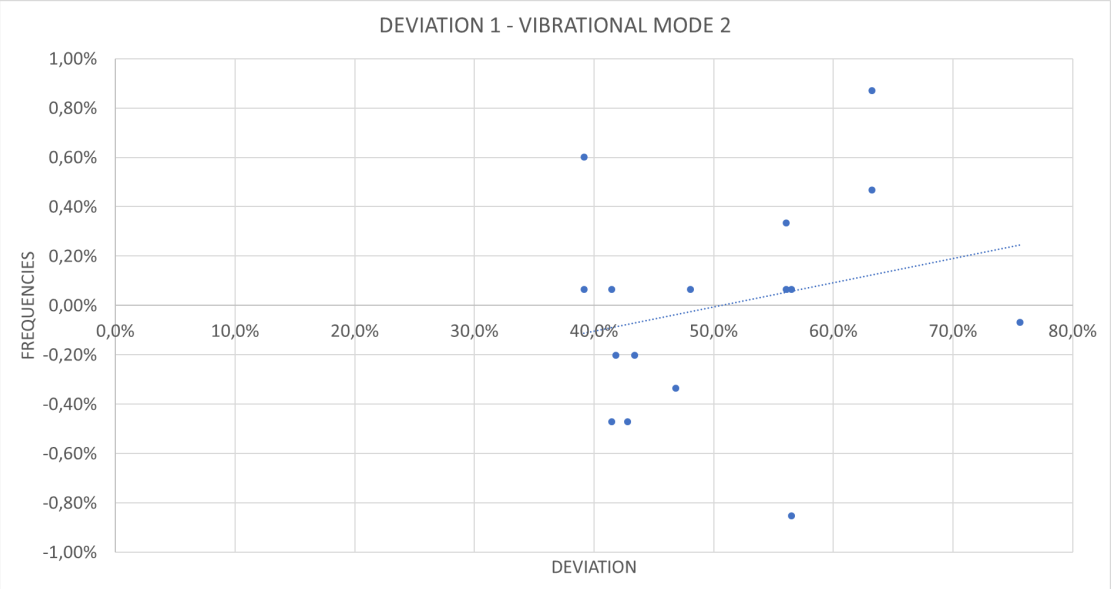

Figure 3.90: Sum of Deviation 1 for Mode 2 - Nickel Based DS Superalloy

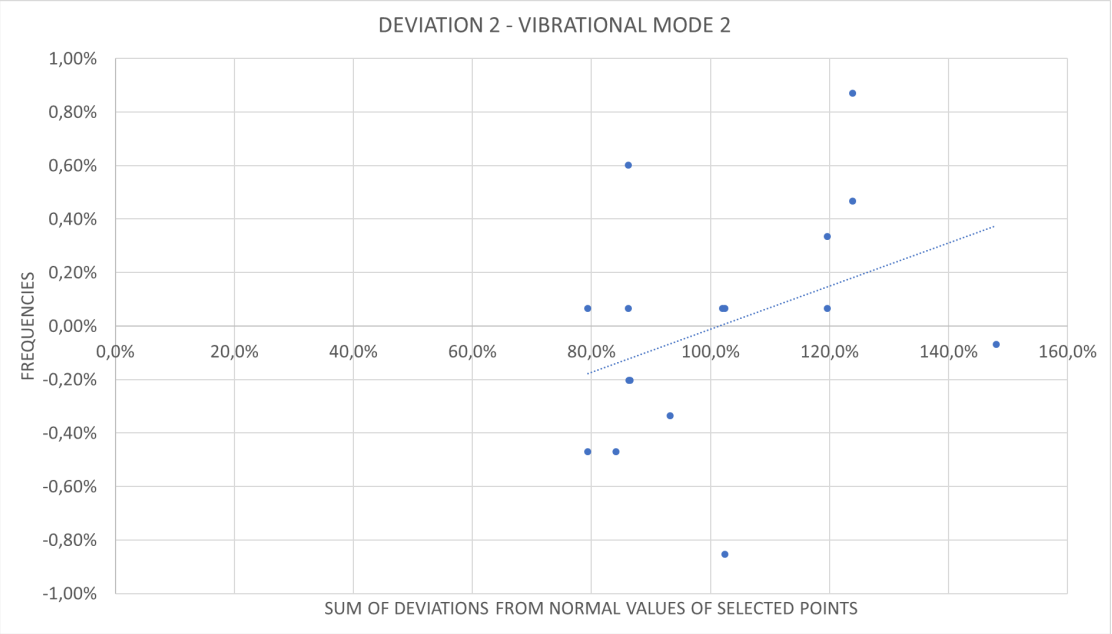

Figure 3.91: Sum of Deviation 2 for Mode 2 - Nickel Based DS Superalloy

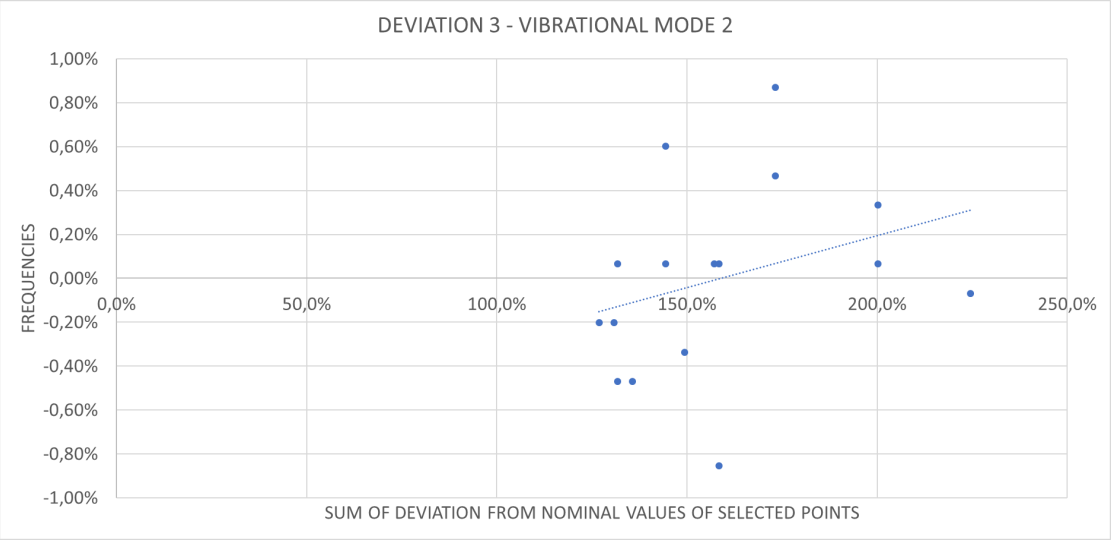

Figure 3.92: Sum of Deviation 3 for Mode 2 - Nickel Based DS Superalloy

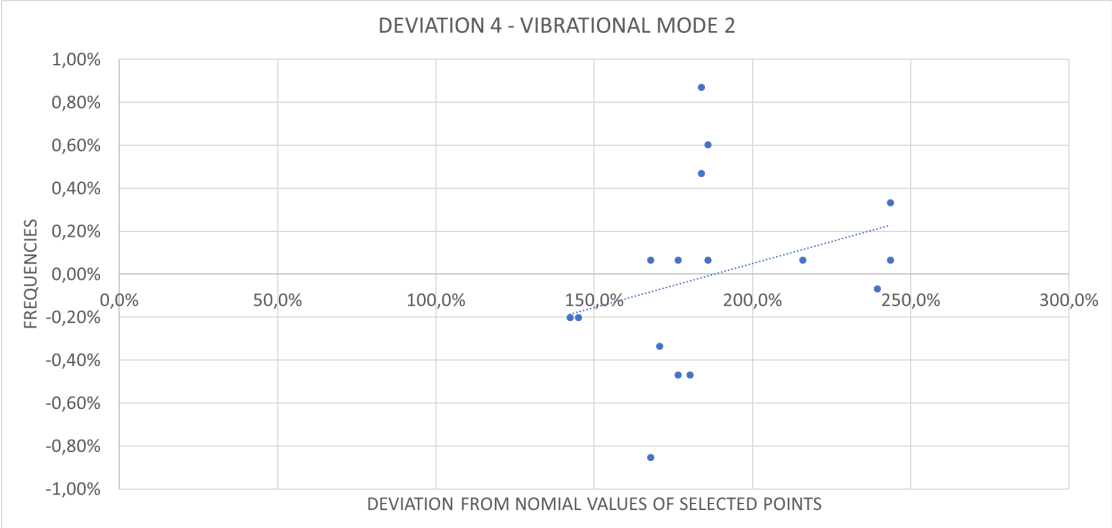

Figure 3.93: Sum of Deviation 4 for Mode 2 - Nickel Based DS Superalloy

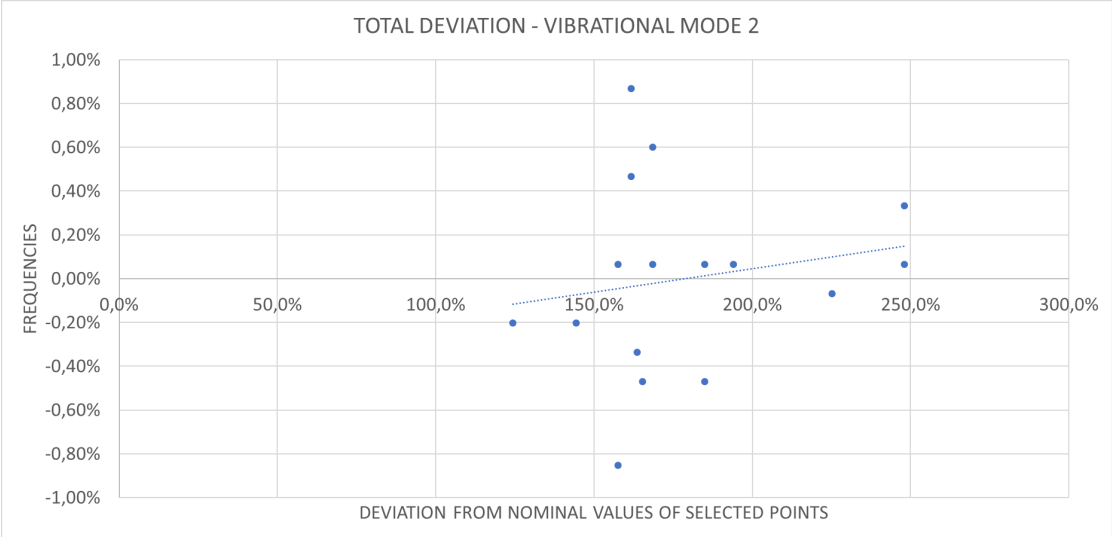

Figure 3.94: Sum of Total Deviation for Mode 2 - Nickel Based DS Superalloy

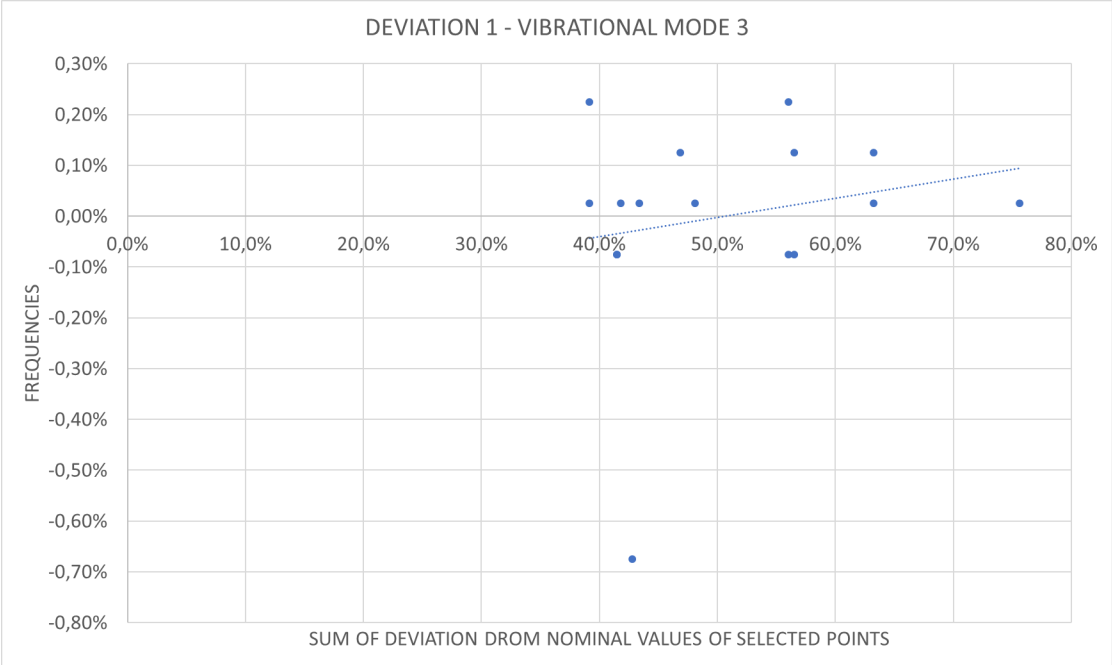

Figure 3.95: Sum of Deviation 1 for Mode 3 - Nickel Based DS Superalloy

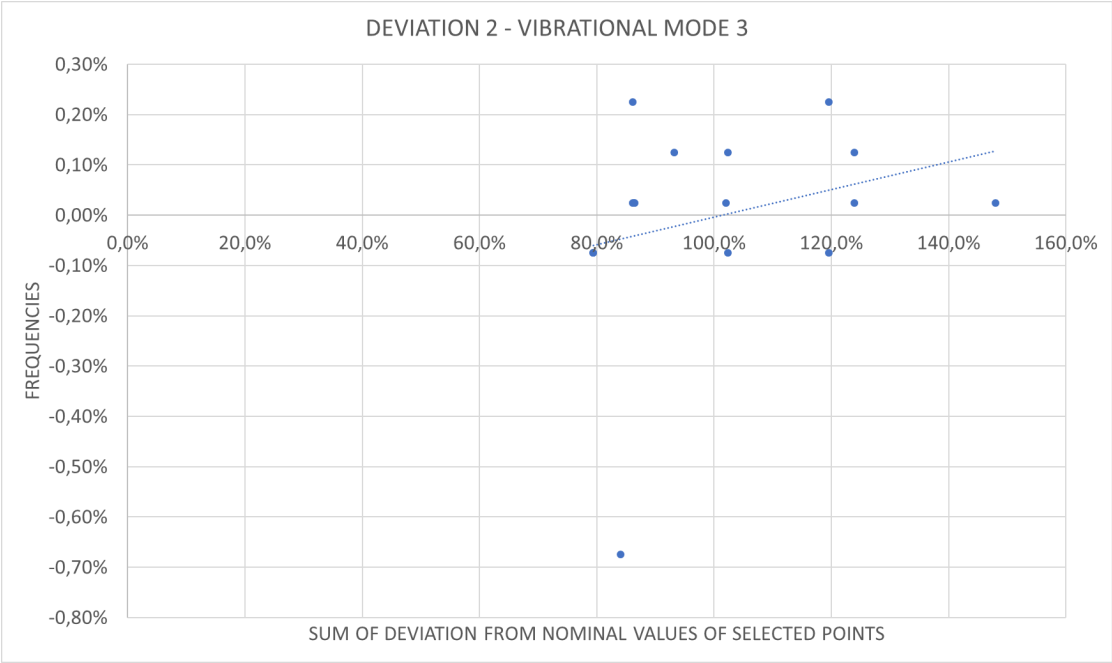

Figure 3.96: Sum of Deviation 2 for Mode 3 - Nickel Based DS Superalloy

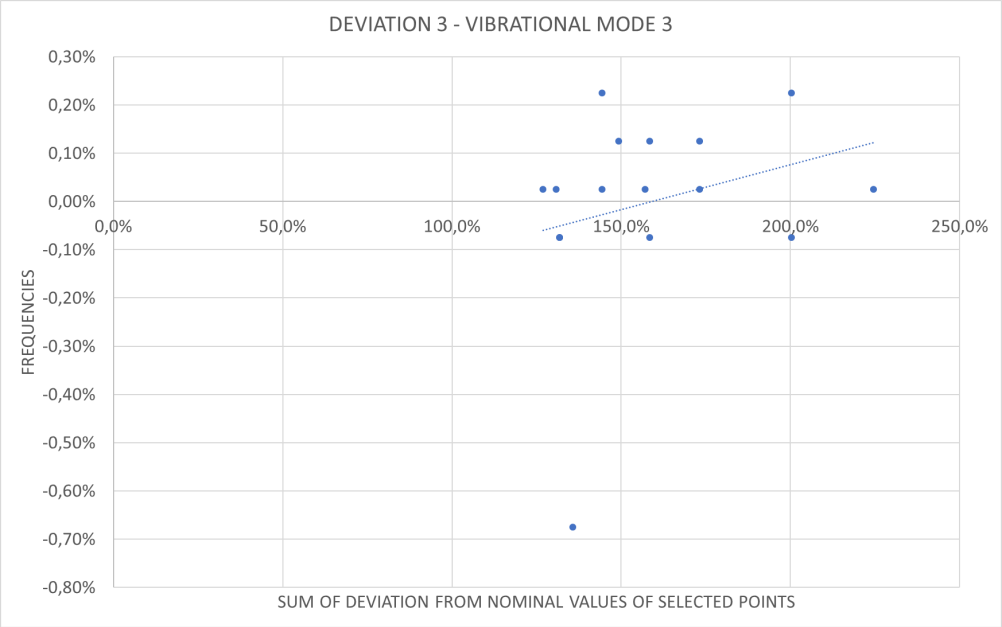

Figure 3.97: Sum of Deviation 3 for Mode 3 - Nickel Based DS Superalloy

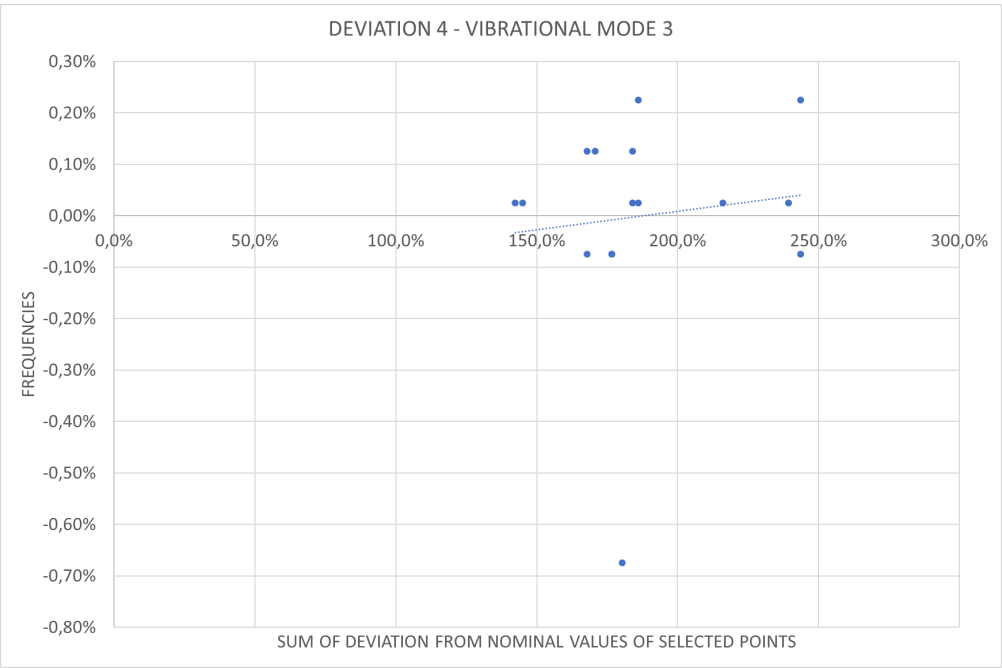

Figure 3.98: Sum of Deviation 4 for Mode 3 - Nickel Based DS Superalloy

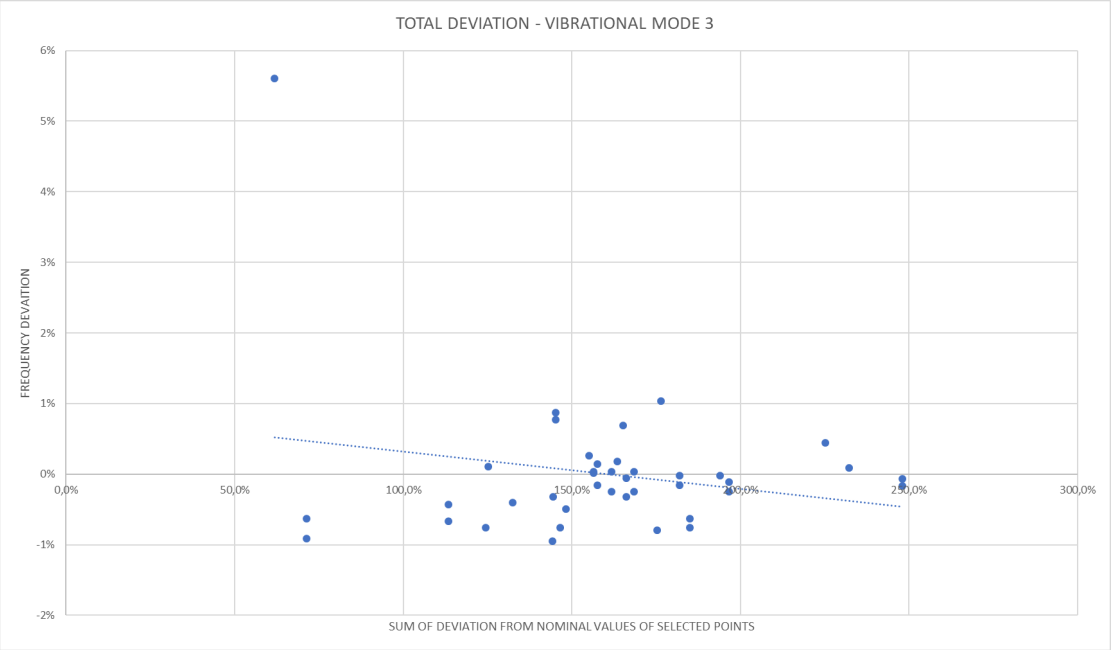

Figure 3.99: Sum of Total Deviation for Mode 3 - Nickel Based DS Superalloy

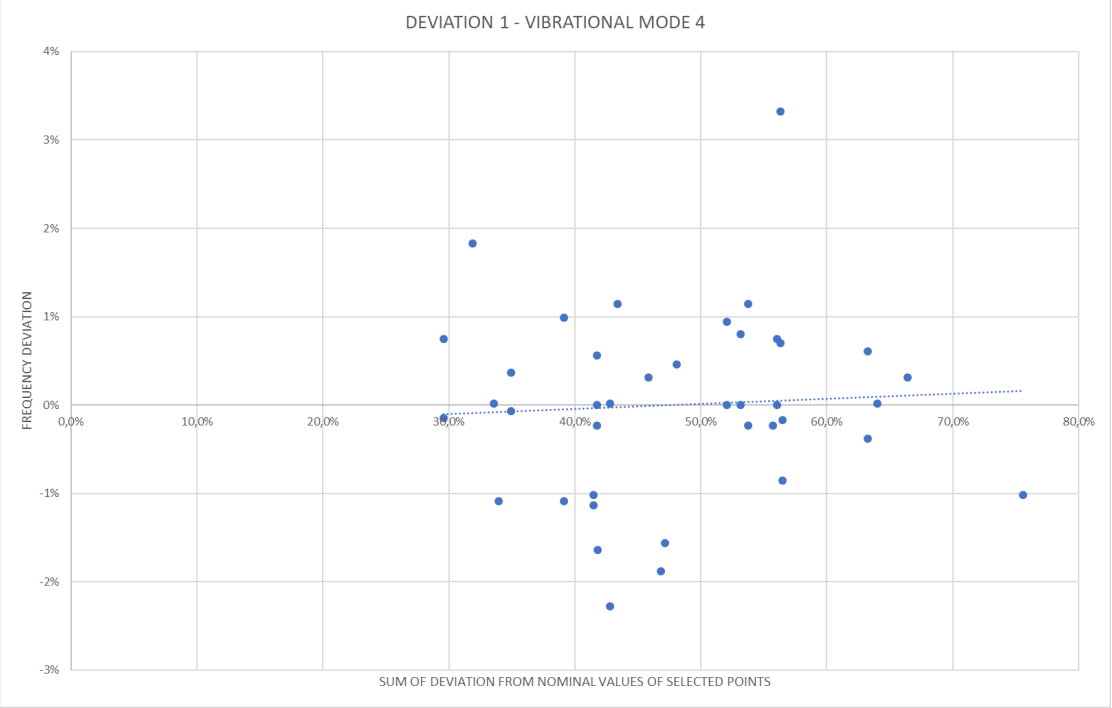

Figure 3.100: Sum of Deviation 1 for Mode 4 - Nickel Based DS Superalloy

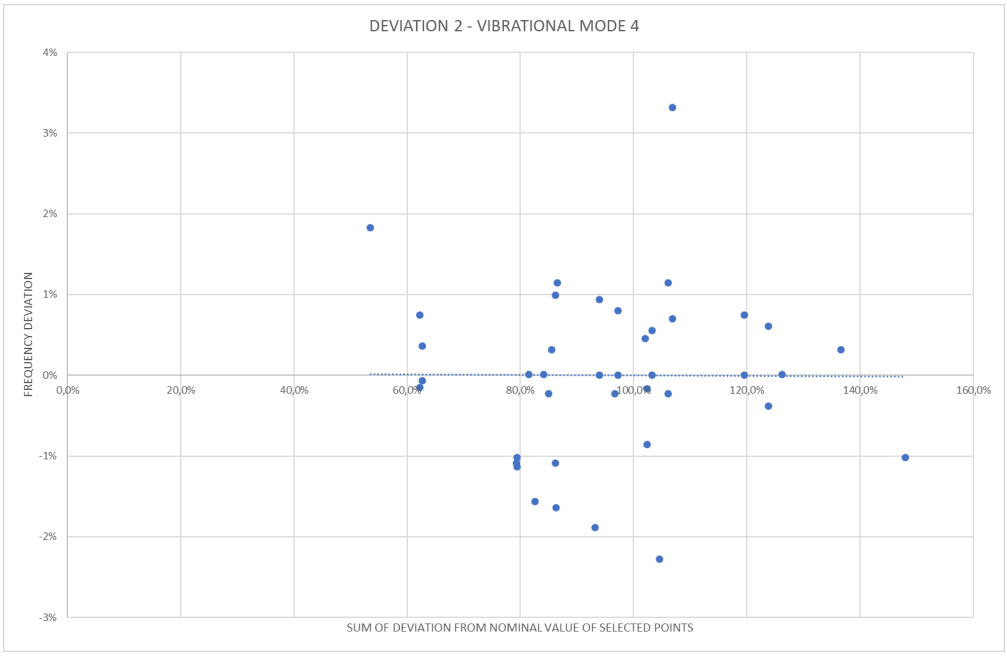

Figure 3.101: Sum of Deviation 2 for Mode 4 - Nickel Based DS Superalloy

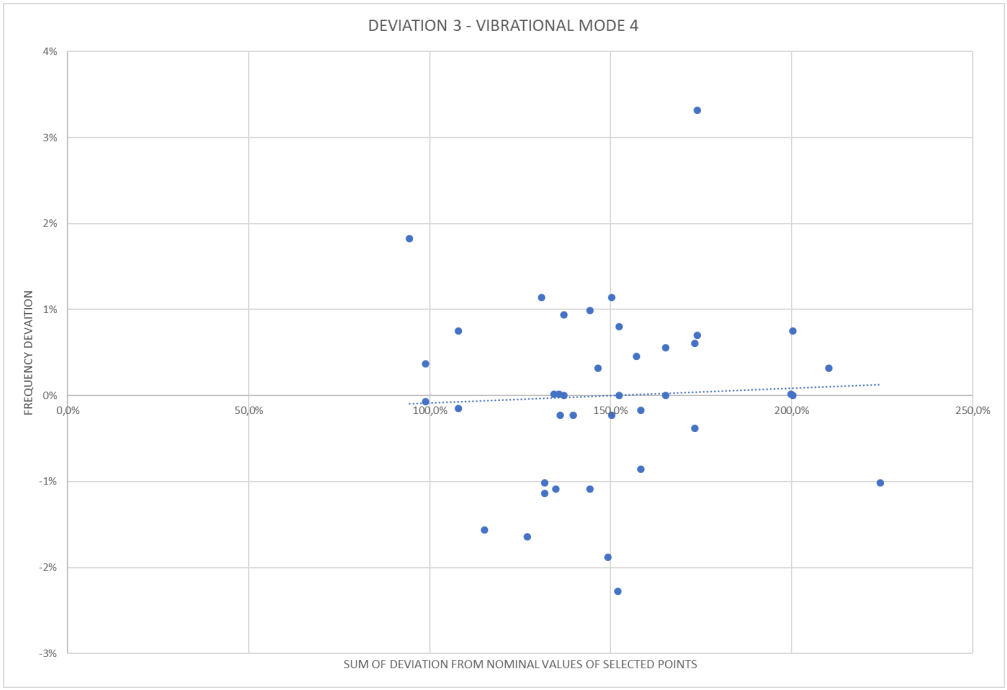

Figure 3.102: Sum of Deviation 3 for Mode 4 - Nickel Based DS Superalloy

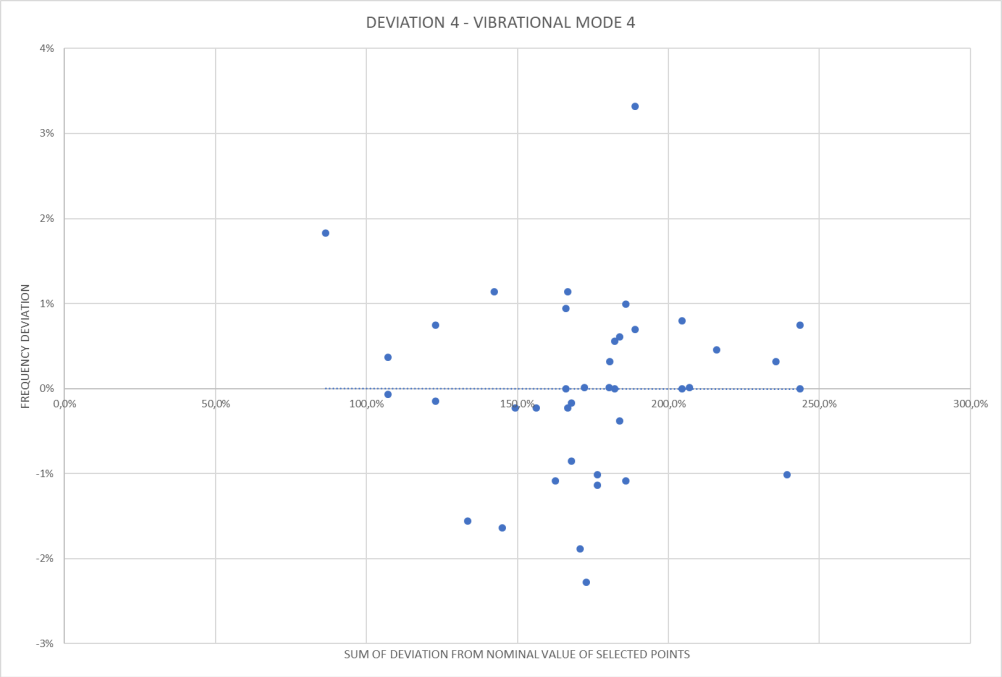

Figure 3.103: Sum of Deviation 4 for Mode 4 - Nickel Based DS Superalloy

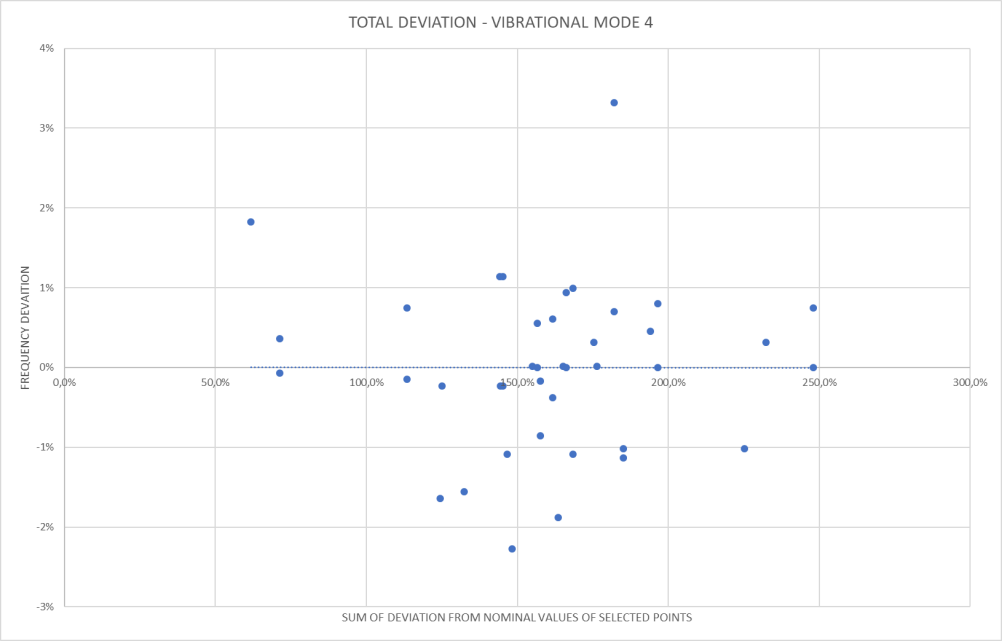

Figure 3.104: Sum of Total Deviation for Mode 4 - Nickel Based DS Superalloy

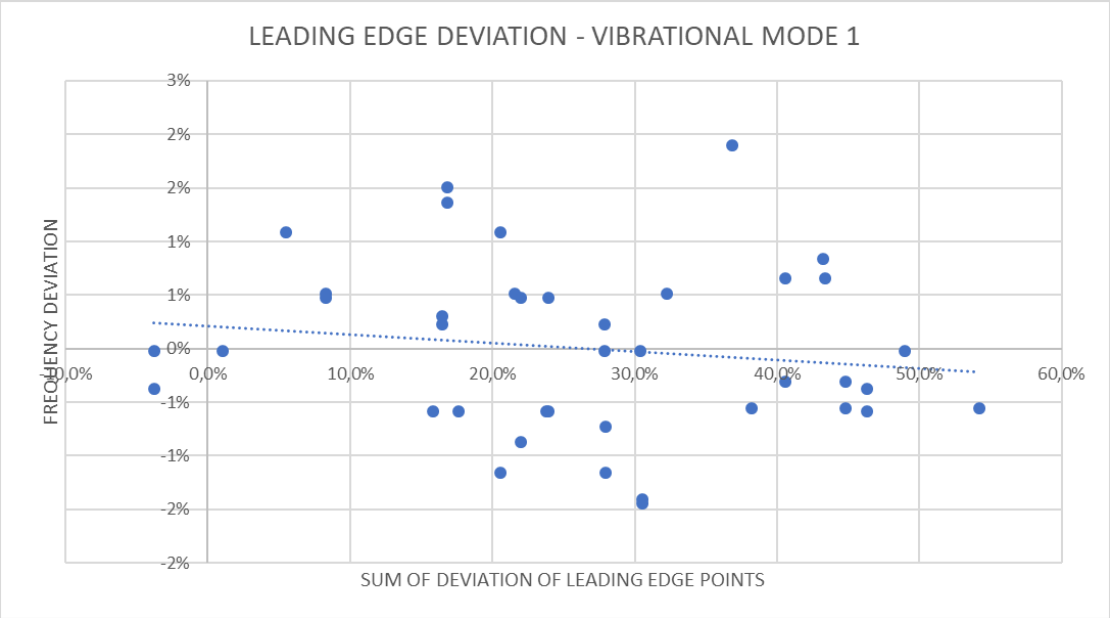

Figure 3.105: Leading Edge Points Deviation for Mode 1 - Nickel Based DS Superalloy

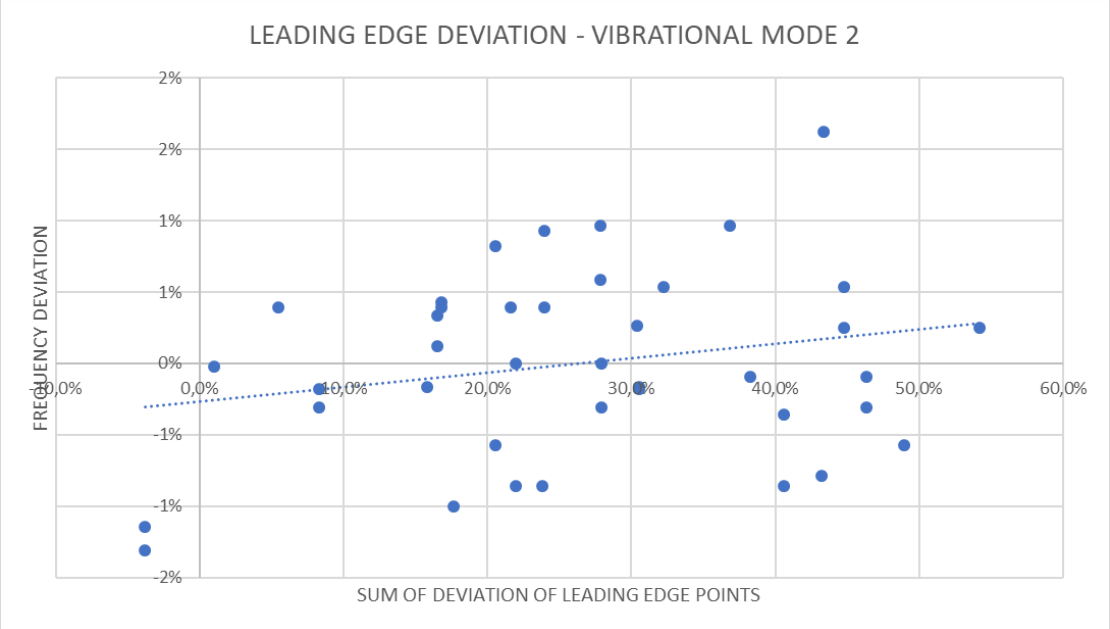

Figure 3.106: Leading Edge Points Deviation for Mode 2 - Nickel Based DS Superalloy

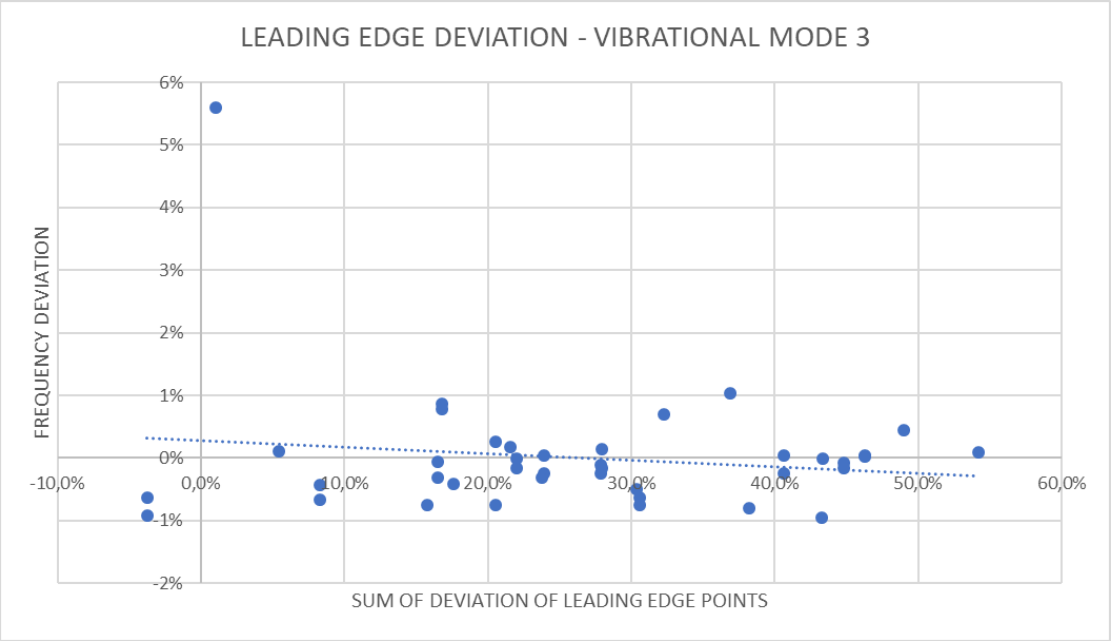

Figure 3.107: Leading Edge Points Deviation for Mode 3 - Nickel Based DS Superalloy

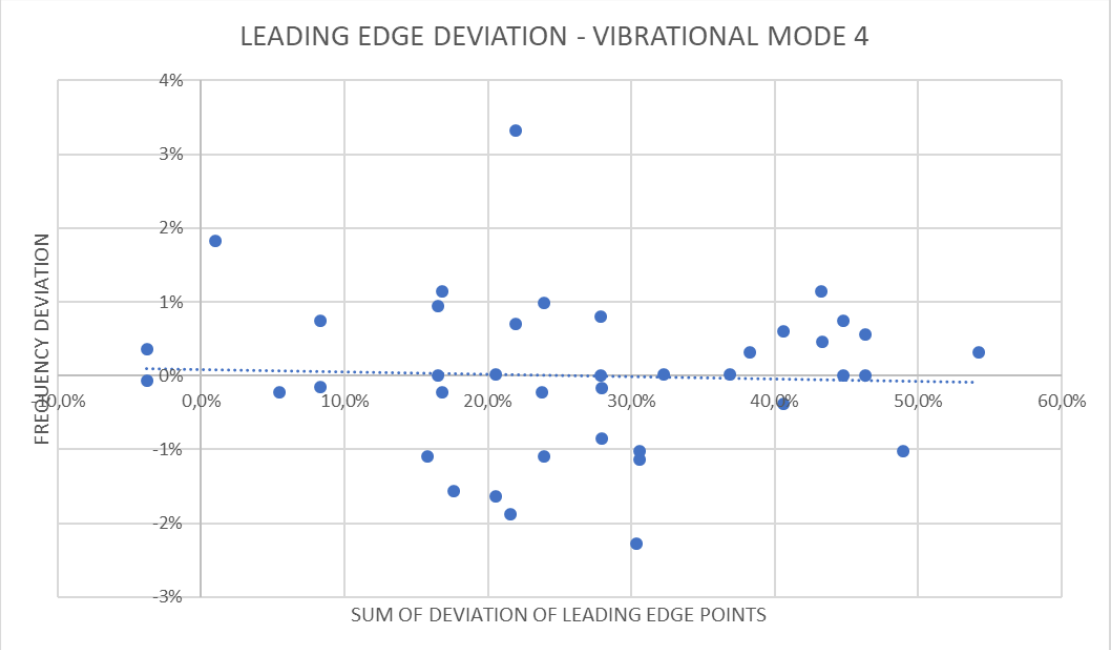

Figure 3.108: Leading Edge Points Deviation for Mode 4 - Nickel Based DS Superalloy

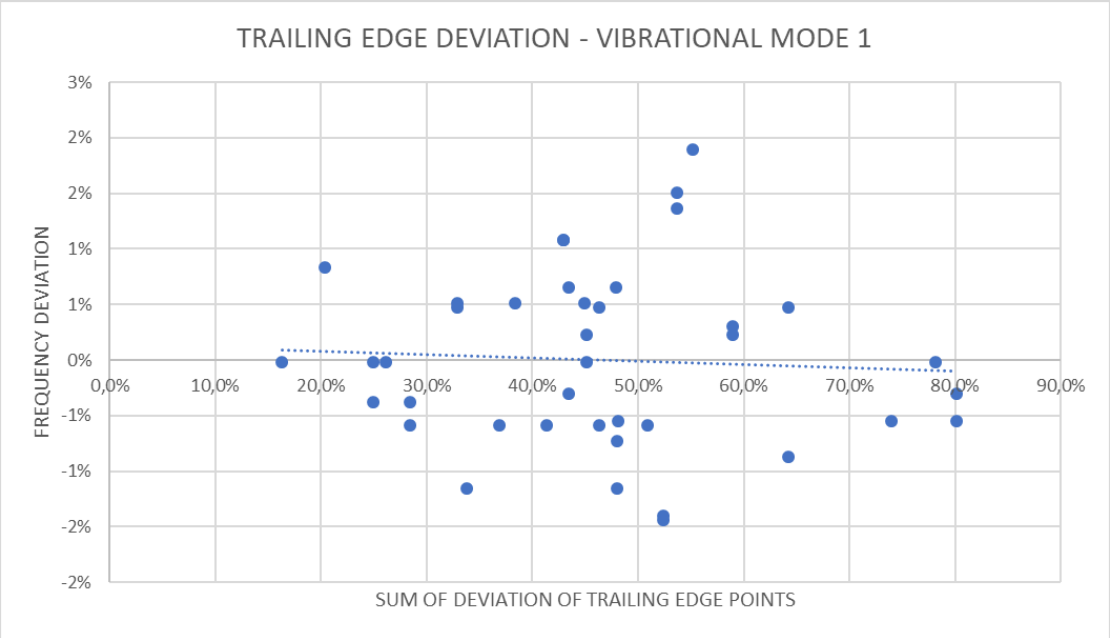

Figure 3.109: Trailing Edge Points Deviation for Mode 1 - Nickel Based DS Superalloy

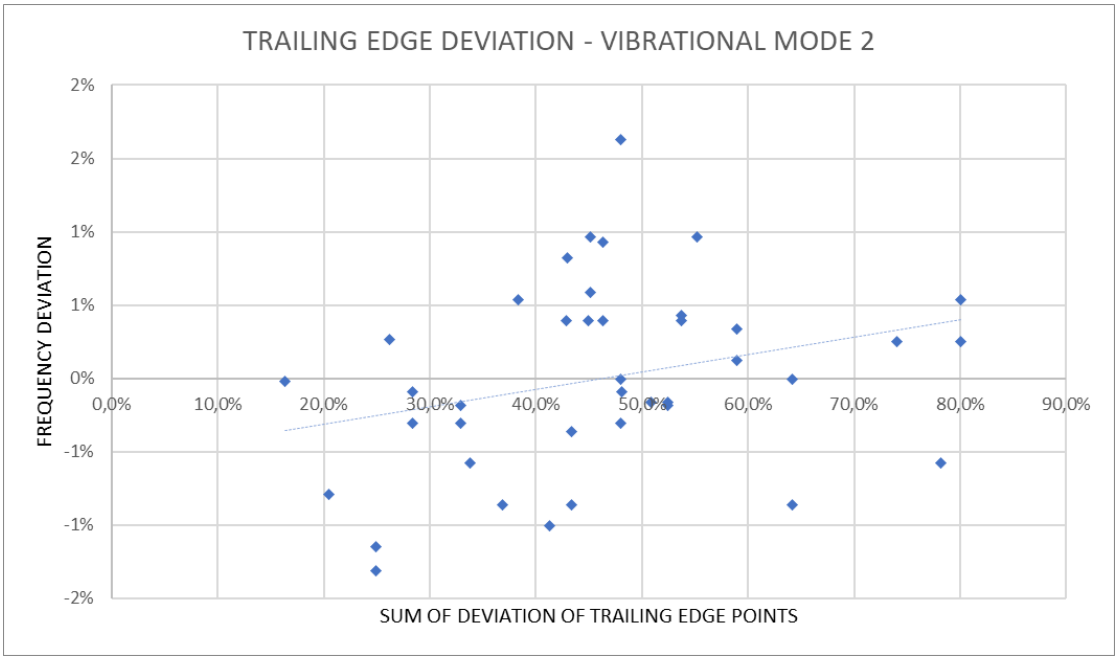

Figure 3.110: Trailing Edge Points Deviation for Mode 2 - Nickel Based DS Superalloy

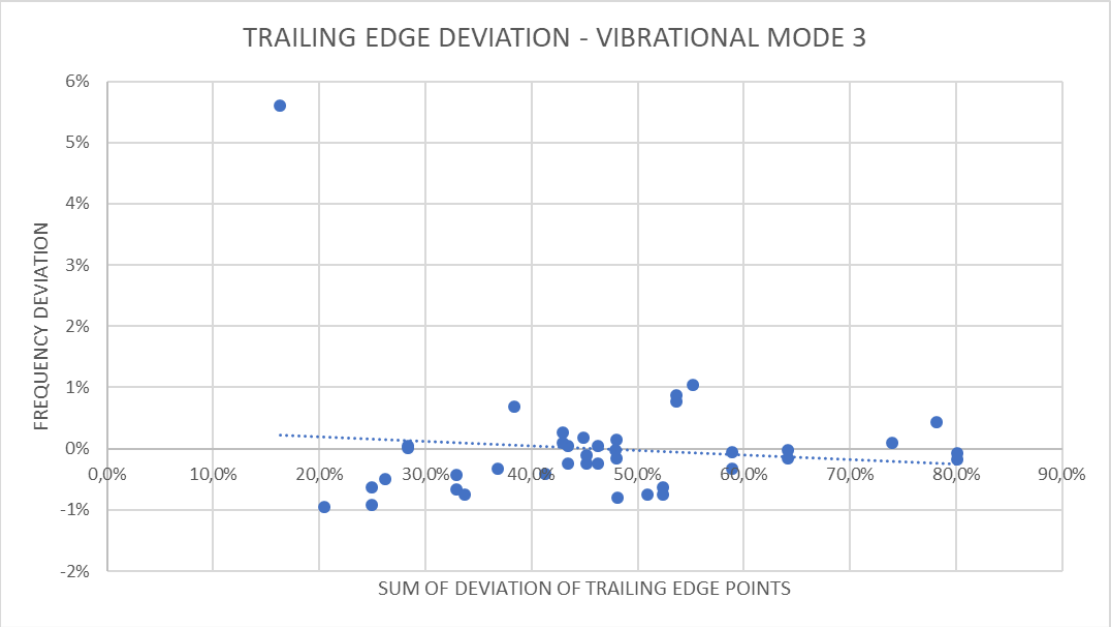

Figure 3.111: Trailing Edge Points Deviation for Mode 3 - Nickel Based DS Superalloy

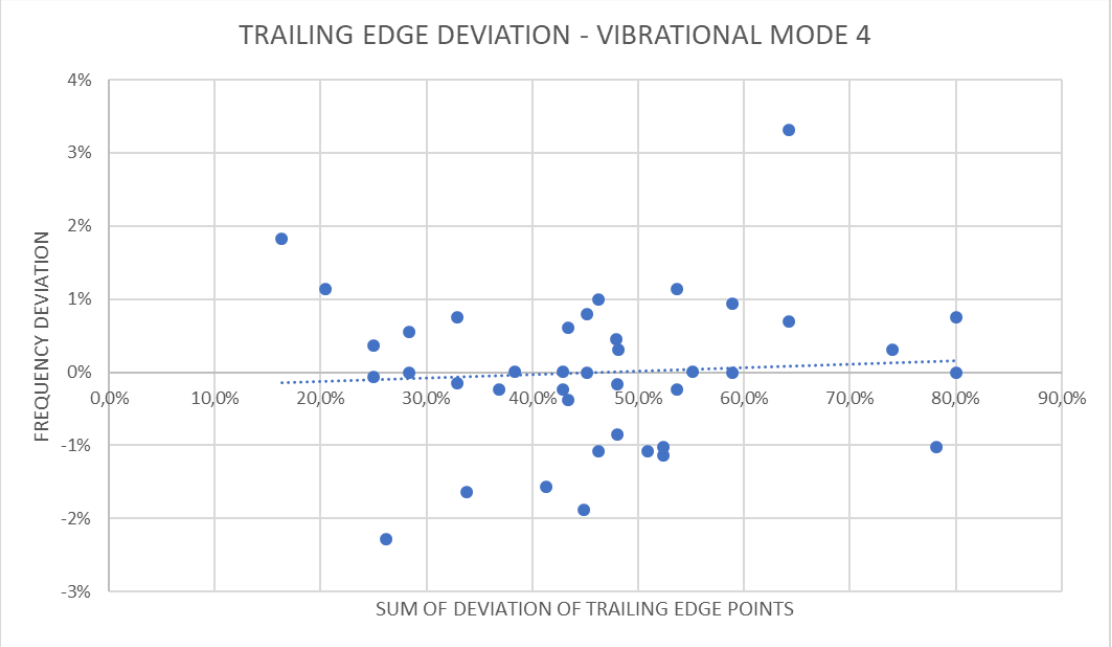

Figure 3.112: Trailing Edge Points Deviation for Mode 4 - Nickel Based DS Superalloy

As clear from graphs for all batches for both materials, in particular from the observation of the trend dotted line, there is not a clear pattern that reconducts a variation in dimensions between the nominal and measured values to the possibility of influence on the measured frequency values. This would have allowed to draw conclusions that further fueled investigating this direction, but since there isn't a recognizable influence, hence the path was not followed further. In addition, as some graphs can show a mild inclination of the dotted line, there is to say that the sparseness of the measured values is far greater than the trend line inclination. In fact, observing the y-axis shows how around 0 up to $1 - 2\%$ were the values the most interested by the trend line, showing how little influence was observable, since the variation for the single blade was bigger (but still acceptable).

Chapter 4

Material Analysis

In this Chapter the focus will be the materials itself used for blade construction in Gas Turbine Blades. Both materials were studied and a brief description is provided.

4.1 The superalloys

Both materials used in TB production are so-called **superalloys**. A superalloy is an alloy that has the ability to operate at a high fraction of its melting point, and are used in situations where high-heat resistance is fundamental, such as aircraft engines[4]. In particular, this section will discuss about **Nickel-Based Superalloys**, an non-standard class of metallic materials with an exceptional combination of high temperature, strength and toughness, able to work in corrosive and/or oxidizing environments [4]. Due to their exceptional resistance to heat, they can tolerate temperatures up to 1050°, with occasional excursions that can go up to 1200°, or right around 90% of their melting temperature [4]. In order to have a clear understanding and know deeply the material, a table containing the percentages of elements of some superalloys used for this purpose is given below 4.1.

Table 1 Compositions of commercial Ni-based superalloys (wt. %, bal. Ni)

Alloy	Cr	Co	Mo	W	Ta	Re	Nb	Al	Ti	Hf	C	B	Y	Zr	Other
Conventionally Cast Alloys															
Mar-M246	8.3	10.0	0.7	10.0	3.0	—	—	5.5	1.0	1.50	0.14	0.02	—	0.05	—
Rene' 80	14.0	9.5	4.0	4.0	—	—	—	3.0	5.0	—	0.17	0.02	—	0.03	—
IN-713LC	12.0	—	4.5	—	—	—	2.0	5.9	0.6	—	0.05	0.01	—	0.10	—
C1023	15.5	10.0	8.5	—	—	—	—	4.2	3.6	—	0.16	0.01	—	—	—
Directionally Solidified Alloys															
IN792	12.6	9.0	1.9	4.3	4.3	—	—	3.4	4.0	1.00	0.09	0.02	—	0.06	—
GTD111	14.0	9.5	1.5	3.8	2.8	—	—	3.0	4.9	—	0.10	0.01	—	—	—

Figure 4.1: Superalloys composition Table, where the composition percentage is given upon Nickel Content

4.2 Isotrpic and Anisotropic Materials

Due to the fact that the two superalloys considered during this thesis, **René 80 and the Nickel Based DS Superalloy** present different properties and structures, a brief explanation about isotropic and anisotropic materials is needed in this section to explain the following chapter's ideas. A material, considered **elastic** if the deformation energy is a state function (work doesn't depend on the process of load, but only on the initial and final state) is also considered **linear** if the stresses are proportional do deformations. Constitutive Equations of a elastic and linear material are expressed with a simple matrix law, the Generalized Hooke Law [5]:

$$\{\sigma\} = [C]\{\epsilon\} \leftrightarrow \{\epsilon\} = [D]\{\sigma\} \tag{4.1}$$

where **[C]** is the stiffness coefficient matrix for elastic behaviour or stress-strain matrix, $\{\sigma\}$ is the stress vector, $\{\epsilon\}$ is the total strain vector and $[D] = [C]^{-1}$ is the compliance matrix. Matrixes [C] and [D], both symmetric [5], change their structure based upon material properties and Reference System.

4.2.1 Anisotropic Materials

In the case of **Anisotropic Materials** (in the industrial sector, anisotropic is intended as **non-isotropic**), the properties of the material, such as **Young's Module** and **G Module**, vary accordingly to the direction considered. When considering DS materials (Fig: 4.2), the structure has the presence of various grains, that can be seen to grow in a preferred direction. The grains inside the component *grow* during the casting process in specified directions, as can be seen from image 4.4. Since the DS material has a number of grains (that differently from a **conventional casting** do not average out making the material isotropic, without a preferred growth direction) the direction of grain growth plays a fundamental role when it comes to frequency assessment, because understanding grain orientation changes property material significantly (this aspect will be evaluated in detail in Chapter 7).

Since the anisotropic material's properties are direction-dependant, the Compliance Matrix can be represented in this form, when correctly oriented:

$$[C] = \begin{bmatrix} 1/E_x & -\nu_{xy}/E_x & -\nu_{xz}/E_x & 0 & 0 & 0 \\ -\nu_{yx}/E_y & 1/E_y & -\nu_{yz}/E_y & 0 & 0 & 0 \\ -\nu_{zx}/E_z & -\nu_{zy}/E_z & 1/E_z & 0 & 0 & 0 \\ 0 & 0 & 0 & 1/G_{xy} & 0 & 0 \\ 0 & 0 & 0 & 0 & 1/G_{yz} & 0 \\ 0 & 0 & 0 & 0 & 0 & 1/G_{xz} \end{bmatrix}$$

Where the typical terms are [6]:

- E_x is the Young's Module in the x direction
- ν_{xy} is the major's Poisson's ratio
- ν_{yx} is the minor's Poisson's ratio
- G_{xy} is the shear modulus in the xy plane

As the matrix is symmetric, the values can be arranged as:

$$\frac{-\nu_{xy}}{E_x} = \frac{-\nu_{yx}}{E_y}, \frac{-\nu_{zx}}{E_z} = \frac{-\nu_{xz}}{E_x}, \frac{-\nu_{yz}}{E_y} = \frac{-\nu_{zy}}{E_z} \tag{4.2}$$

And the relation between E, G and ν (with the respective pedices) has to be computed using the Compliance's Matrix. The independent values are **five**: E_x, E_z, ν_{xy}, ν_{yz}, G_{yz}.

DS Materials

Directionally-Solidified Materials, such as the one that was used in this Thesis's Work, are a particular case of Anisotropic Materials, that experience different properties in different direction, so that the Compliance Matrix, when non oriented in a particular way, assumes the following form;

$$\mathbf{C} = \begin{bmatrix} C_{11} & C_{12} & C_{13} & C_{14} & C_{15} & C_{16} \\ & C_{22} & C_{23} & C_{24} & C_{25} & C_{26} \\ & & C_{33} & C_{34} & C_{35} & C_{36} \\ \text{S} & & & C_{44} & C_{45} & C_{46} \\ & \text{Y} & & & C_{55} & C_{56} \\ & & \text{M} & & & C_{66} \end{bmatrix}$$

When, on the other hand, the coordinate system is aligned with the grain growth direction (or reference direction), the compliance matrix therefore becomes [7]

$$[C] = \begin{bmatrix} 1/E_1 & -\nu_{12}/E_1 & -\nu_{23}/E_1 & 0 & 0 & 0 \\ & 1/E_1 & -\nu_{23}/E_1 & 0 & 0 & 0 \\ & & 1/E_3 & 0 & 0 & 0 \\ S & & & 1/G_{23} & 0 & 0 \\ & Y & & & 1/G_{23} & 0 \\ & & M & & & 2(1+\nu_{12})/E_1 \end{bmatrix}$$

Where for easier presentation, there was the index transformation as follows;

$$(x, y, z) \Rightarrow (1,2,3) \tag{4.3}$$

Due to the **smaller** number and **bigger** dimension of grains when compared to Conventional Casting Materials, DS materials have, as said before a preferential direction (or orientation) 4.2.

4.2.2 Isotropic Material

When considering **isotropic materials**, during the conventional casting process the grains inside materials grow in every direction without a preferential one, thus at the end of the process the entire component will have thousands of grains in thousand of directions, therefore averaging out and presenting symmetry in the behaviour, without a preferential direction (since every grain grows in a different direction, the complete component will not have a prevailing direction). Isotropic Materials have the same mechanical properties in every direction, hence [C] and [D] are identical (for structure and values) in every reference system. This simplifies and streamlines **significantly** the presentation of the material. The matrixes then can be represented in this form:

$$[C] = \begin{bmatrix} C_{11} & C_{12} & C_{13} & 0 & 0 & 0 \\ & C_{22} & C_{23} & 0 & 0 & 0 \\ & & C_{33} & 0 & 0 & 0 \\ & \mathrm{S} & & \frac{C_{11}-C_{12}}{2} & 0 & 0 \\ & \mathrm{Y} & & & \frac{C_{11}-C_{12}}{2} & 0 \\ & & \mathrm{M} & & & \frac{C_{11}-C_{12}}{2} \end{bmatrix}$$

from which is evident how the independent coefficient number is **two**. Since, as said before the [C] and [D] matrixes are identical, considering one or another would not chance. Another fundamental equation that has to be written is the dependance of **G** from **E** and **Poisson's Coefficent,** ν:

$$G = \frac{E}{2(1+\nu)} \tag{4.4}$$

This formula, in this form, is only applicable to Isotropic Materials.

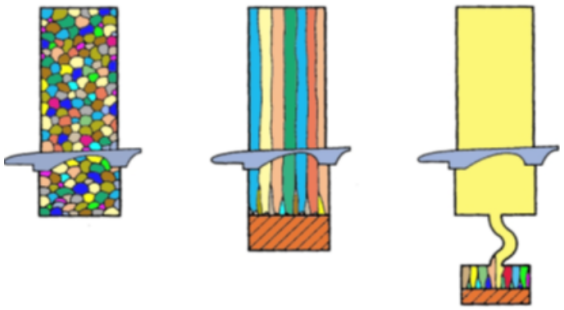

Figure 4.2: Different types of alloys, conventional graining, directionally solidified (DS) and single crystal (SX) [8]

4.3 René 80

The first material of the two that was the focus of this thesis is a superalloy called René 80. René 80 is a nickel superalloy mainly used in the aerospace field to produce blades for low-pressure aeronautical turbines [9]. The alloy was initially developed in the 1980s by General Electric as a castable alloy with high resistance to rupture, thermal fatigue, and hot corrosion resistance [9]. It is a isotropic alloy whose main components can be observed in Table 4.1. The alloy offers an excellent combination of creep resistance, oxidation resistance, and thermal stability, crucial for turbine hot-section components [4], and due to its capability of working with high temperatures and high stress environments [4] it was chosen as the main structural material for the construction of for the third stage of the turbine [10] (not only it sees use in GT, but also for Jet Engines). Due to the demanding environment in which the materials ends up working in, the alloy René 80 exhibits high-temperature inelastic behaviour that cannot be accurately captured by separate plasticity and creep laws. As shown in this [10] conference paper, a unified constitutive model - incorporating rate dependence, cyclic softening and static recovery - is required to provide realistic stress-strain predictions for cast René 80 in service. For this thesis' work creep and fatigue were not investigated, but a deeper understanding of the material, its behaviour and working conditions was needed.

4.4 The Anisotropic Nickel Based Superalloy

The new material for blade construction, that for simplicity in this section will be addressed as **DS Superalloy** is a Nickel-Based superalloy, whose main components, other than Nickel, are various and give significant properties to the alloy. The alloy is widely used, similarly to René 80, for environments where high corrosion, heat and stress resistance is needed (hence the use case in Turbine Blades, beginning with the case of turbine blades for aircraft engines [11]). It was developed as a better alternative to older superalloys and even though presents a superior corrosion resistance, it presents some challenges regarding castability, like most DS superalloys[1], as it is prone to suffering from hot-tearing during directional solidification, during the casting process as most DS superalloys, motivating research into its cracking mechanisms and alloy design [11]. In particular, the **DS** as said before stands for **Directional Solidification**, which is a casting method in which columnar grains grow in a preferred crystallographic direction (Fig: 4.4),

[1]Cracking during casting is a well known problem for DS superalloys, well-known and researched by the casting industry[11]

thereby reducing transverse grain boundaries. Directional solidification is type of solidification that occurs from farthest end of the casting and works its way towards the sprue [12]. A representation of the casting process is given below (Fig: 4.3) Especially useful, Directionally solidified (DS) superalloys have become a primary

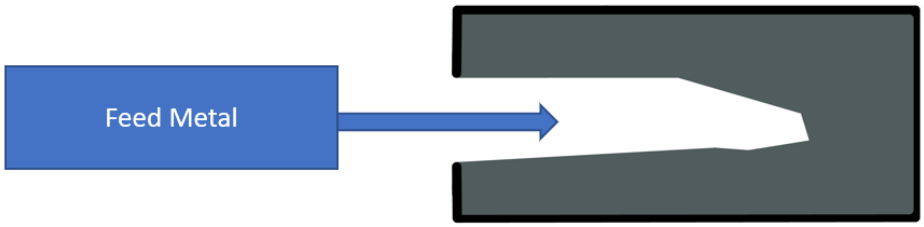

Figure 4.3: Directional Solidification Representation, where feed metal is the molten material

and fundamental material choice for turbine blade applications, in a consistent amount of fields [13]. The extensive use of Nickel Based DS Superalloys in IGTs is due to their balanced performance of high creep strength, excellent hot-corrosion resistance, and good castability [14]. In addition to the excellent properties of the materials, modern gas turbines end up using directionally solidified (DS) Nickel superalloys which also hold a higher cyclic life resistance and an improved creep rupture strength compared to their conventionally cast (CC) version, making them a better choice for the most demanding applications [15]. This gives a direct answer of why DS superalloys chosen over conventional casting: better cyclic life (fatigue) and creep rupture strength. Also, it supports the need to consider anisotropic behavior during testing and subsequent assessment.

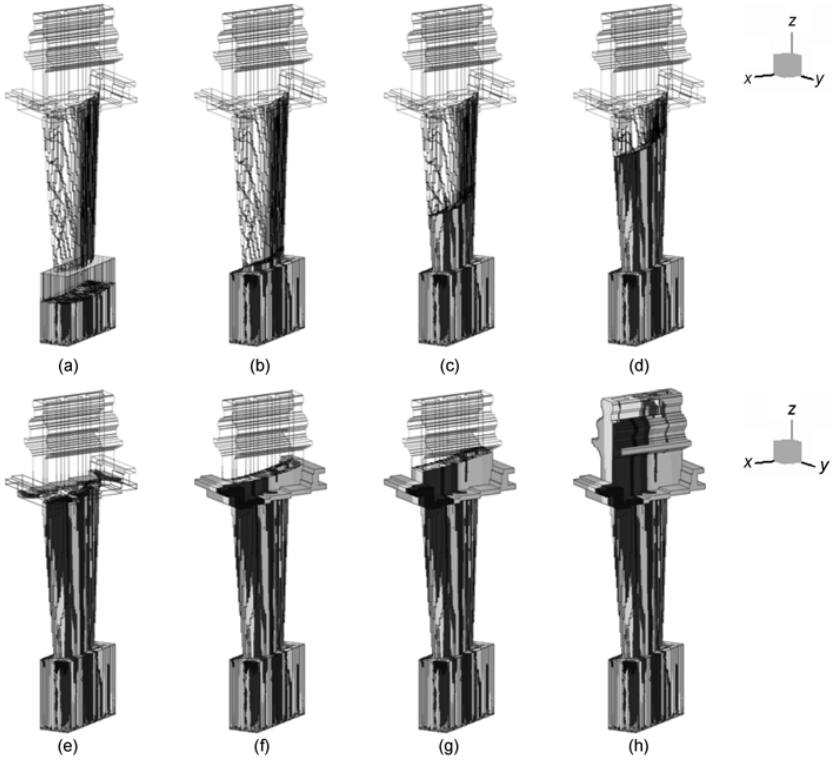

Figure 4.4: Grain growths in the turbine blade casting during solidification. In these figures, different grey scales represent different columnar grains [7]

Chapter 5

Calculations

Calculations needed for the assessment of the initial part of the activity are mandatory to have a deep and complete sense of understanding of the complex problem. Hence, a series of calculations were performed, beginning with the single TB blade in Renè 80 superalloy and after in a variable spectrum of scenarios in order to asses thoroughly the dependance of the solution by a various number of parameters. As it is easily understandable, the first step of the aforementioned work consists in having sufficient Meshes and models to experiment and work with, therefore, beginning with the meshes derived from Chapter 2 a substantial amount of calculations was performed. To synthethize [1]:

1. **1'900'000 Nodes** in Renè 80 (both using Databases 1 and 2) and Nickel Based New DS Superalloy

2. **900'000 Nodes** in Rene 80 (both using Databases 1 and 2)

3. **800'000 Nodes** in Renè 80 (both using Databases 1 and 2) and Nickel Based New DS Superalloy

4. **700'000 Nodes** in Renè 80 (both using Databases 1 and 2) and Nickel Based New DS Superalloy

5. **Automatic Mesh** (auto-generated by Ansys WB) in both materials and both databases

[1]Such quantity of meshes and calculations was not specifically needed if not for comparison purposes, and to show how results were affected by the meshing process

5.1 Mesh Influence

The fundamental principle before launching and analysing any type of calculation is to asses the influence of the mesh on the results obtained. The meshing process, that involves the creation of the mesh in different situations (with the broach block, without it, with the fir-tree lobes meshed differently...) has to be as detached as possible from influencing the results of the calculations, since the situation where it does would include the addition of possible mistakes and errors. To asses the influence of the meshing process on the calculations, the scheme that ensures it is the following: perform a number of calculations until the relative difference of frequency between them gets under an acceptable threshold[2]. As briefly hinted before, the material in which the calculation are performed is not important (when a calculation is launched, a series of material properties such as Young's Module E, Density ρ, G, and many more are required by the software in order to converge to solution) because the idea in this section is to find the ***relative variation between meshes*** that is due to the different number of nodes, elements and meshing technique. The different cases studied are the following, every single one with **Renè 80 in Databases 1 and 2**: 1,9 million Nodes, 900'000 Nodes, 800'000 Nodes and 690'000 Automatically Generated mesh, with the following results: The

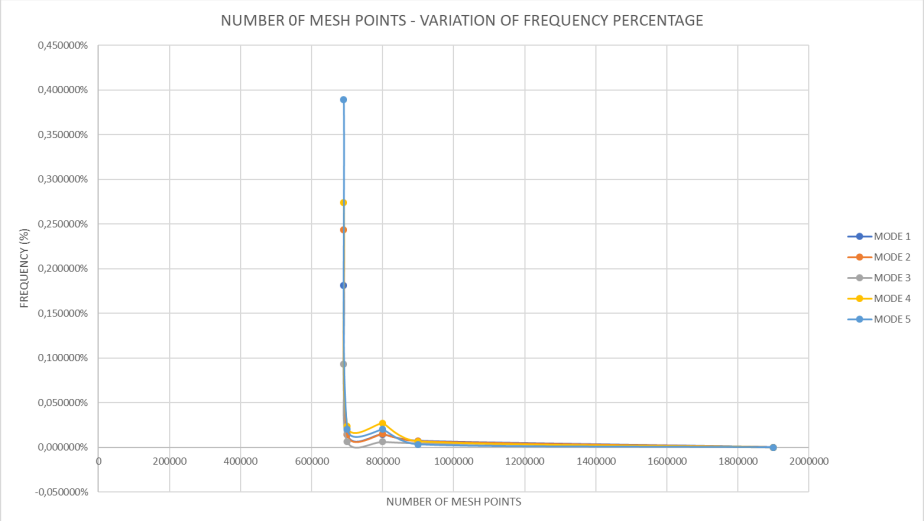

Figure 5.1: The mesh influence visualized

graph shows really quickly how the variation is definitely **negligible**. This is

[2]The value of the "acceptable" difference is not fixed. It is a value based on the phenomenon to measure: if the variation is order of magnitude minor than the values calculated, then the variation between meshes can be considered zero, or negligible.

clear as the results with the worst accuracy are around 0.4% and the best settle at **less than** 0.05%, while the expected variation (accuracy) for the cases taken into consideration is around $1\% - 4\%$. This confirms that even the mesh that was automatically generated with less points, hence the *least* precise, is still far from reaching the **inaccuracy** related to material's properties variation, different databases and general discrepancies. With this results kept in mind, from now on, even though every calculation was still performed with the most accurate [3] (Shown in Figure 5.2) mesh available, it is safe to assume that the results obtained are to be considered **Mesh Indipendent**.

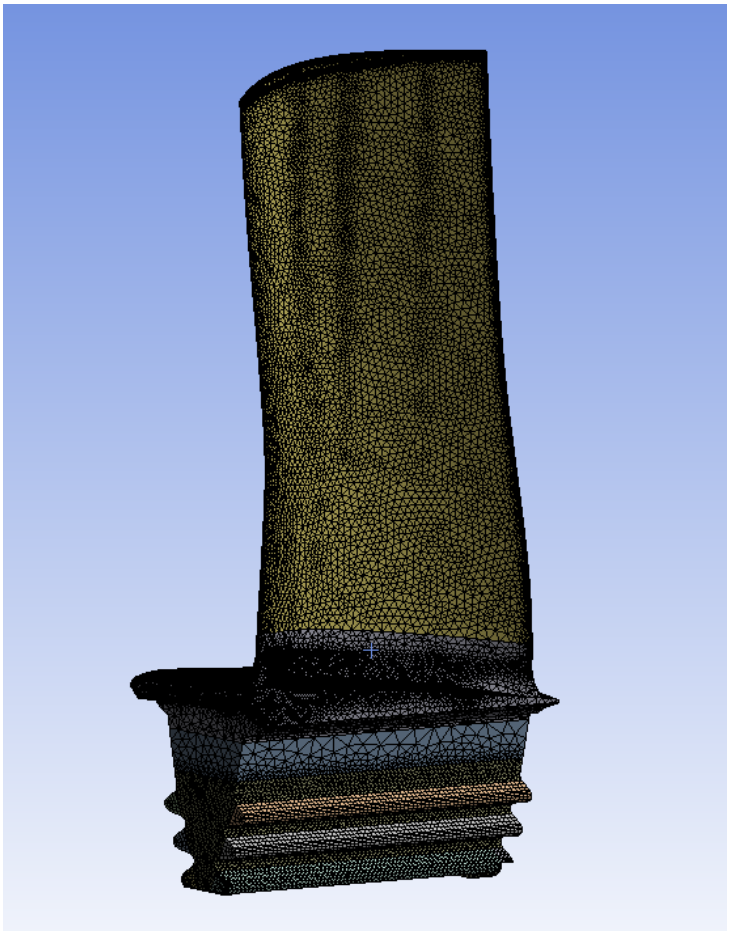

Figure 5.2: The TB Blade in question, pictured here after the meshing process. The Mesh displayed here is the 1,9 Million Nodes

[3] In this case, the 1,9 Million Nodes' one. This refers to the *most accurate* of the batch taken into consideration

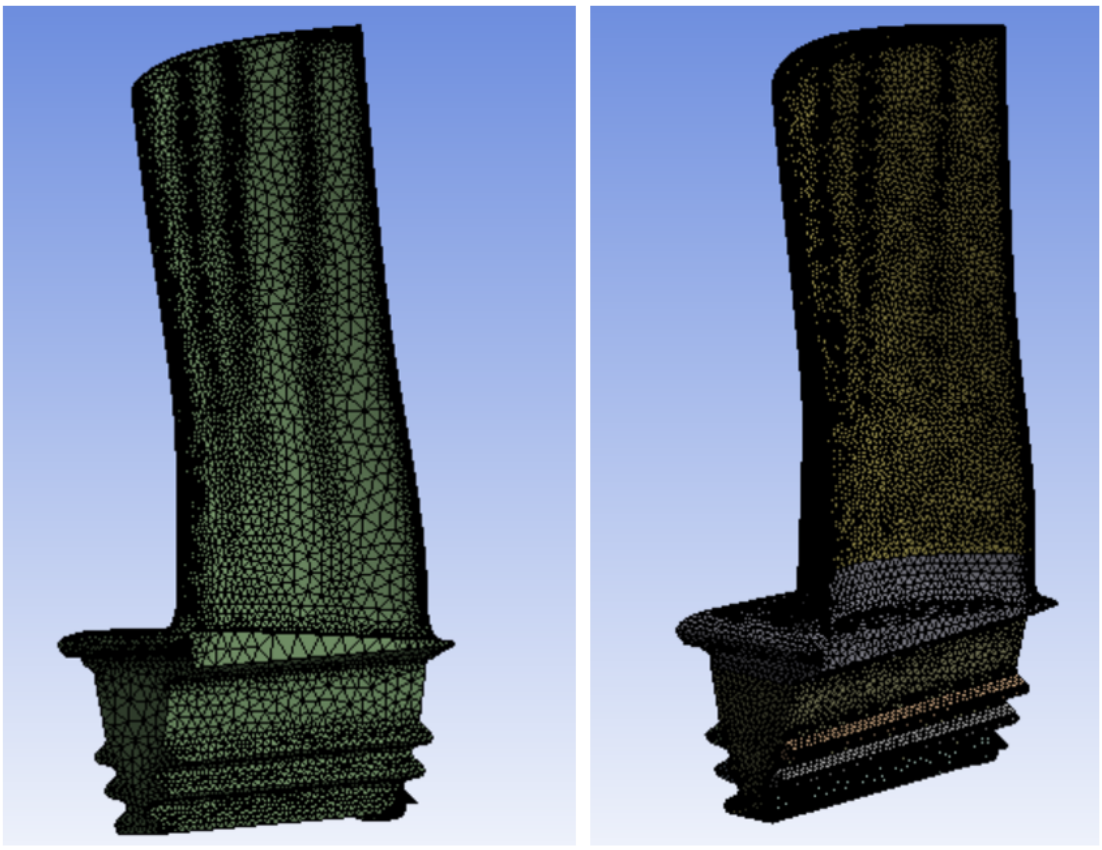

Figure 5.3: Comparison Between 800'000 and 600'000 Meshes

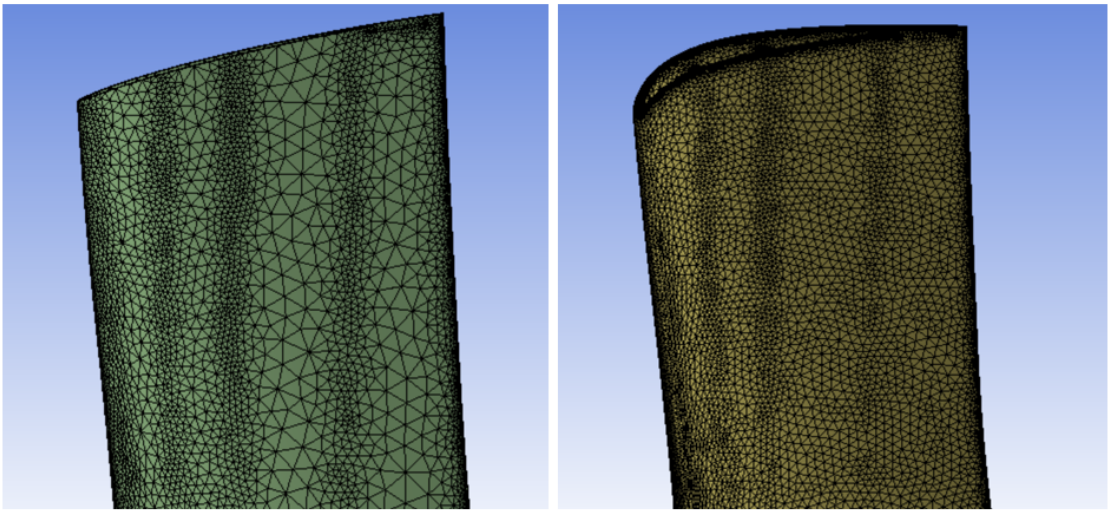

Figure 5.4: Mesh Closeup Showing differencies in the blade section

5.2 Constraints Analysis

Constraints play a fundamental role in the Modal Frequency assessment. This is especially true when considering turbine blades that have different and geometrically complex constraints, like fir tree lobes.

5.2.1 Infintely Rigid Constraints

This type of constraints is one of the easiest example to implement in any FEM software, as the part of the model that is needed to constrain is highlighted in the **Launch File** with a command line, and the software itself will consider the part set in place. This type of constraint was used not only to assess mesh independence in calculations, but also to understand how the blade's frequency and modes were affected when constrained in different parts and when made out of different materials. In particular, in this condition, a series of calculations were performed with different conditions:

1. **One lobe couple Constrained**: both constraining (separately) **Lobe 1** and **Lobe 3** (Fig: 5.5);
2. **Two lobes couples Constrained**: constraining (simultaneously) **Lobe 3** and **Lobe 2** (Fig: 5.5);
3. **All three lobes couples Constrained**: constraining **Lobes 1,2,3** (Fig: 5.5)

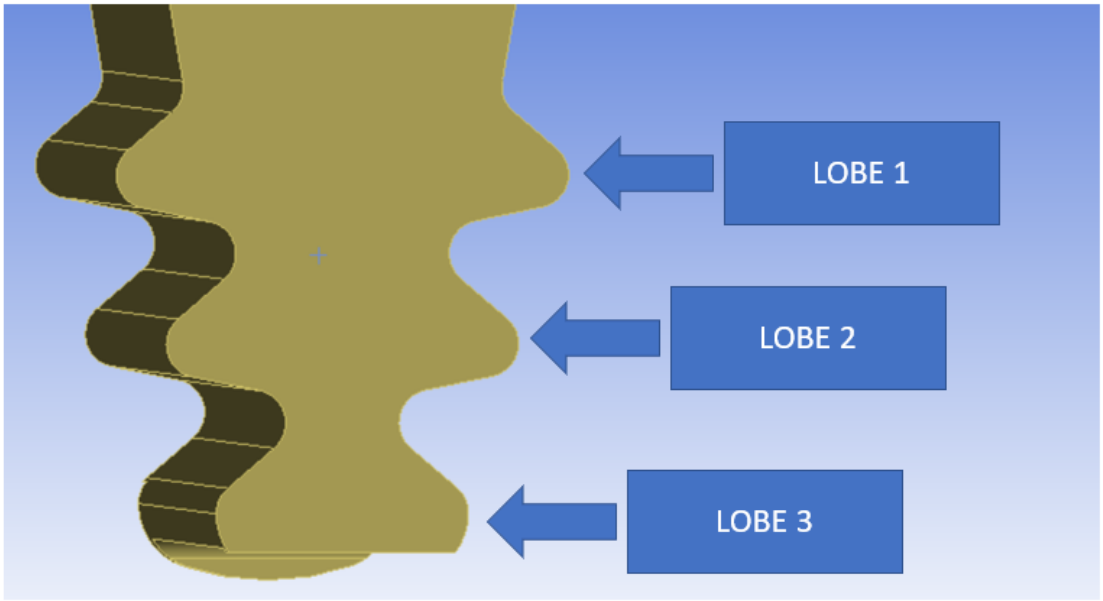

Figure 5.5: Rapresentation of the blade's lobes and enumeration

One Lobe Couple Constrained

The one lobe constrained situation poses both a great way to better understand the modal behaviour and a interesting way to mimic the real world behaviour of the broach block, depending on the couple of lobes constrained. In the situation of having just one lobe couple is the closest to a test bench broach block possible, since that kind of apparatus is designed in order to have only the first lobe (starting from the blade) anchored in place. This scenario present itself only if the constrained lobe is the first one starting from the top, as it is easy to imagine, so referencing from the Fig: 5.5, that would imply constraining **Lobe 1**. The case of constraining the lowest two lobes, on the other hand, was investigated only to familiarize with the modal behaviour of the blade in different case scenarios and understanding frequencies more in detail (the constrained parts are **Lobe 3**).

1 CONTACT	MODE 1	MODE 2	MODE 3	MODE4	MODE 5	MODE 6
Lobe 3	-45%	-23%	-12%	-17%	-23%	-10%

Table 5.1: Lower Lobe constrained frequency deviation

Where the deviation is calculated as usual:

$$\text{Deviation of Frequency} = \left(\frac{\text{Calculated Value}}{\text{All 3 Lobes Calculated Value}} - 1 \right) \cdot 100 \tag{5.1}$$

As expected, by constraining only the lower lobe, we obtain smaller value of frequency. This in an expected effect, since, as it is known from the theory [16]

$$f \propto \frac{1}{L} \cdot \sqrt{\frac{E}{\rho}} \tag{5.2}$$

where L in particular is the length of the body from the constrain to the free tip. So, as expected, a longer L (the blade gets constrained lower than the first lobes) results in a smaller f. When on the other hand the constrained lobe was the upper one, or from Fig. 5.5 **Lobe 1**, the values were very close to the measured one, since the **Broach Block** is constraining only the higher lobe, and very close to the case of **All Lobes Constrained**, since the L to be used in the formula 5.2 is the value **from constrain to tip**. A tab with both scenarios is listed below;

1 CONTACT TOP	MODE 1	MODE 2	MODE 3	MODE4	MODE 5	MODE 6
Measured	0%	1%	-6%	-2%	4%	-3%
3 Lobes - Calc	0%	0%	0%	-2%	-1%	0%

Table 5.2: Measured and Calculated with 3 Lobes constrained when compared to the first lobe only

As imagined, when the deviation was calculated between the all three and Upper only lobes constrained, the deviation was really negligible.

Two Lobes Constrained

This calculation was performed, as before, to asses the frequency modifications connected to the different lengths from tip to constraint. As before, Deviation of frequency was calculated in the same exact way. Results are shown in the Table 5.3 As expected, frequencies were not as small as the **One Lobe Constrained**

2 CONTACTS	MODE 1	MODE 2	MODE 3	MODE4	MODE 5	MODE 6
	-12%	-9%	-3%	-7%	-14%	-4%

Table 5.3: Two Lobes Constrained Frequency Deviation

situation, but sort of in the middle ground.

All Three Lobes Constrained

This Calculation was the most used case in order to asses initial modal behaviour. A initial hint at the behaviour of the all constrained case was already given in the 5.2, but to more clearly explain the modal behaviour, a representation of the Vibrational Modal Form is given Below. An underformed blade representation 5.6 is given below as well.

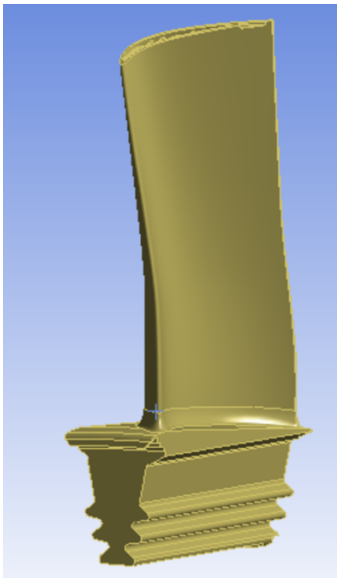

Figure 5.6: The blade when undeformed

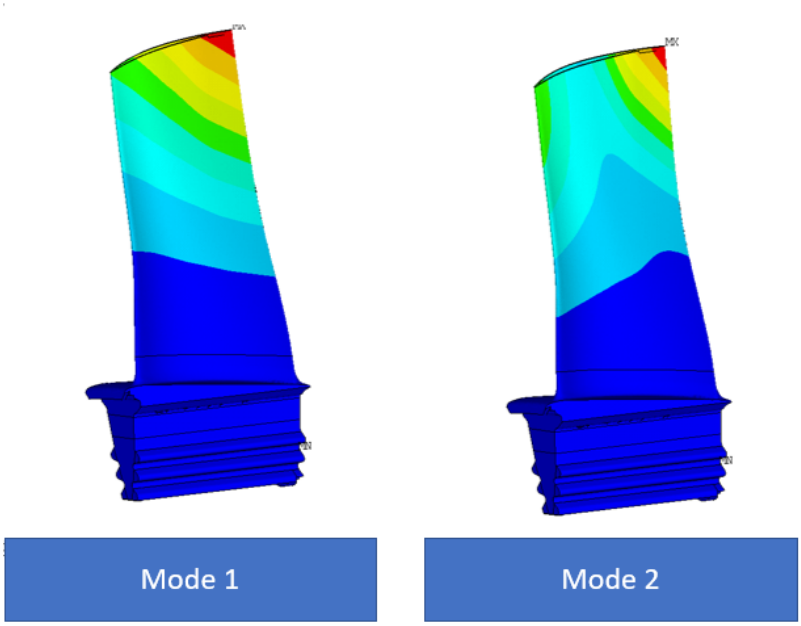

Figure 5.7: Vibrational Modes 1 and 2

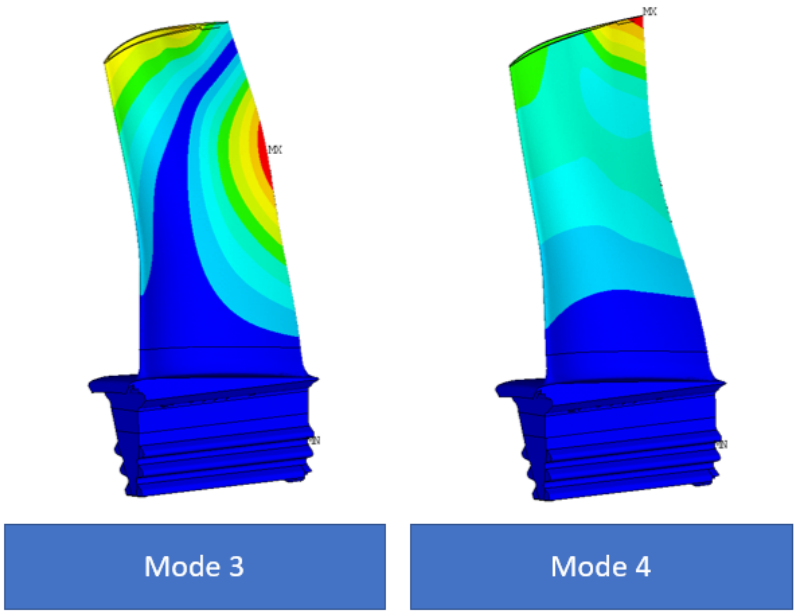

Figure 5.8: Vibrational Modes 3 and 4

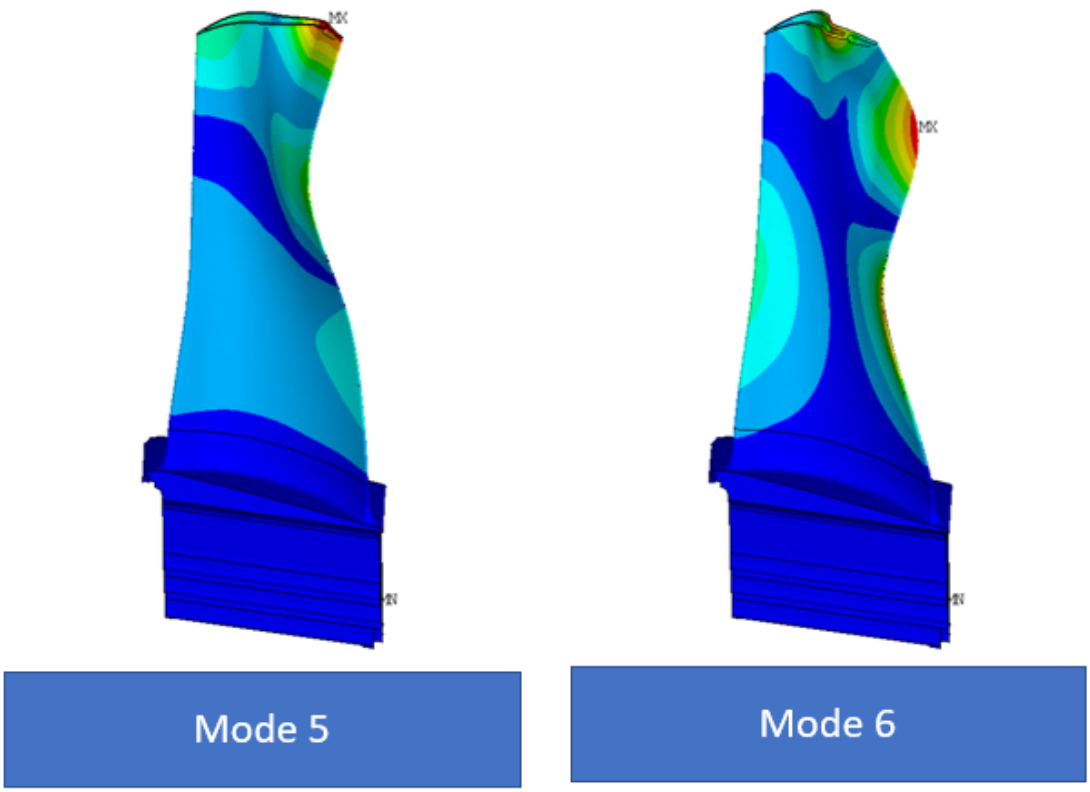

Figure 5.9: Vibrational Modes 5 and 6

Where the Deviation is calculated as follows:

$$\text{Deviation of Frequency} = \left(\frac{\text{Calculated Value}}{\text{Measured Value}} - 1\right) \cdot 100 \tag{5.3}$$

5.2.2 The broach block

Since the blade during testing is constrained into a broach block and then hit with a hammer in order to excite it and allowing for frequency assessment, using a broach block was the best idea when it came with a real world comparison between the calculations and the measured results. Indeed, almost all calculations from now on were performed **with** the broach block, since it was the most accurate case possible in order to compare the results with testing results. A model of the broach block was already modeled by AEN's Mechanical Integrity Team, and was made available in order to be assembled with the FEM blade itself. The idea of assembling the blade into the broach gave some issues as contacts have to be established with precision in order not to have problems with model convergency.

The Broach Block, even though it is considered rigid, is **not infinitely** rigid. This gives more resemblance to a real-type constraint, where the support has some degree of compliance. In order to fix the blade onto the block, underneath the blade, in a purposely designed groove, lays a **intermediate piece** (as seen from Fig 5.10), a mechanical component that transfer pressure coming from underneath the block to the blade, effectively securing it in place and not allowing any movement or slipping. With this component, blade-broach contact is assured. It is the same digital representation of the real one, making the entire model as close to reality as possible.

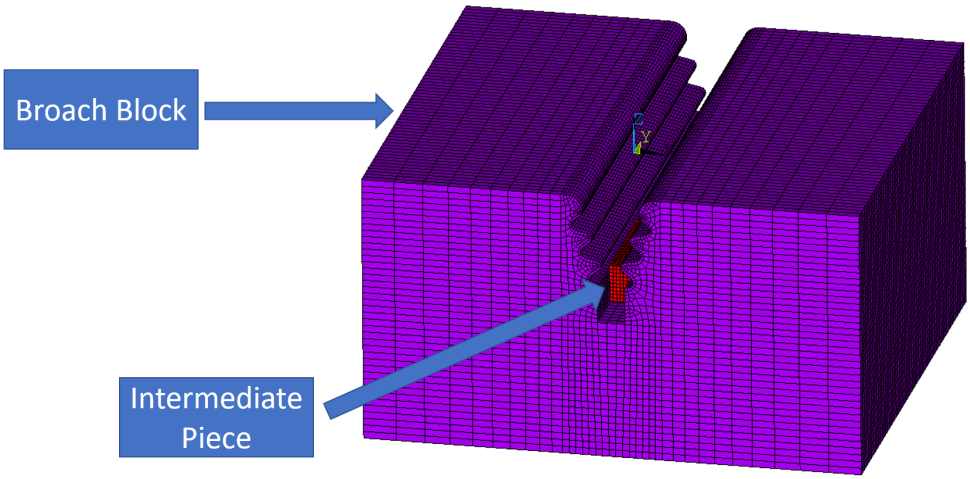

Figure 5.10: Broach Block and Intermediate Piece assembly, used for assessment

5.2.3 No Constraints Case

Real life issues of this type of evaluation

Due to the fact that a TB blade made out of a Nickel Based superalloy such as the René 80 weights **scores of kilograms**, a real world test is impractical to say the least, since the two main used methods in the industry for this purpose, that are:

- Hanging the blade from a surface and then perturbating the blade with a hammer;
- Laying the blade on a cushion and perturbating it with a hammer;

end up, even if at a small scale and sometimes negligibly, either slightly interfering with the measurements or do not give extremely clear results (hence the reason of using a Broach Block). This is the case due to the fact of having the mass of the blade itself, since in the first case a single thread of wire would need to be thick and strong to support the object, thus interfering with the measurement, while in the second case scenario the cushioning piece would be heavily deformed under the blades' own weight that would not behave like a cushion any more, but as a hard surface, making measurements more susceptible to interferences.

5.3 Results Analysis

In this section a brief discussion of the results obtained with calculations is given for in both René 80 and Nickel Based DS Superalloy in the different scenarios described before. After the results there is a short explanation of the deviations, and how they are to be interpreted.

5.3.1 René 80

Results for the Broach Block calculated frequencies with René 80 was, as expected, close to the measured values. The deviation between the measured case and the calculated case, observable in the tab: 5.4, shows the percentages for every mode up to the eighth. As usual, the deviation is calculated with the following formula

$$\text{Deviation of Frequency} = \left(\frac{\text{Calculated Value}}{\text{Measured Value}} - 1 \right) \cdot 100 \tag{5.4}$$

where the reference values were the calculated frequencies (averaged) for the broach block case

Modes	M1	M2	M3	M4	M5	M6	M7	M8
Values	-0,81%	1,00%	-3,32%	-4,07%	1,49%	-1,39%	0,60%	-0,61%

Table 5.4: Values of Deviation of Calculated over Measured

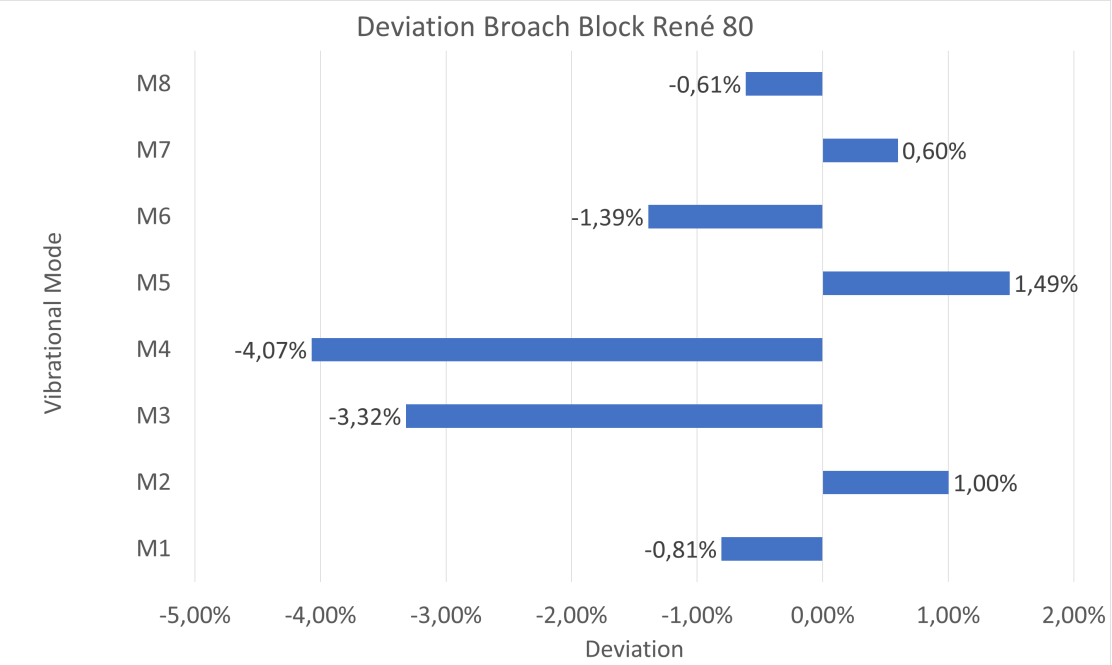

Figure 5.11: Broach Block Deviation Values - René 80

As it can be observed from both the table 5.4 and the Fig: 5.11, the deviation for the **first two modes only** is around **1 %**, hence we can conclude that the values of frequency around those two modes are quite accurate.

5.3.2 Nickel Based New DS Superalloy

After familiarising with the problem with the René 80 Model with and without the broach block, the next step was to asses the results with the values of the Nickel Based New DS Superalloy. For this purpose, the model assembled in the broach block was used, with the new material properties.

Issues with measures

Due to the difficulty of correctly assessing the frequency of the measured blade during physical testing, there was the need to correctly assign the batch of measures to the correct vibrational mode. This comes from the fact that measuring the frequency, even for a number of blades, becomes significantly more complex as the vibrational mode number becomes bigger. Assessing the first two frequencies is straightforward 5.12, while assessing the higher modes gets progressively more complex, posing the need for some analysis later. The issue was solved by observing the graphs after importing them into Excel and sorting them in the correct

vibrational mode.

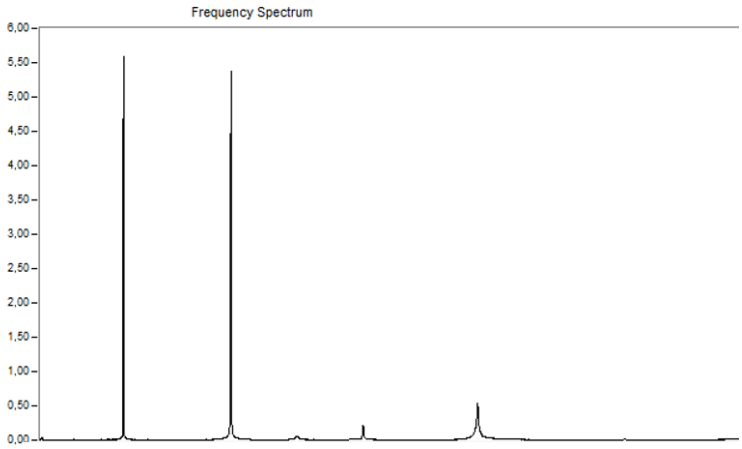

Figure 5.12: The frequency spectrum as seen by the operator. After the first two frequencies, assessing the numbers gets more and more complicated, since amplitude peaks of vibrational modes and external interferences become comparable

5.3.3 Results

The following graph (5.13) shows the results graphed with the associated deviation, after the correction mentioned in the section before. The deviation, as usual, was calculated as follows:

$$\text{Deviation of Frequency} = \left(\frac{\text{Calculated Value}}{\text{Measured Value}} - 1\right) \cdot 100 \tag{5.5}$$

A table for easy reading of results is also provided 5.5.

Deviation	**M1**	**M2**	**M3**	**M4**	**M5**	**M6**	**M7**	**M8**
	8,10%	6,79%	2,34%	2,55%	0,57%	0,22%	-0,27%	-3,54%

Table 5.5: Deviation table for Broach Block and the New DS anisotrpic Superalloy

This result is significant, and has to be discussed briefly. When considering the results, a comparison between René 80 and the New Material has to be done in order to understand how the two materials compare and to investigate the discrepancy in accuracy. This was the first step to correctly asses differences and establish a starting point. The values for the two materials are significantly different, because if the first experiences a discrepancy of around **4.07% at maximum** (but on the fourth mode), the new material is off by **more than 8** %. This is the main objective of the thesis, assessing the difference, understanding the main reasons

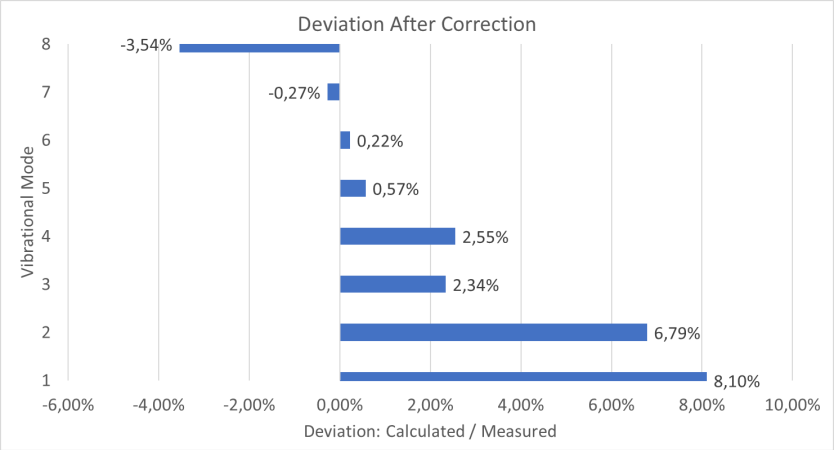

Figure 5.13: Deviation of Values from Measured ones

behind it and then bring the conclusions in order to give a clear answer. What was investigated after was done in order to see how different scenarios affected results, and what was the best possible outcome to be obtained.

Chapter 6

The effect of Turbolators

In the first part, as a way to simplify calculations, models and results, a decision was made to remove and omit turbolators from the blade, making for an easier model to mesh, assemble, and run. As it is easy to understand, this meant having a easier geometry to work with but at the same time a further from truth batch of results, since the real blade is equipped with turbolators. Results then, up to this point, were affected by the issue of being biased and not reflecting the truth as far back as the model. After assessing first-hand results, and observing discrepancies, it was deemed **necessary** to **let go of the aforementioned simplification**. Consequently, as a decision about finding out what the impact of turbolators was for frequency assessment in blades was made, a complete model with all the components in its full original form was prepared, again, starting from the original blade. The Model in question was meshed directly from the original CAD design with **two** different meshes and then firstly assessed without the broach block and then assembled in it. Both cases were studied and gave very promising results. The first assessment, without the broach block, was still particularly useful in order to understand what the impact was when compared to previous calculations (e.g. the calculations without broach block), even if they could not be compared with the measured values. The performed calculations were done in order to asses if the turbolators gave any type of contribution in the modal solution and in the frequency assessment. This calculations, since the effect of turbolators **previously unknown** were particularly useful, paired with some tuning of the material, in order to have a value of correction for further uses of the blade calculations and give an explanation of the behaviour of those structures during modal analysis. The idea of including the turbolators came from the idea of making the model as close to reality as possible, and working with the realest possible case scenario from this chapter on, hence, as said before, letting go of the first simplification.

6.1 Vibrational Modes Analysis

After running the first calculation the results that were obtained gave a pretty promising idea about the fact that turbolators are actually giving some important and **NON NEGLIGIBLE** difference of around **three percent decrease** for the first two vibrational modes. The higher modes, that were measured up until the *eighth mode*, were not affected wrongly, and in contrast to what was previously expected, the results didn't seem to be affected by the presence of turbolators. The most affected modes were of course the first two, but with really promising results. The results can be visualized in the image below 6.1

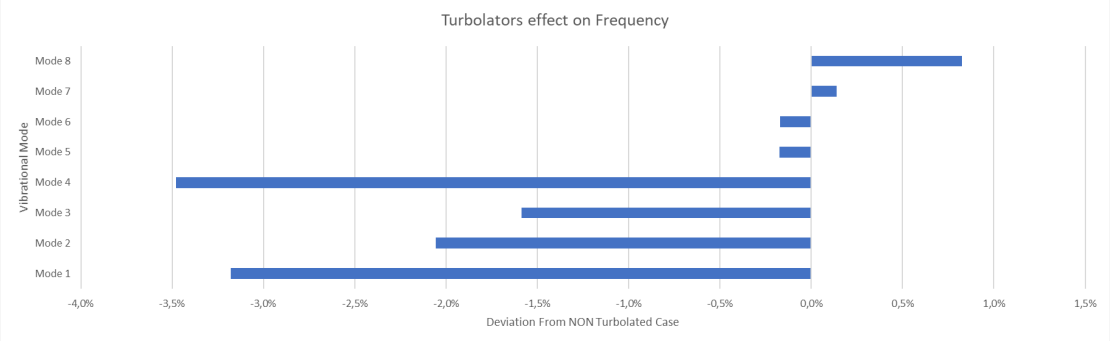

Figure 6.1: Turbolators Effect on Blade Frequency. The case was compared with the calculations done without the broach block and the model without turbolators.

DEV	M1	M2	M3	M4	M5	M6	M7	M8
	-3,2%	-2,1%	-1,6%	-3,5%	-0,2%	-0,2%	0,1%	0,8%

Table 6.1: Table of deviation of frequencies with the turbolators when compared with results without them

This result confirms that the presence of those structures cannot be ignored, and thus the former considerations about their negligible effect cannot be applied to the problem in question. More importantly, it leads into the right direction when it comes to frequency assessment, lowering the measured frequencies and allowing for values closer to the measured ones.

Since those results were obtained the broach block - constrained model was considered in order to obtain more real word and more accurate results.

6.2 Turbolators and the Broach Block Model

The aforementioned results gave some promising results that are quite important and need to be investigated further. Since the results with the infinitely rigid constraints were not comparable with the measured frequencies, there was the need to assemble the newly considered blade with turbolators with the model broach block, in order to obtain results that can be compared with measurement and draw subsequent conclusions. Starting as usual with the formula used for calculating the deviation 6.1

$$\text{Deviation of Frequency} = \left(\frac{\text{Calculated Value with Turbolators}}{\text{Measured Value}} - 1 \right) \cdot 100 \quad (6.1)$$

it can be observed in the following graph the newly obtained results 6.2;

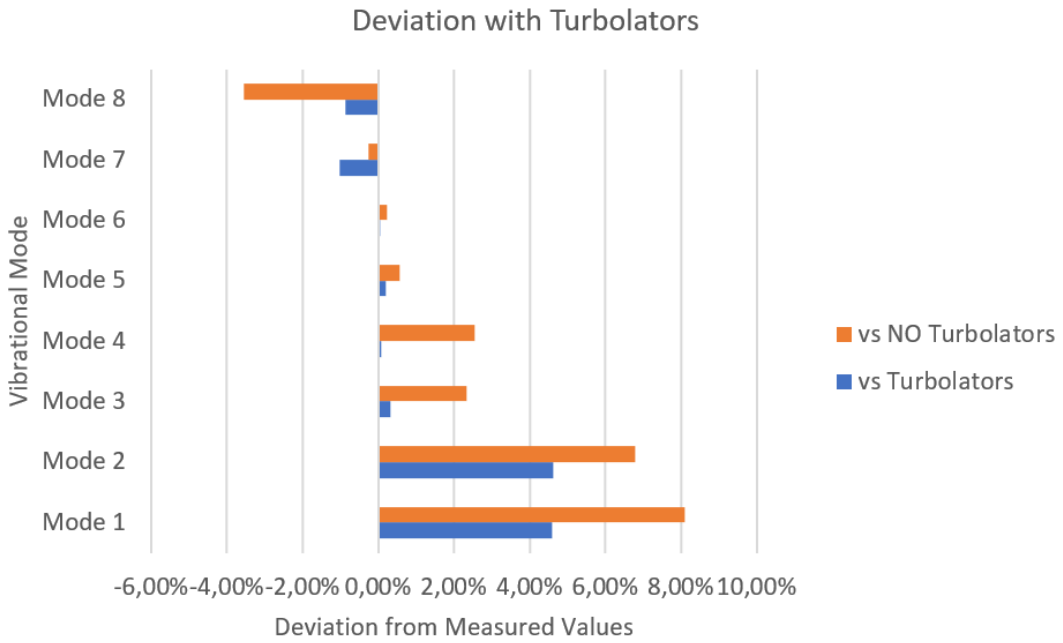

Figure 6.2: The deviation from measured with and without turbolators

The values of the newly calculated frequency not only is closer to the reference (the measured values) but also makes the model closer to the real world scenario. For this reason, from this chapter on, turbolator-equipped model will be the standard and every calculation from now on will include them.

Chapter 7

Grain Orientation

Materials such as **the New Nickel Based DS Superalloy** are so called anisotropic (for a more detailed description, reference the chapter 4), meaning their properties depend on the direction considered. Due to this particular characteristic, they tend to behave pretty differently depending on the orientation of the grain of the component. What does it imply practically? When the material solidifies, the internal grains tend to align at an angle of **zero degrees**, but only ideally. In reality every section of the blade will solidify with a different grain angle, leading to the need of defining an acceptable cone (regarding the **x, y and z axis** of grain orientation). This means there is another degree of uncertainty to be considered. This will hence be the focus of this Chapter.

7.1 How grains orientation is defined

In the image below 7.1 is possible to observe a rendering of a blade with an angle of deviation from the nominal values. The maximum and minimum acceptable values in order to have a usable blade (that fits into the specification's guidelines) is $+20°$ **and** $-20°$ respectively, in every single axis direction. In order to asses results in the **worst possible scenario** it was decided to perform calculations using the extremes values to see how the maximum possible orientation behaves. As it is easy to understand, normal production blades fit into a way narrower cone of orientation, and those extremes pose just a limit to the validation phase during the construction phase of the blade. The assessment of the grain orientation is a destructive procedure that involves **an acid attack** on the blade, rendering it impossible to be used for any structural purpose, and thus impossible to test for frequency assessment after (this explains why the values are statistical and given in a cone of acceptability rather than singularly. Checking the results causes the blade to be impossible to measure after). Since rotating the blade around the z axis

would mean **just** having a different orientation of the whole blade, the overall result wouldn't change much [1]. In order to explore all the different possible situations, the blade was tested in every single case possible, meaning the solution was calculated with both the broach block and without it.

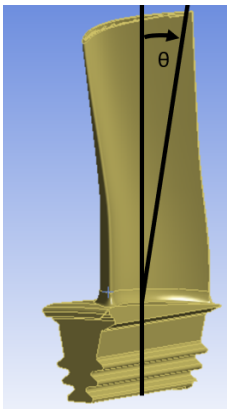

Figure 7.1: Grain Orientation Visualized. The angle θ can be both positive and negative

7.2 Infinitely Rigid Constraints

In this first case scenario, the blade is held in place by giving infinitely rigid constraints on the upper two teeth of the fir tree, while the orientation of the grains variates in **both x and y axis**, in accord with the diagram 7.2. When referencing a name of an axis and subsequently "adding" or "subtracting" a value of θ, it refers to the action of rotating that axis according to the value specified, as shown in the image 7.2. Results summary is given in table 7.1. As a reminder, the deviation is calculated with this formula:

$$DEVIATION = \left(\frac{VALUE}{REFERENCE} - 1\right) \cdot 100 \tag{7.1}$$

NOTE: The reference values are the calculated values with an orientation for x, y, z axis equal to $0°$

[1]For the sake of completeness, a couple of calculations were performed for the blade without the broach block. They highlighted and proved the aforementioned fact. Results can be observed in the Appendix B.

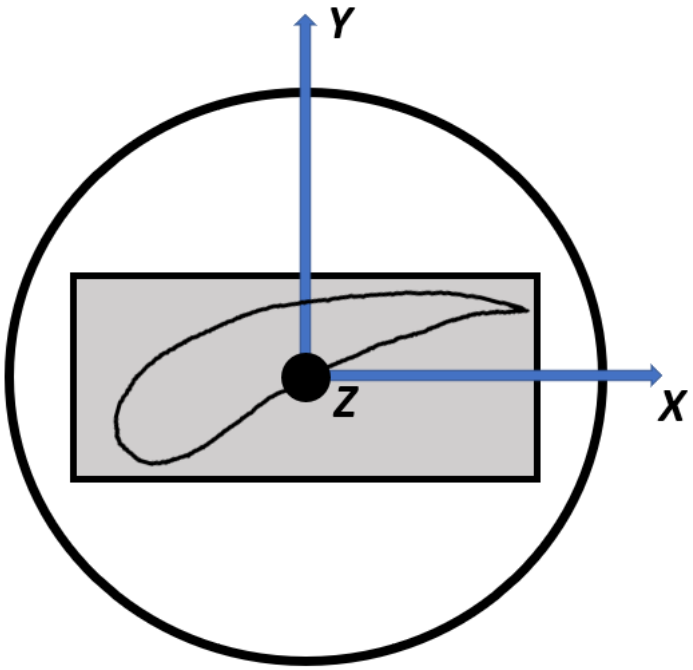

Figure 7.2: The blade (in grey) with axis viewed from above. This is the same orientation of coordinate system used in Ansys Mechanical

Deviation	Mode 1	Mode 2	Mode 3	Mode 4	Mode 5	Mode 6	Mode 7	Mode 8
x + 20	4,5%	-2,1%	1,7%	5,6%	-2,0%	-1,0%	1,2%	3,0%
x - 20	1,5%	3,0%	-4,4%	0,1%	2,2%	0,3%	-1,5%	-0,8%
y + 20	1,9%	-0,5%	1,0%	1,1%	-0,4%	-0,7%	1,7%	1,4%
y - 20	9,5%	0,8%	-2,8%	4,3%	2,9%	-3,3%	-0,7%	-0,3%

Table 7.1: Deviation from calculated with different grain orientations

To better visualise results, the following graphs are provided:

As it is clear from the graphs for the different grain orientations, there is not a single situation where the orientation would help to reach a better frequency overall. Some modes do actually perform better with a different grain orientation, but this would mean having to deal with worse results in different situations. Since this is unacceptable (even if the first two modes do really bear more weight than the higher ones, it is clear that having useless results for most of the modes, and in a randomic disposition, isn't an acceptable case scenario). For this reason it was concluded that there is not an orientation that is worth investigating separately.

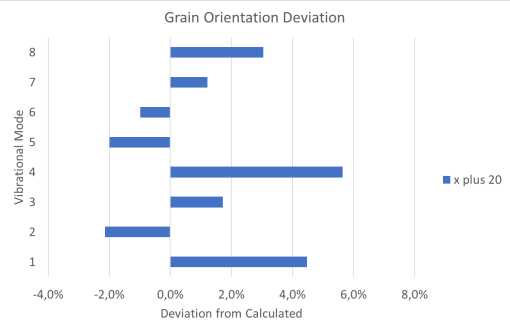

Figure 7.3: Influence of X + 20°

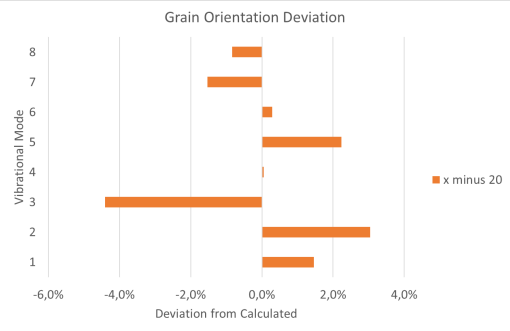

Figure 7.4: Influence of X - 20°

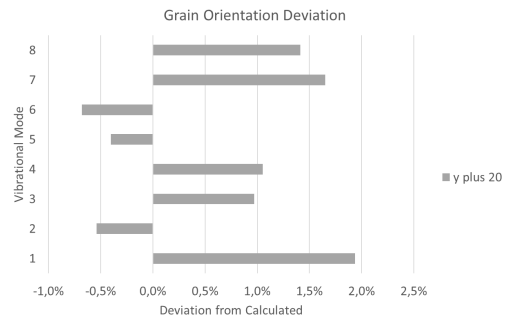

Figure 7.5: Influence of y + 20°

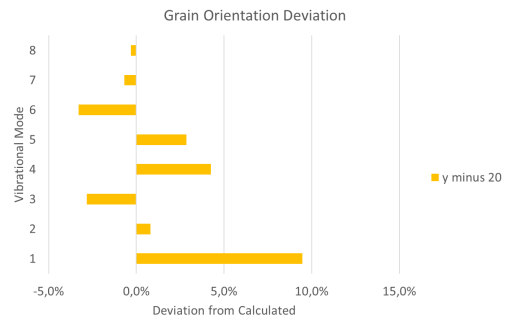

Figure 7.6: Influence of y - 20°

7.3 The Broach Block Effect

Since blades get tested into a broach block it is vital to always check if the broach block effect, that is not infinitely rigid as the constraints set into the software, is important enough to modify or alter results. For this reason it was decided to mount the blade in the broach block again and launch calculations as before. The results, shown in the tabs below, are divided into the values obtained with the deviation from the calculated values ("Deviation from Calculated"), where the calculated values are those obtained with the grain deviation angle set to 0°. Equal to before, the formula used for deviation is the following:

$$DEVIATION = \left(\frac{VALUE}{REFERENCE} - 1\right) \cdot 100 \tag{7.2}$$

Deviation	Mode 1	Mode 2	Mode 3	Mode 4	Mode 5	Mode 6	Mode 7	Mode 8
x + 20	14,2%	6,3%	-1,6%	0,4%	3,7%	-2,5%	-2,2%	-1,2%
x - 20	6,5%	2,0%	2,4%	1,6%	-1,7%	-1,8%	2,2%	0,9%
y + 20	11,3%	4,3%	4,1%	4,0%	-0,4%	-1,0%	1,1%	1,2%
y - 20	10,8%	8,8%	-0,1%	0,4%	3,1%	0,0%	-1,6%	-0,3%

Table 7.2: Deviation from Measured Values - Different Grain Orientation

Deviation	Mode 1	Mode 2	Mode 3	Mode 4	Mode 5	Mode 6	Mode 7	Mode 8
x + 20	9,2%	1,6%	-1,9%	0,3%	3,5%	-2,6%	-1,2%	-0,3%
x - 20	1,8%	-2,6%	2,1%	1,6%	-1,9%	-1,8%	3,2%	1,8%
y - 20	6,4%	-0,3%	3,7%	3,9%	-0,6%	-1,0%	2,1%	2,1%
y - 20	5,9%	3,9%	-0,4%	0,3%	2,9%	0,0%	-0,6%	0,6%

Table 7.3: Deviation from Calculated - Reference to zero degrees orientation

In order to have a clear visualization of results, in addition to those two tables, the following graphs are provided.

To give a more complete understanding, the following two graphs show all the previous solutions combined:

As it is clearly visible from every single graph shown above, there is not a single variation that would allow the frequency of every single mode to get closer to measured, and the variation are pretty randomic, indicating that there is not a better orientation to investigate thoroughly. Since variations of orientation do not give a better result than zero orientation, and that the ***zero degrees orientation is the best result possible***, the grain orientation idea was not investigated further. As a reminder: the real grain orientation of the blade is not, as said before, so deviated from zero. The real value is likely around the zero degrees orientation, even if not absolutely zero. During the production process the solidification of the grain can vary a little, and even differently in different parts of the blade. For this reason, changing grain orientation to the entire blade is a simplification itself.

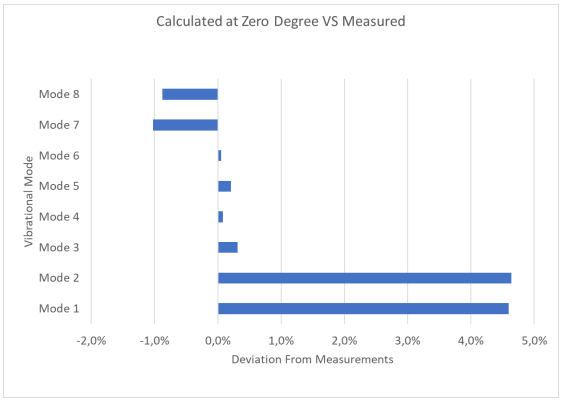

Figure 7.7: Deviation from Calculated at zero degrees of orientation

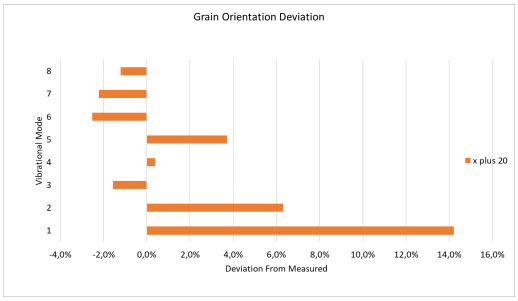

Figure 7.8: Influence of X + 20°

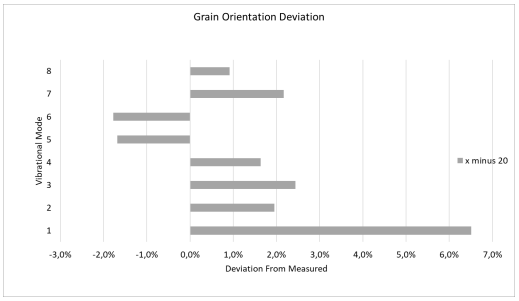

Figure 7.9: Influence of X - 20°

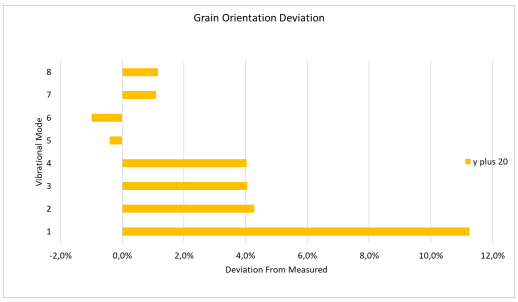

Figure 7.10: Influence of Y + 20°

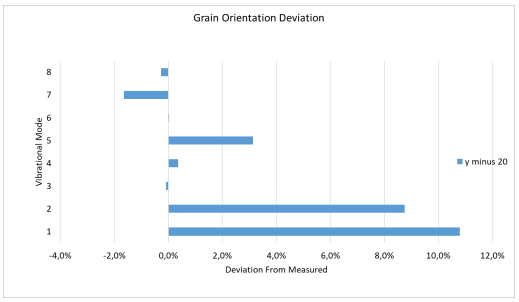

Figure 7.11: Influence of Y - 20°

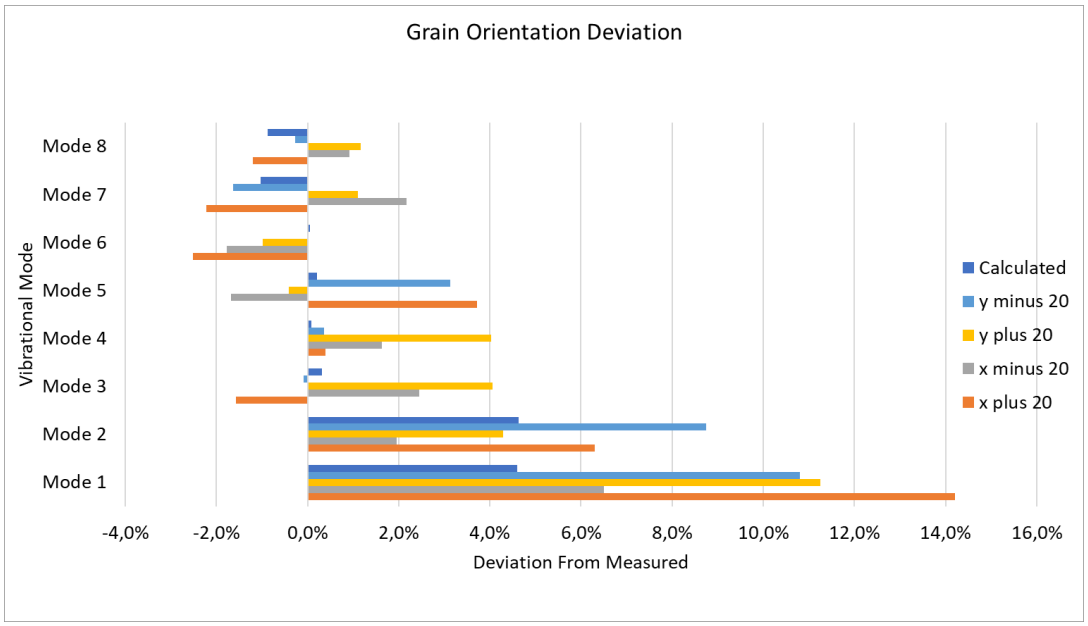

Figure 7.12: The complete overview of the deviation of every single variation of orientation from the calculated values

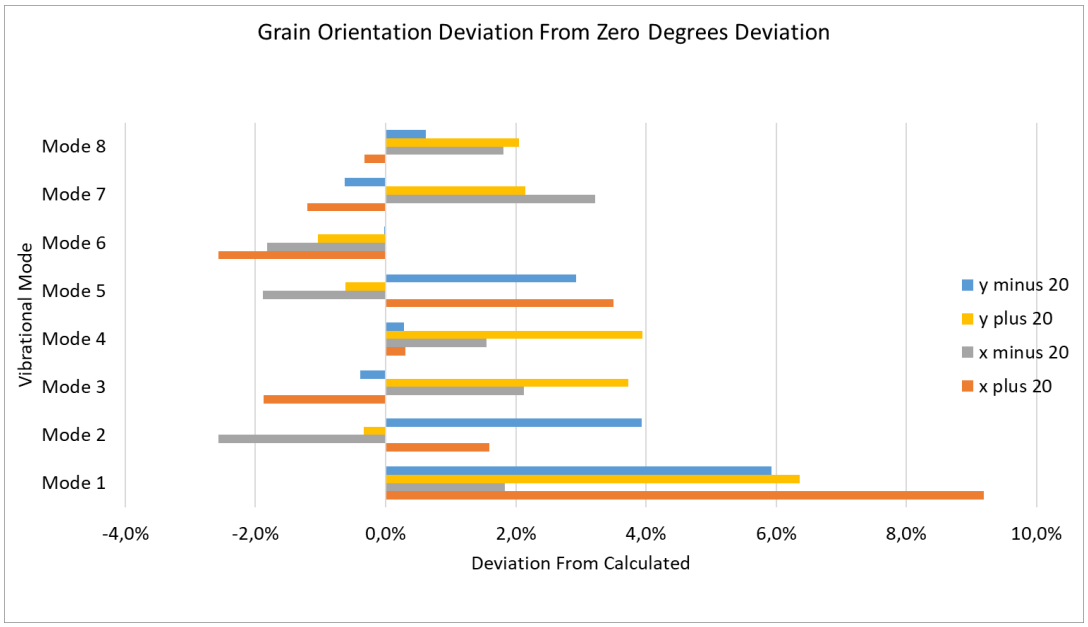

Figure 7.13: The complete overview of the deviation of every single variation of orientation from the measured values

Chapter 8

The Optimization of E and G

In order to obtain a model that would have been able to correctly calculate the values with a level of accuracy comparable to the René 80 case. This was initially made just by correcting the E and G modules with a fixed variable, in order to get close to the values of the measured frequencies. This was the first of **three types** of tuning, all of whom gave different results.

8.1 Finite Value Correction

The first idea was the simplest to implement and to test, which consisted of correcting the values of **E and G separately and together** with a fixed value, in order to fix one specific frequency at a time. The idea behind how the **correcting value** was obtained is the following;

$$\text{since } f \propto \sqrt{E} \rightarrow \frac{f_{new}}{f_1} = \frac{\sqrt{E_{new}}}{\sqrt{E_1}} \rightarrow E_{new} = \underbrace{\left(\frac{f_{new}}{f_1}\right)^2}_{k} \cdot E_1 \tag{8.1}$$

where E_1, and f_1 are respectively the values of the untuned E and frequency, while the *new* values are the one to target, so the f_{new} is the value of the measured frequency for the considered vibrational mode. k is the constant that gets multiplied to the Young's Module in order to *fix* the relative frequency (that in this case would be f_1). The deviation was calculated with the following formula;

$$\text{Deviation of Frequency} = \left(\frac{\text{Value of Calculated Frequency}}{\text{Measured Frequency}} - 1\right) \cdot 100 \tag{8.2}$$

With that method, the results obtained are the following;

E only, k = 0.8649

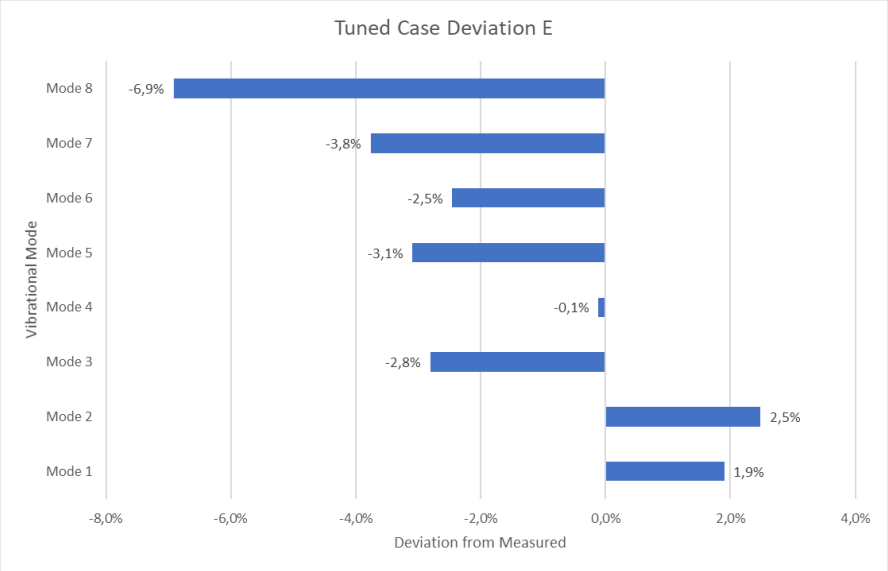

Figure 8.1: Deviation of Frequencies after Correcting E with k

E and G, k = 0.8649

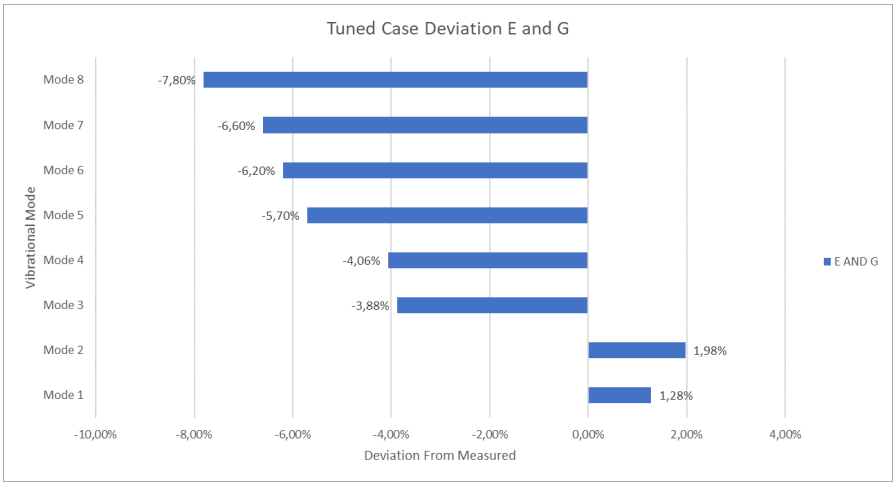

Figure 8.2: Deviation of Frequencies after Correcting E and G with k

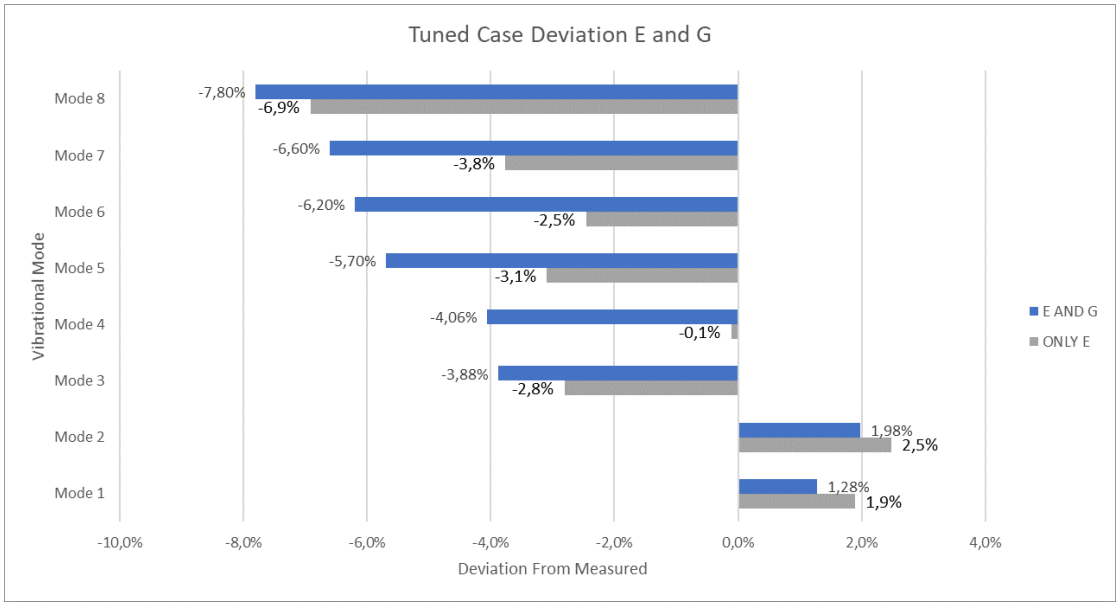

Figure 8.3: Confrontation between correcting E and G and only E

E and G, k = 0.873

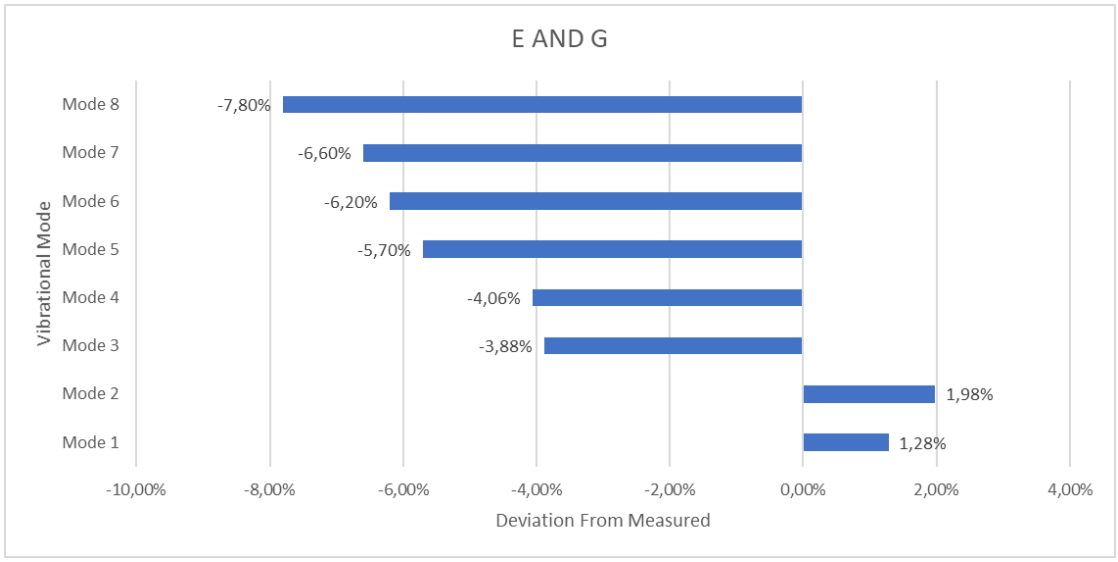

Figure 8.4: Deviation of Frequencies after Correcting E and G with k

All the cases give the same type of results when it comes to the optimization process. They rigidly shift all the frequencies backward or forward according to the value that was used to correct one single frequency. This kind of optimization isn't ideal, as it doesn't address most frequencies, but just gives a temporary solution for when it comes to having a model that correctly predicts a single frequency value. For this reason, it was decided to consider multiple frequencies at a time

8.2 Algebraic System Resolution

Another idea that was investigated was to consider the first **four modes** and the values of E_x, G_x, E_z, G_z, from the material properties, and by matching the values like this, and solving the associated **4x4 Algebraic System** for every iteration. For every frequency, there was a ***target*** and a ***initial value***. For the first **Proper 1 - 4** optimizations, the relationships were the following;

$$f_{\text{target}}(\text{Mode 1}) \rightarrow E_x, f_{\text{target}}(\text{Mode 2}) \rightarrow E_z \tag{8.3}$$

$$f_{\text{target}}(\text{Mode 3}) \rightarrow G_x, f_{\text{target}}(\text{Mode 4}) \rightarrow G_z \tag{8.4}$$

This resolution had the issue of having the frequencies tied to a single value, but nonetheless gave some promising results, that are listed below; **Important Note:** "AS" followed by a number refers to the "Algebraic System" method, while the number refers to the iteration. The iterations were made as follows;

$$\text{Initial, non tuned values of E, G and } f \rightarrow \text{New E and G values} \Rightarrow f_{new} \tag{8.5}$$

where "$\rightarrow$" stands for *solving the algebraic system* and "$\Rightarrow$" for *running calculations with the obtained values* of E and G and fining f. The second iteration would have used the E, G and f from the first iteration in order to find the **new** E and G, and so on for all the following iterations.

AS 1

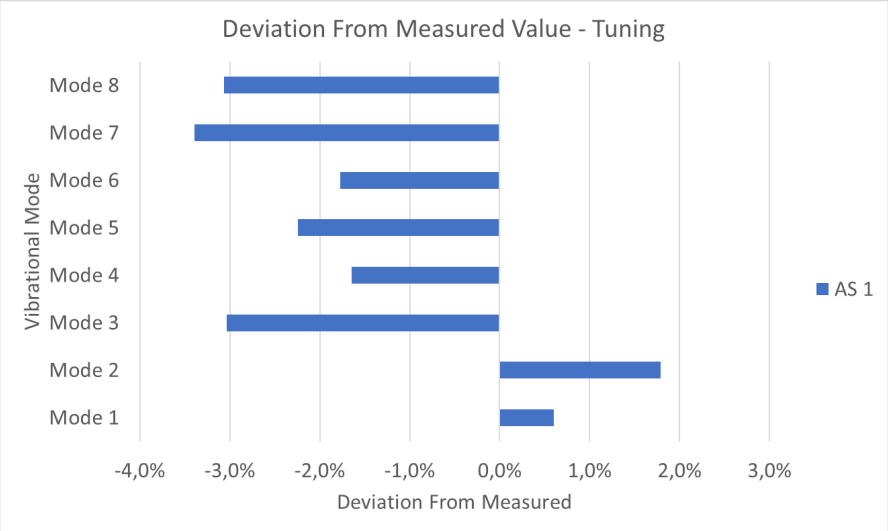

Figure 8.5: Deviation of Frequency for the 1^{st} iteration

AS 2

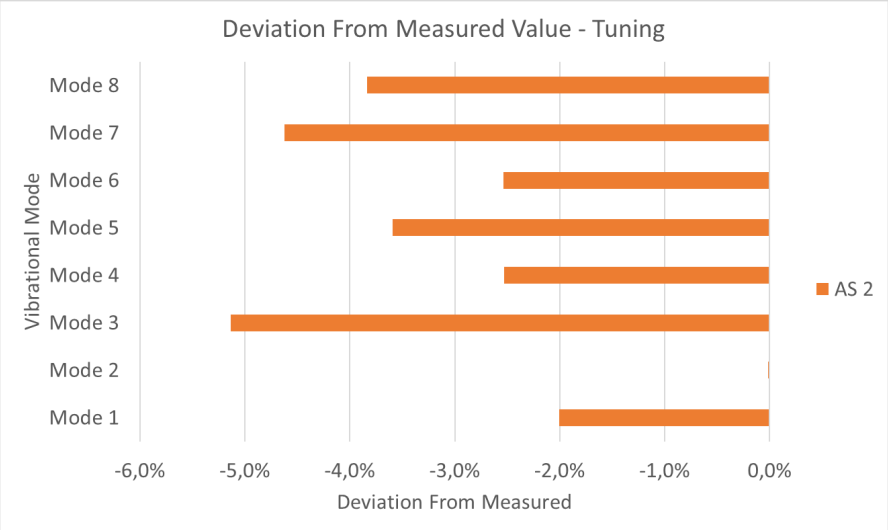

Figure 8.6: Deviation of Frequency for the 2^{nd} iteration

AS 3

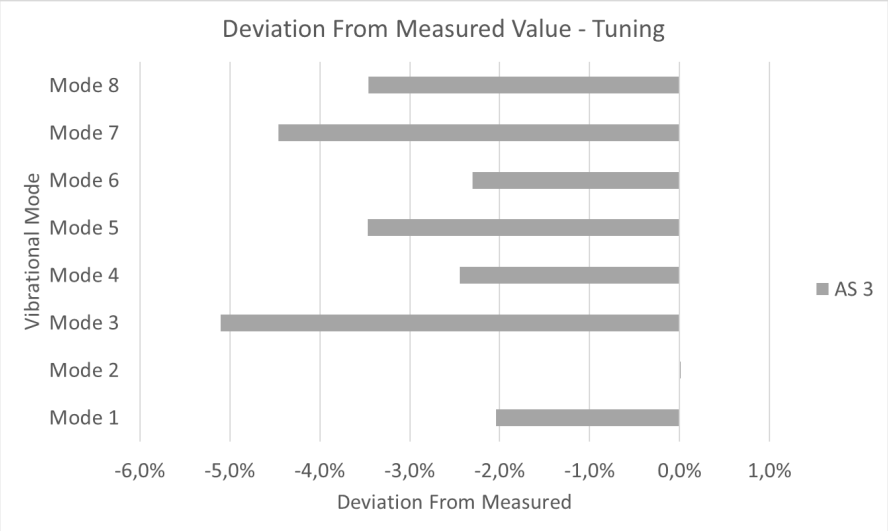

Figure 8.7: Deviation of Frequency for the 3^{rd} iteration

AS 4

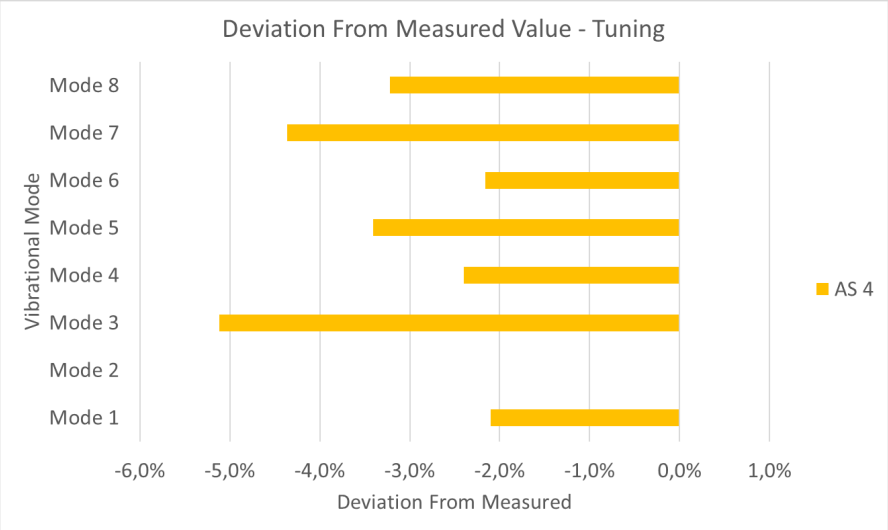

Figure 8.8: Deviation of Frequency for the 4^{th} iteration

AS 5

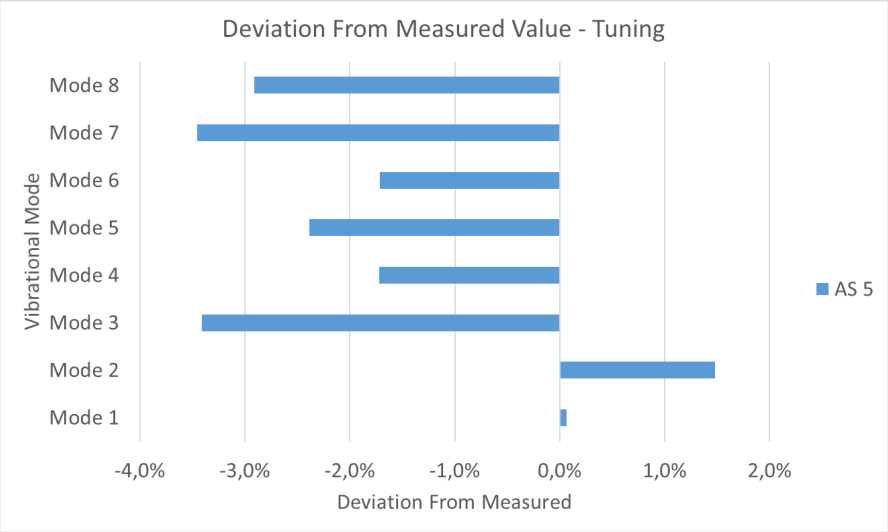

Figure 8.9: Deviation of Frequency for the 4^{th} iteration

Theoretical

This case was treated differently. After observing that the values of E and G were **not** obeying to the material's properties laws, it was decided to try and force the case of AS1 to obey to the rules of 4.2.1. So by forcing the compliance matrix to be respected in order to obtain the values of E and G, the results of the calculations performed were the following;

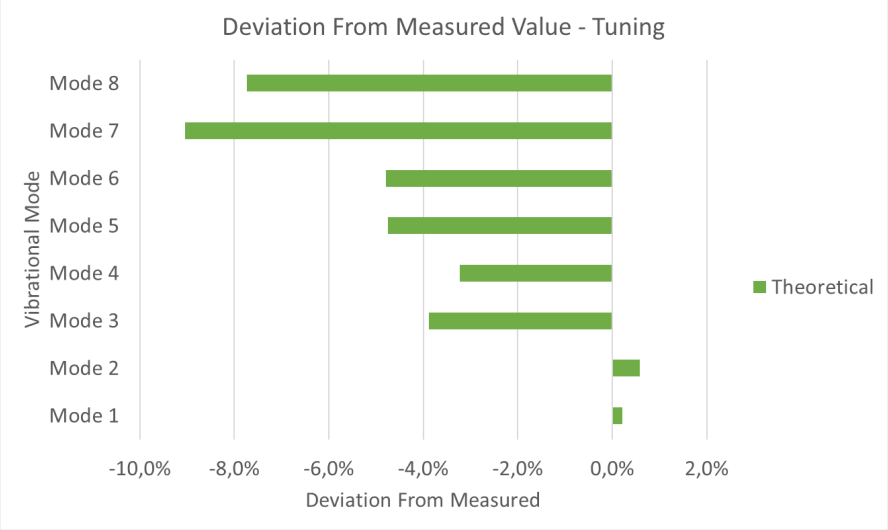

Figure 8.10: Theoretical Deviation

All the presented results can be summarized in the following graph (8.11) and table (8.1);

Deviation	M1	M2	M3	M4	M5	M6	M7	M8
AS 1	0,6%	1,8%	-3,0%	-1,6%	-2,2%	-1,8%	-3,4%	-3,1%
AS 2	-2,0%	0,0%	-5,1%	-2,5%	-3,6%	-2,5%	-4,6%	-3,8%
AS 3	-2,0%	0,0%	-5,1%	-2,4%	-3,5%	-2,3%	-4,5%	-3,5%
AS 4	-2,1%	0,0%	-5,1%	-2,4%	-3,4%	-2,2%	-4,4%	-3,2%
AS 5	0,1%	1,5%	-3,4%	-1,7%	-2,4%	-1,7%	-3,5%	-2,9%
Theoretical	0,2%	0,6%	-3,9%	-3,2%	-4,7%	-4,8%	-9,0%	-7,7%

Table 8.1: Final recap table

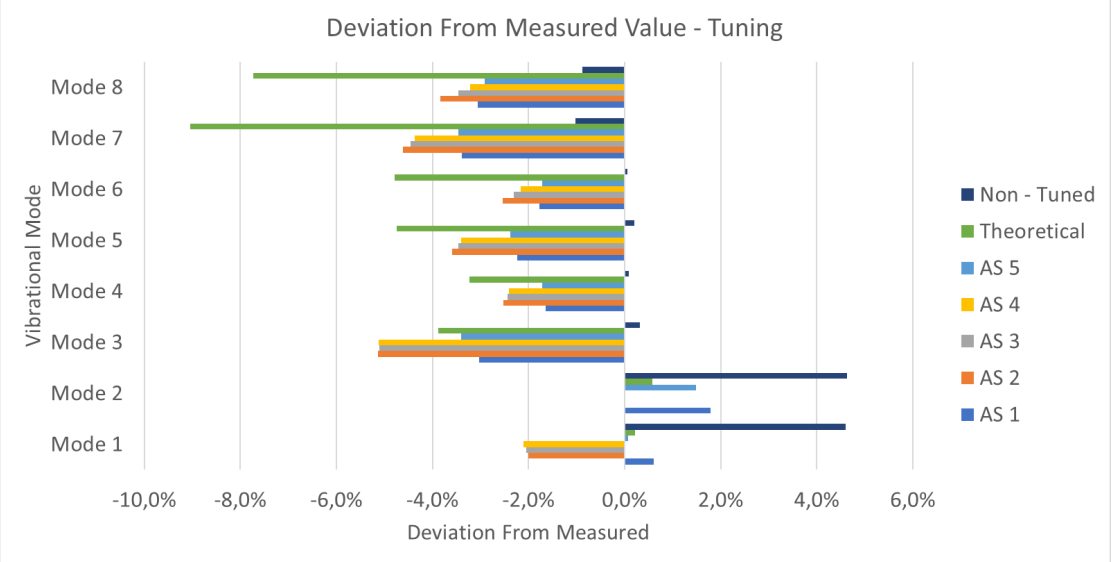

Figure 8.11: Final Recap Graph of AS. Non-Tuned case is also inserted for reference.

8.2.1 The Test Plate

The test plate is a slab of the same Nickel Based Superalloy Material made with standard measures in order to measure material properties accurately and precisely in a scientifically validated scenario. In order to compare results in the exact same way as it was done in the part of material assessment and testing initially (by the material's team), it was decided to test **some** of the tuning iteration on the test plate as well, in order to compare them to the untuned result and see how the deviation compared as well. Only four modes were compared since they were the only one clearly comparable.

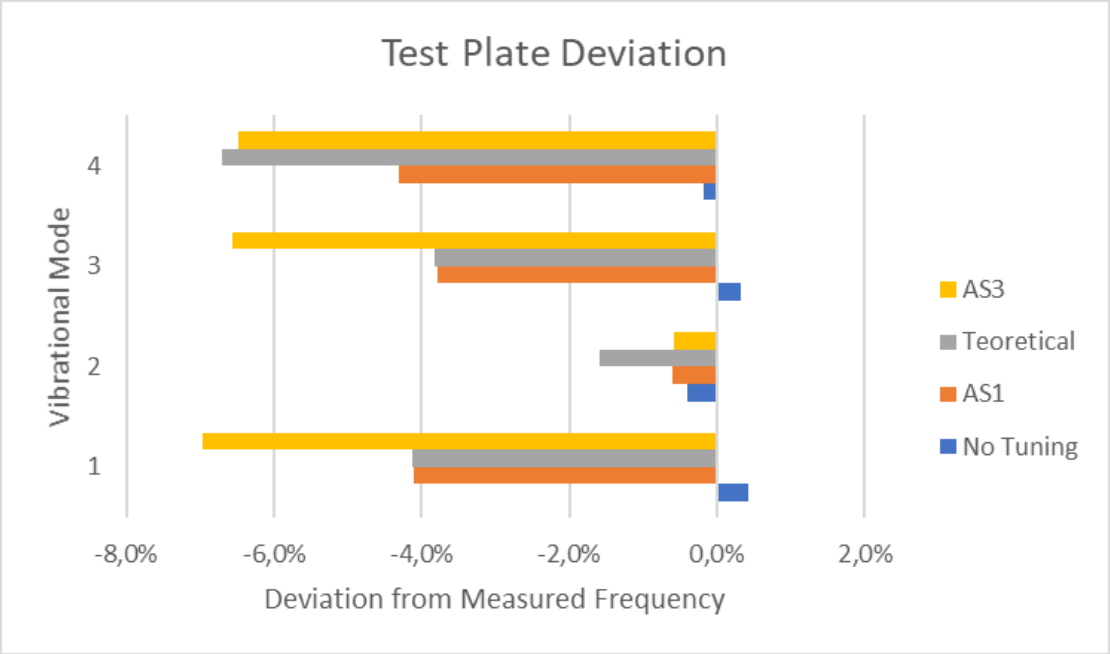

Figure 8.12: Test Plate Results

As it can be observed from the graph, the case of NO TUNING is clearly the best case scenario possible, showing that the initial values provided were backed by solid evidence and empirical data. This results underlines how the complex shape of a blade can inherently complicate results and needs proper consideration.

8.3 Matlab Code Optimization

After observing results on all the **AS** cases, it was decided to more finely optimize the two frequencies of the first two most important modes. After observing tab :8.2, it is clear how, for the first two frequencies, the values of G do not play a fundamental role (they have a variation of around $0 - 1\%$ usually, except for the Theoretical case), hence it was decided to specifically focus on the values of the other values (E_x and E_z) in order to finely tune the values of the first two vibrational modes. That shows that even when considering the values for E and G, **only the values of E influence significantly the first two frequencies**. Of course G values are useful, and clearly have to be studied, but when it comes to the first two vibrational modes they tend to me **mostly** influenced by the Young's Module rather than the G module, since are close to a purely flexional mode rather than a torsional mode. Even in the Theoretical case, when imposing a variation of 35%, the first two vibrational modes do not appear to be greatly influenced. For this reason, from now on, the focus will be on the most influential parameters.

Deviation	Ex	Ez	Gx	Gz
AS1	-9%	-9%	-1%	0%
AS2	-10%	-15%	0%	0%
AS3	-7%	-14%	0%	0%
AS4	-5%	-15%	0%	0%
AS5	-7%	-10%	0%	0%
Theoretical	-9%	-9%	-35%	0%

Table 8.2: Variation of E, G in different optimizations

In order to obtain a tuning process that was sufficiently and mathematically correct, it was decided to focus specifically on the **first two modes and their frequency**[1]. In order to better optimize the process, it was decided to use **MatLab** and more specifically a code that worked as described below;

1. First, since there was no clear analytical function linking E_x, E_Z, f_1 and f_2, using a series of data from previous cases (all the AS cases) for both frequencies and Young's Module, using the MatLab **scatteredInterpolant** function, a interpolative function was created.

2. Second, after plotting the planes, and using the measured frequencies for the first two modes as targets, an error function was defined

[1]The first two modes are the most important for the purpose of de-tuning (for frequency) and because are the two easiest to measure correctly and precisely, as can be seen in 5.12

3. Lastly, using function **lsqnonlin**, the values of Optimized E_X and E_z were obtained.

When referencing "iterations", in this case, it is regarding to the fact that with the newly calculated values, they were used as more input points for the first step (so every iteration has more input points in order to obtain a more precise optimization).

The following images offer a visual representation of the two functions bonding the frequencies and the E of the material;

$$f_1(E_x, E_z) \text{ and } f_2(E_x, E_z) \tag{8.6}$$

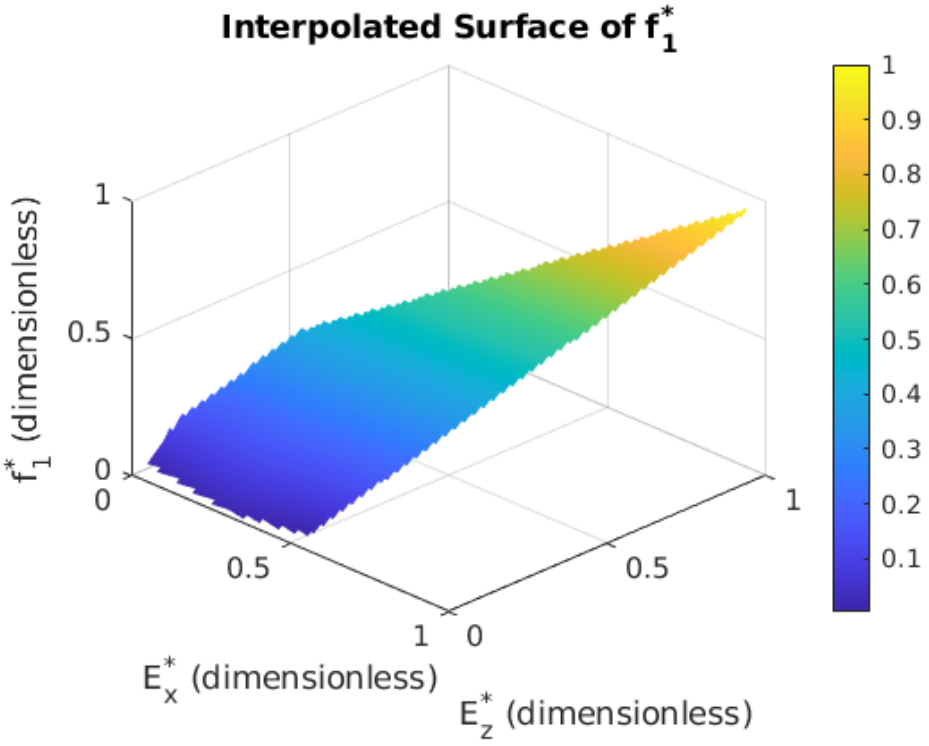

Figure 8.13: First Mode frequency interpolated function visualized (dimensionless)

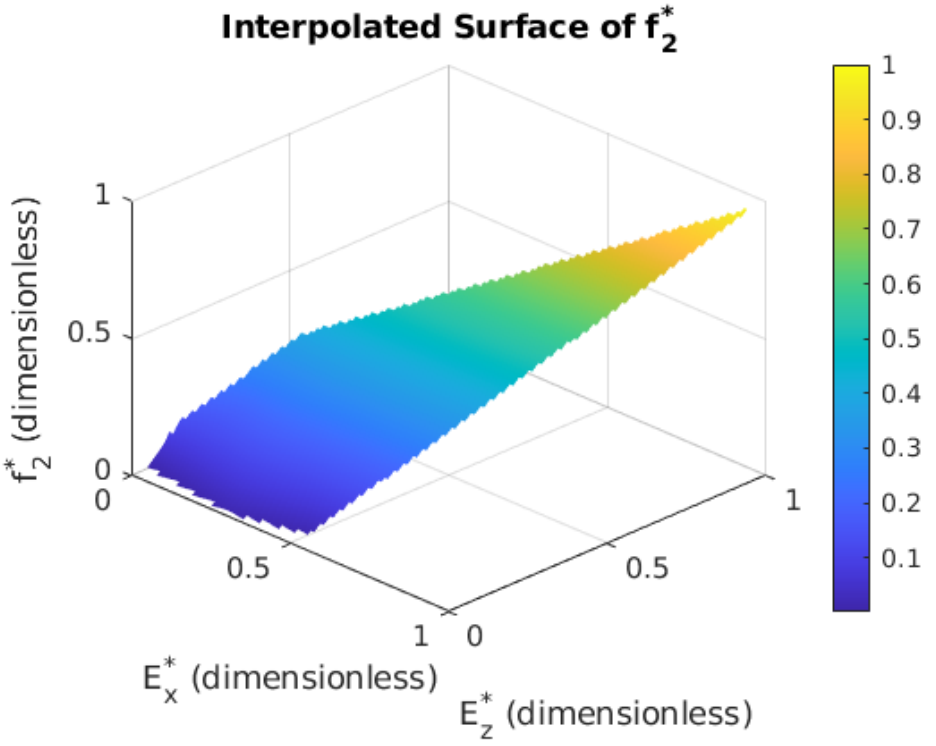

Figure 8.14: Second Mode frequency interpolated function visualized (dimensionless)

MatLab Iteration 1

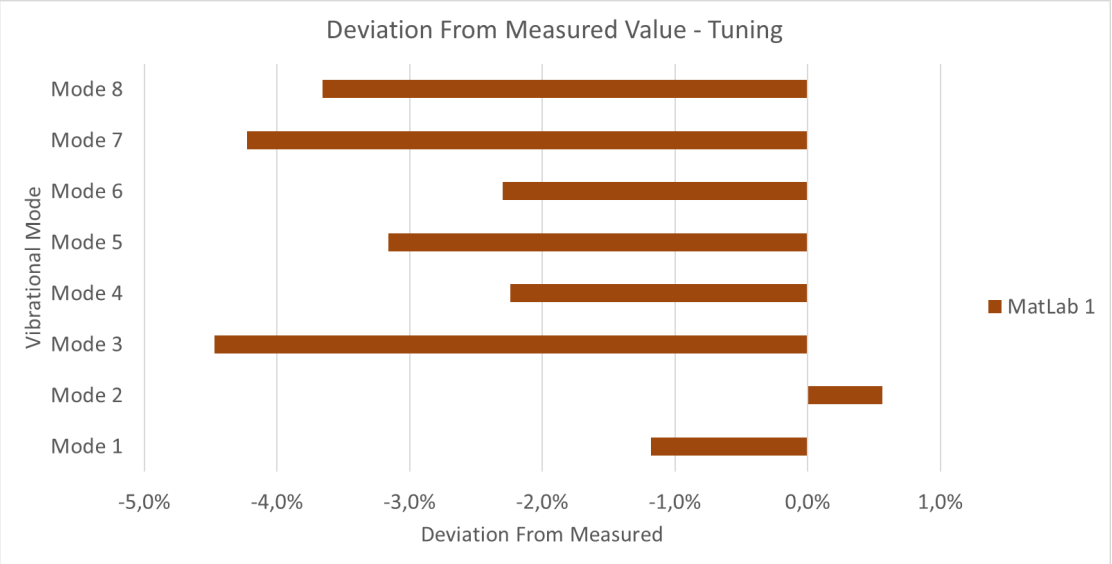

Figure 8.15: MatLab Iteration 1 Deviation

MatLab Iteration 2

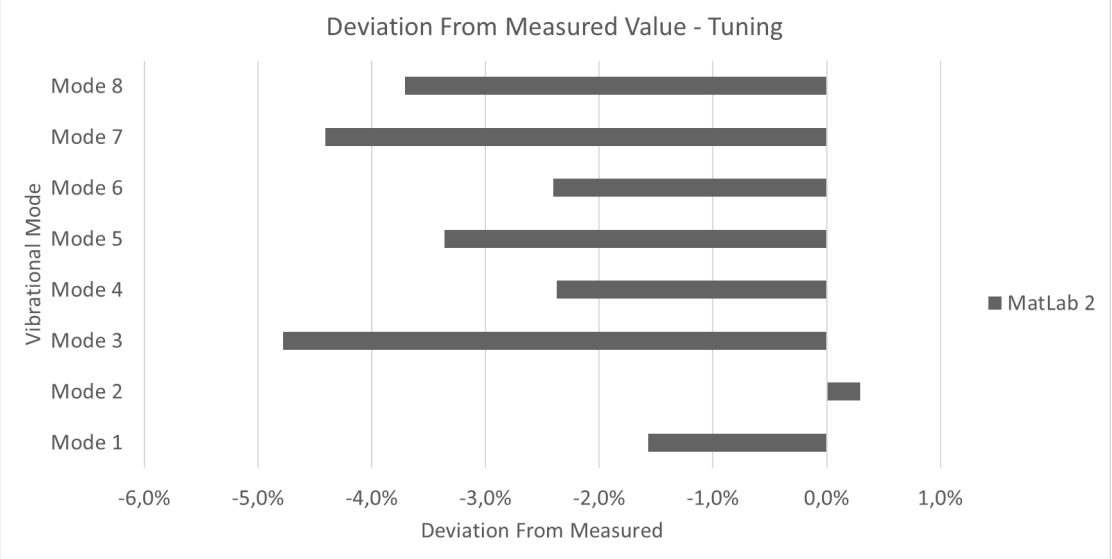

Figure 8.16: MatLab Iteration 2 Deviation

MatLab Iteration 3

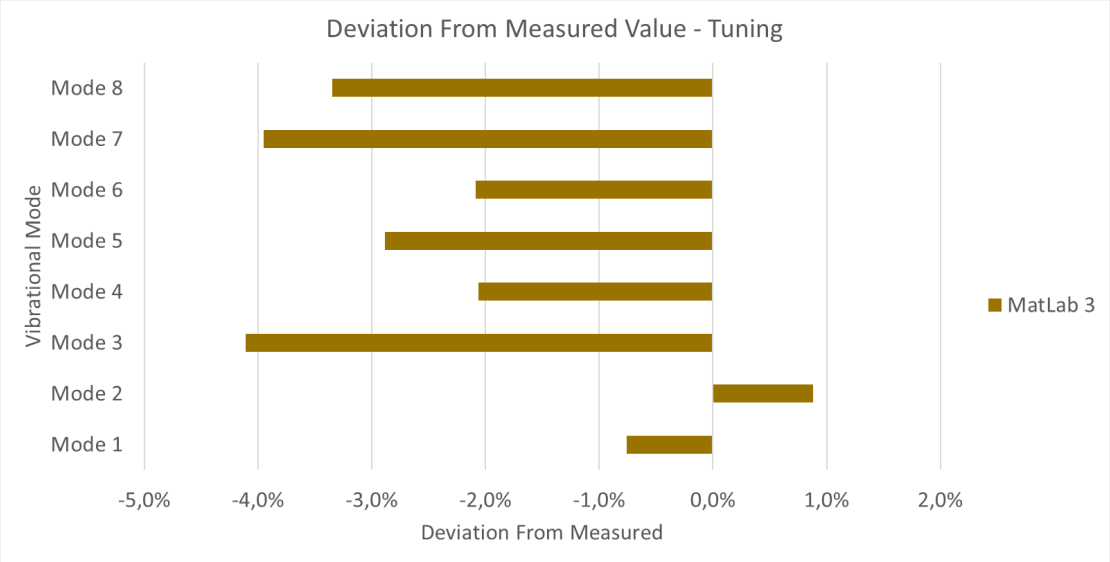

Figure 8.17: MatLab Iteration 3

MatLab Iteration 4

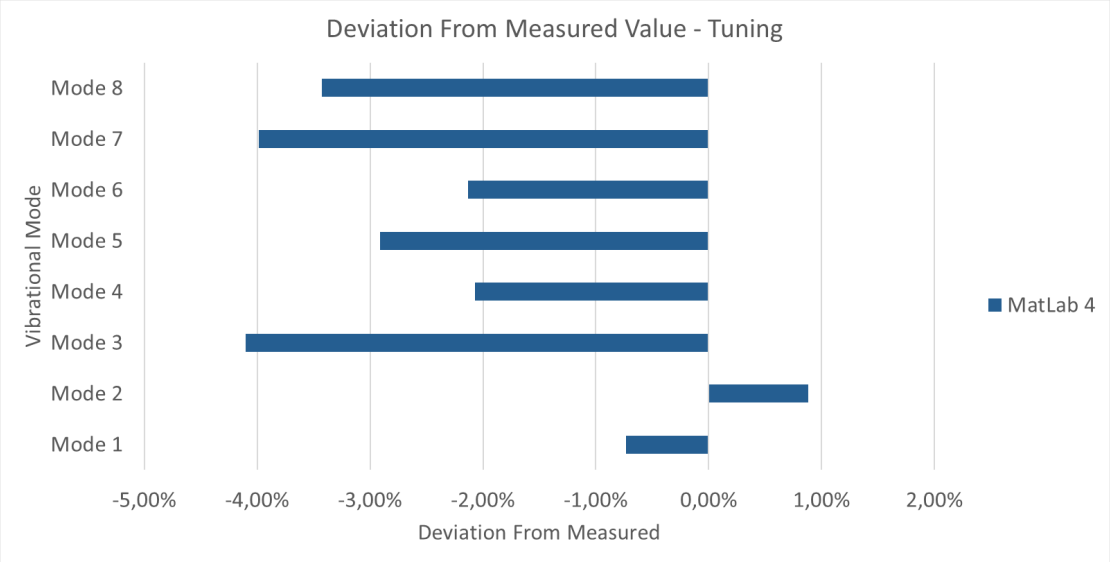

Figure 8.18: MatLab Iteration 4

To recap all the iterations, the following graph (8.19) and table (8.3) are provided;

	M1	M2	M3	M4	M5	M6	M7	M8
MatLab 1	-1,2%	0,6%	-4,5%	-2,2%	-3,2%	-2,3%	-4,2%	-3,7%
MatLab 2	-1,6%	0,3%	-4,8%	-2,4%	-3,4%	-2,4%	-4,4%	-3,7%
MatLab 3	-0,8%	0,9%	-4,1%	-2,1%	-2,9%	-2,1%	-3,9%	-3,3%
MatLab 4	-0,73%	0,88%	-4,10%	-2,07%	-2,91%	-2,13%	-3,98%	-3,43%

Table 8.3: Recap MatLab Table

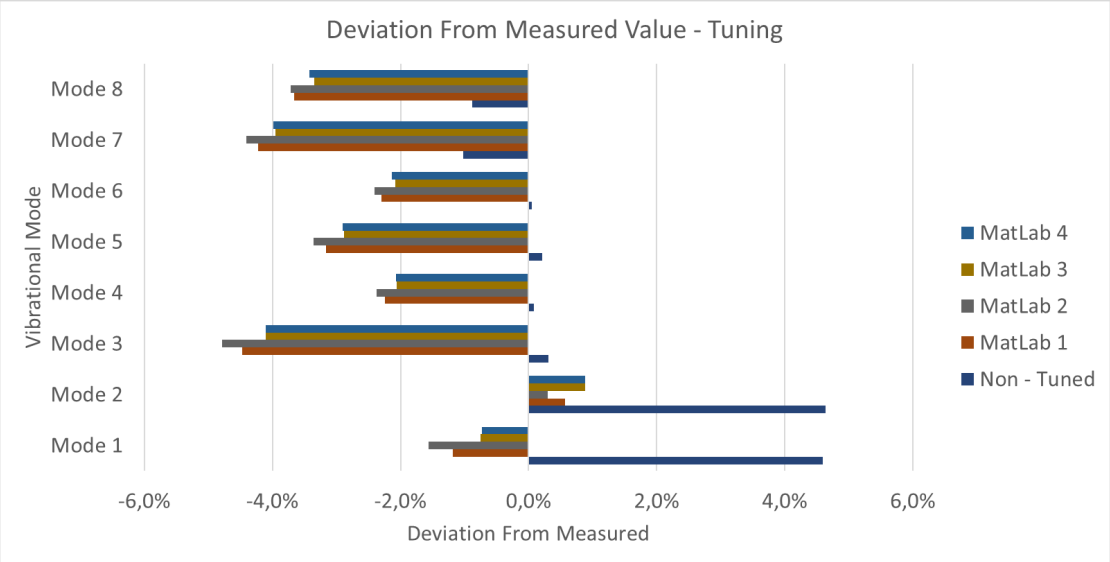

Figure 8.19: Matlab final graph recap. Non Tuned case inserted for Reference

This optimization not only gave results for the first two modes comparable to the René 80, but also considered both frequencies at the same time, differently from the AS cases, making for a more raffinate results. This optimization, with results in the magnitude of **0.7 and 0.8 %** for the first two modes, offers a model particularly useful to assess frequencies in the future.

8.3.1 Optimization Conclusion

Clearly the MatLab optimization has the most accurate results when it comes to the first two vibrational modes, as the entire code was developed in order to optimize them. An important aspect not to neglect is the importance of the AS results as well. Not only they were obtained by using only a linear system, but their numerous results were used in the MatLab optimization code and gave a batch of useful results to be used in the optimization and helped archieve the more accurate results. Since clearly the first two modes were the most important (as seen in Fig: 5.12) and easier to measure, tuning the two frequencies in the needed order of magnitude gives an important result in order to properly calculate and tune the blade frequencies for further assessments.

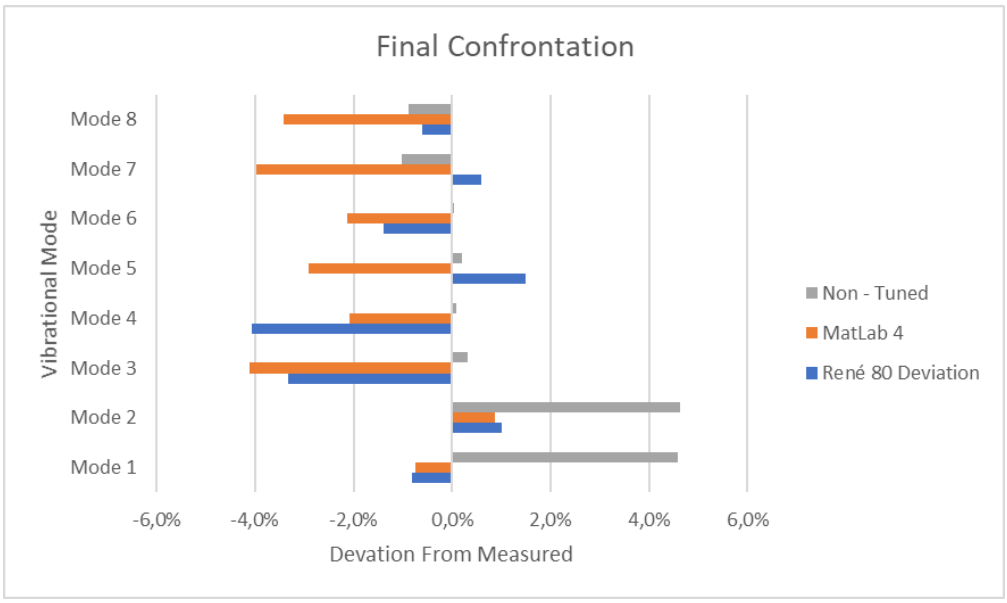

Figure 8.20: Final Confrontation between cases. With the final MatLab case the situation is really comparable with the René 80 situation

Chapter 9

Calculation Index

9.1 Introduction

This document was redacted as a part of the Master's Thesis in Aerospace Engineering to have a clear and easy to consult index of every calculation launched, and the expected results.

9.2 Indefinitely Rigid Constraints

In this section the Blade is constrained with **INDEFINITELY RIGID CONSTRAINTS**, making results independent from the constraints's type.

9.2.1 New Nickel Based DS superalloy

New Nickel Based DS superalloy: anisotropic alloy
CALCULATIONS PERFORMED:

- **ALL 3 FIR TREE LOBES CONSTRAINED, NO TURBOLATORS**: Used for assessing results and proving that mesh independent calculation results were provided

  1. **1.9 million Nodes GUIDED Mesh**: Most accurate mesh, to have the best results possible;
  2. **900'000 Nodes GUIDED Mesh**;
  3. **800'000 Nodes GUIDED Mesh**;
  4. **700'000 Nodes GUIDED Mesh**;
  5. **600'000 Nodes AUTOMATICALLY GENERATED Mesh**;

- **ALL 3 FIR TREE LOBES CONSTRAINED, WITH TURBOLATORS**: Used to assess turbolators influence on modal response

  1. **690'000 Nodes AUTOMATICALLY GENERATED Mesh**

- **UPPER TOOTH OF FIR TREE LOBE CONSTRAINED ONLY, WITH TURBOLATORS**: Used to assess turbolators influence on modal response

  1. **2.6 Million Nodes AUTOMATICALLY GENERATED Mesh**
  2. **690'000 Nodes AUTOMATICALLY GENERATED Mesh**
  3. **2.6 Million Nodes Auto Mesh**
     - **+20 DEGREES, X AXIS**
     - **-20 DEGREES, X AXIS**
     - **+20 DEGREES, Y AXIS**
     - **-20 DEGREES, Y AXIS**

- **UPPER TOOTH OF FIR TREE LOBE CONSTRAINED ONLY, NO TURBOLATORS**: used for assessing results of different type of constraints

  1. **700'000 Nodes GUIDED Mesh**

- **NO LOBES CONSTRAINED - FREE VIBRATING BLADE**: used to asses how the material properties were found and comparison

  1. **+20 DEGREES, X AXIS**
  2. **-20 DEGREES, X AXIS**
  3. **+20 DEGREES, Y AXIS**
  4. **-20 DEGREES, Y AXIS**
  5. **+20 DEGREES, Z AXIS**
  6. **-20 DEGREES, Z AXIS**

- **MIDDLE TOOTH OF FIR TREE LOBE CONSTRAINED ONLY, NO TURBOLATORS**: used for assessing results of different type of constraints

  1. **700'000 Nodes GUIDED Mesh**

9.2.2 RENE 80 Database 1

RENE 80 Database 1: nickel based superalloy, whose properties refer to database 1

CALCULATIONS PERFORMED:

- **ALL 3 FIR TREE LOBES CONSTRAINED, NO TURBOLATORS**: Used for assessing results and proving that mesh independent calculation results were provided

  1. **1.9 million Nodes GUIDED Mesh**: Most accurate mesh, to have the best results possible;
  2. **900'000 Nodes GUIDED Mesh**;
  3. **800'000 Nodes GUIDED Mesh**;
  4. **700'000 Nodes GUIDED Mesh**;
  5. **600'000 Nodes AUTOMATICALLY GENERATED Mesh**;

- LOWER LOBE OF FIR TREE LOBE CONSTRAINED ONLY, NO TURBOLATORS: Used for assessing results and proving that mesh independent calculation results were provided

- LOWER TWO LOBES OF FIR TREE LOBE CONSTRAINED ONLY, NO TURBOLATORS: Used for assessing results and proving that mesh independent calculation results were provided

- HIGHER LOBE FIR TREE LOBE CONSTRAINED ONLY, NO TURBOLATORS: Used for assessing results and proving that mesh independent calculation results were provided

- MIDDLE LOBE FIR TREE LOBE CONSTRAINED ONLY, NO TURBOLATORS: Used for assessing results and proving that mesh independent calculation results were provided

RENE 80 Database 2: nickel based superalloy, whose properties refer to database number 2

CALCULATIONS PERFORMED:

- **ALL 3 FIR TREE LOBES CONSTRAINED, NO TURBOLATORS**: Used for assessing results and proving that mesh independent calculation results were provided

  1. 1.9 million Nodes GUIDED Mesh

9.3 Broach Block

In this section the goal was to asses the real frequency related to the measurements, since the broach block is not infinitely rigid.

9.3.1 RENE 80

RENE 80: nickel based superalloy, whose properties refer to database 1
CALCULATIONS PERFORMED:

- **1.9 million Nodes GUIDED Mesh**: Most accurate type of mesh in order to compare results to the real measurements
- **Original Calculation**: the model that AEN's employees made, non modified.

9.3.2 Nickel Based DS Superalloy

Calculation used in order to solve the issue presented. The problem was that the original model didn't match with the measured results.

- **1.9 Million Nodes Guided Mesh BONDED**: This calculation was performed in order to asses and solve problems with the model and the small sliding issues
- **1.9 Million Nodes Guided Mesh SERIAL**: the "*Serial*" Badge was only given in order to distinct it from the "Bonded". This calculation was the one performed with everything sorted out and solved, in order to asses results precisely
- **2.6 MILLION NODES, WITH TURBOLATORS**: used to asses the effect of turbolators on the blade itself
- **2.6 MILLION NODES; WITH TURBOLATORS - GRAIN ORIENTATION**: used to asses the influence of grain orientation on modal behaviour
  - **+ 20 DEGREES, X AXIS**
  - **- 20 DEGREES, X AXIS**
  - **+ 20 DEGREES, Y AXIS**
  - **- 20 DEGREES, Y AXIS**

9.4 TUNING OF THE MATERIAL PROPERTIES

Since calculations and values didn't match, some routes to asses issues were paved. The first one was the fine tuning of the material's properties

CALCULATIONS PERFORMED:

- **1.9 Million Nodes Guided Mesh SERIAL**: with modifications regarding **E AND G** with a coefficient of **0,873**
- **1.9 Million Nodes Guided Mesh SERIAL**: with modifications regarding **E AND G** with a coefficient of **0,8649**
- **1.9 Million Nodes Guided Mesh SERIAL**: with modifications regarding **ONLY E** with a coefficient of **0,873**
- **AS1 1.9 Million Nodes Guided Mesh SERIAL**
- **AS2 1.9 Million Nodes Guided Mesh SERIAL**
- **AS3 1.9 Million Nodes Guided Mesh SERIAL**
- **AS4 1.9 Million Nodes Guided Mesh SERIAL**
- **AS5 1.9 Million Nodes Guided Mesh SERIAL**
- **Theoretical 1.9 Million Nodes Guided Mesh SERIAL**
- **Matlab 1 1.9 Million Nodes Guided Mesh SERIAL**
- **Matlab 2 1.9 Million Nodes Guided Mesh SERIAL**
- **Matlab 3 1.9 Million Nodes Guided Mesh SERIAL**
- **Matlab 4 1.9 Million Nodes Guided Mesh SERIAL**
- **Matlab 5 1.9 Million Nodes Guided Mesh SERIAL**

9.4.1 Test Plate

Used in order to compare results with already given material properites

- **AS1**
- **AS3**
- **Theoretical**
- **NON Tuned**

Chapter 10

Conclusions

After careful consideration of all the above results, conclusions regarding the work done can be drawn and discussed as follows. It is clear how the presence of small, in-tolerance deviation from nominal values of some sections, points or grouping of points of the blade can be considered negligible when compared with the deviation of frequency encountered between calculations and measured, both considering René 80 and the New DS Anisotropic Superalloy. The trend line clearly expressed how the value spread between points was much greater than the value of the angular coefficient of the trend line. And since all blades that were considered were manufactured and evaluated within standard, the issue was to be found somewhere else.

After clearing out eventual discrepancies and having ruled out the possible issues with meshing (assessing that results were mesh-independent), the results obtained regarding the turbolators, and their non-negligible effect was established. This meant having to consider them for all the following calculations and that their contribution in the modal behaviour, even though not being structural, still had influence that could not be ignored. The understanding of this fact came as a surprise, since there was no prior knowledge that this was the case. Not only the positive impact of turbolators made their presence the model a step closer to the real blade, but also the frequency close to the measured values, ensuring that the modification was in the right direction, and that the simplification was good only for the initial assessment.

The other important aspect to touch is the grain orientation of the material. The grain orientation not only poses a great challenge when it comes to assessing the correct angle for the single blade to measure, as an acid attack is needed to discover the real value of the angle itself, but since, as discovered, the best orientation is the default one, or zero degrees. This is an important statement, as it shows that if grains are oriented differently than what was considered before, values of deviation go further than the optimal 0 - value leads the deviation further from lowering,

and resulting in a lower value.

In addition to that, in order to obtain a model that could be used for testing and assessing at ambience temperature the values, the tuning of the material gave some important and interesting insights on material properties and influence on different frequencies and behaviours. The idea of tuning came from the fact of having the possibility to create a set of material properties values that could help bring the results closer to the real measurements, hence decreasing the deviation to the smallest value possible.

As it could have been expected, the tuning process of the material, paired with the consideration of the turbolators gave a useful insight as how the different things end up influencing things in the modal behaviour of the blade. The case scenario that was considered clearly only took into consideration only the biggest and most important things that could have influenced the modal behavior, and clearly taking into account a wider range of smaller issues would have helped even more to understand how the complete overall workings and effects of the vibrating blade, but the issues of considering all the smaller details would have required times incompatible with a MSc Thesis' Work, so the decision on focusing of the most influential variables was made, still obtaining very valuable and useful results.

In conclusion this thesis helped to better visualize and frame the different parameters that influenced the vibrating frequencies and behaviour of the blade, and gave some unexpected results, nowhere to be imagined in the beginning.

Appendix A

Turbulators

In this Appendix, a brief explanation about what are turbolatos and why are they used is given. As already discusses in chapter 6, during the initial studies they were removed only in order to simplifying calculations and models, but since a more precise and complete result was needed, the simplification was let go and subsequenly re-added. As cooling turbine blades is a fundamental part of gas turbines, several methods were developed in order to improve the heat transfer rates between the cooling channels of the blades and hot gases outside of it [17].

The presence of turbulators in internal cooling passages is primarily needed and intended in order to overcome the inherently poor heat-transfer performance of smooth channels [18]. The internal cooling of those TB has to heavily rely on mechanisms that can break the cooling fluid (air) boundary layer in order to promote intense mixing (as shown in Fig: A.1) both locally and averaged on the entire surface [18]. They achieve this by inducing local flow acceleration and subsequent recirculation, which substantially enhances convective heat transfer [19]. The implementation of such elements has become fundamental since the engine firing continuous temperature rise, and in order to maintain mechanical integrity and life duration of TB [19]. In conclusion, turbulators work by altering the near-wall flow field by inducing secondary vortical structures and periodic (cyclic) separation and reattachment cycles A.1. Those described mechanisms disrupt the thermal boundary layer and help increasing the local heat-transfer coefficients along the turbolated inner surfaces [19]. This section shows how turbolators are used for thermal reasons, but end up, as shown in this thesis's work, having also modal behaviour effects.

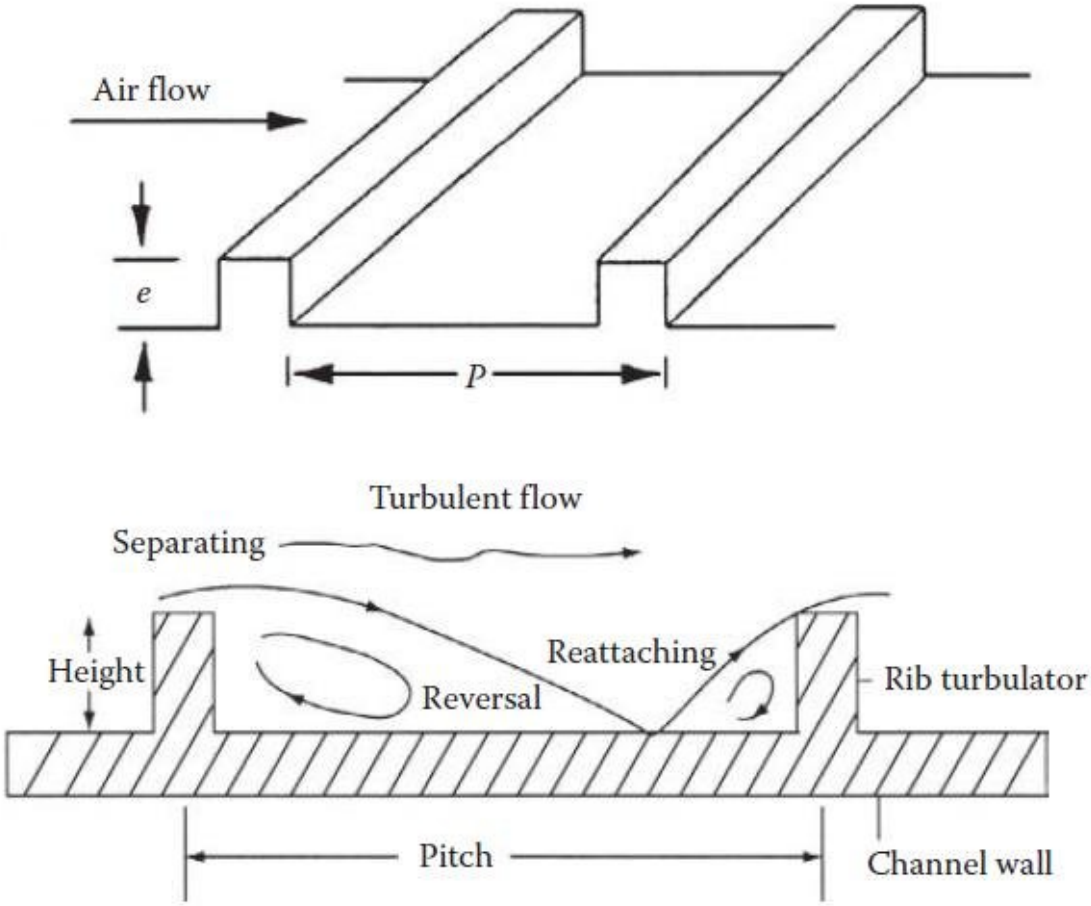

Figure A.1: Schematics of the turbolators method of working inside a Gas Turbine Blade[20]

Appendix B

Extra Calculations

In this section there is a grouping of all the calculations performed that were not needed as results specifically, but rather as proofs of statements.

B.0.1 Z - Axis Variation for Grain Orientation

As described in 7 changing the orientation along the z **- axis** doesn't have any effect on the frequency response. The adimensionalized values are shown in the table below. Tiny discrepancies are due to the numerical method used to perform calculations, and are thus completely negligible. **The reference values are the calculated values with an orientation for** x, y, z **axis equal to** $0°$

Deviation	Mode 1	Mode 2	Mode 3	Mode 4	Mode 5	Mode 6	Mode 7	Mode 8
z + 20	0,00%	0,00%	0,00%	0,00%	0,00%	0,00%	0,00%	0,00%
z - 20	0,00%	-0,01%	-0,01%	-0,01%	-0,01%	-0,01%	-0,04%	-0,01%

Table B.1: Deviation from non - oriented values for z-axis

Bibliography

[1] Ansaldo Energia S.p.A. Website For turbines. *https://www.ansaldoenergia.com* (cit. on pp. 3–6).

[2] R. Marsilio. *Appunti di Macchine*. Lecture notes, Politecnico di Torino. 2022 (cit. on p. 8).

[3] E. Martelli. *Motori Per Aeromobili*. Lecture notes, Politecnico di Torino. 2024 (cit. on p. 8).

[4] Tresa M. Pollock and Sammy Tin. *Nickel-Based Superalloys for Advanced Turbine Engines: Chemistry, Microstructure, and Properties*. JOURNAL OF PROPULSION AND POWER Vol. 22, No. 2. 2006 (cit. on pp. 73, 77).

[5] M. Gherlone. *Corso di Strutture Aeronautiche*. Lecture notes, Politecnico di Torino. 2024 (cit. on p. 74).

[6] *Ansys Help Guide*. Software Help Guide. 2024 (cit. on p. 74).

[7] Hang Zhang, Qingyan Xu, Ning Tang, Dong Pan, and Baicheng Liu. «Numerical simulation of microstructure evolution during directional solidification process in directional solidified (DS) turbine blades». In: *Science China Technological Sciences* 54 (May 2011). DOI: 10.1007/s11431-011-4607-6 (cit. on pp. 75, 79).

[8] Ansaldo Sviluppo Energia. *Internal Presentation*. Property of AEN (cit. on p. 76).

[9] Pietro Antonio Martelli; Antonio Sivo; Flaviana Calignano; Emilio Bassini; Sara Biamino; Daniele Ugues. *Parameters Optimization and Repeatability Study on Low-Weldable Nickel-Based Superalloy René 80 Processed via Laser Powder–Bed Fusion (L-PBF)*. Politecnico di Torino. 2023 (cit. on p. 77).

[10] J. H. Laflen V. G. Ramaswamy R. H. Vanstone and D. C. Stouffer. *Development of a unified constitutive model for an isotropic nickel base superalloy Rene 80*. Conference Paper, NASA. April 1, 1988 (cit. on p. 77).

[11] Jian Zhang. *HOT TEARING IN DIRECTIONALLY SOLIDIFIED NI-BASED SUPERALLOYS*. TMS (The Minerals, Metals Materials Society). 2004 (cit. on p. 77).

[12] *https://en.wikipedia.org/wiki/Directional$_s$olidification* (cit. on p. 78).

[13] A. et al. Long. *Anisotropy in Creep Behavior of a Directionally Solidified Ni-Based Superalloy at 980 °C and 1070 °C*. 2025 (cit. on p. 78).

[14] R. Bürgel; J. Grossmann; O. Lüsebrink; H. Mughrabi; F. Pyczak; R.F. Singer and A. Volek. *DEVELOPMENT OF A NEW ALLOY FOR DIRECTIONAL SOLIDIFICATION OF LARGE INDUSTRIAL GAS TURBINE BLADES*. Superalloy. 2004 (cit. on p. 78).

[15] Roland Mücke. *A Mathematical Framework for Cyclic Life Prediction of Directionally Solidified Nickel Superalloys*. 2011 (cit. on p. 78).

[16] S. Zucca. *Corso di Dinamica dei Rotori per Applicazioni Aerospaziali*. Lecture notes, Politecnico di Torino. 2024 (cit. on p. 85).

[17] Jasem Alrajhi. *Computational Study of Turbulence and Recirculation Effects in Turbine Blade Cooling Channel*. Global Journal of Researches in Engineering. September 2024 (cit. on p. 128).

[18] J.-C. Han. «Turbine Blade Internal Cooling Passages with Rib Turbulators». In: *Journal of Turbomachinery* 116.1 (1994), pp. 123–134. DOI: 10.1115/1.2928389 (cit. on p. 128).

[19] L. Hu, Y. Zuo, M. Zhang, and W. Chen. «Heat Transfer Enhancement in Turbine Blade Internal Cooling Channels using Rib Turbulators». In: *Energies* 18.13 (2025), p. 3296. DOI: 10.3390/en18133296 (cit. on p. 128).

[20] Dutta Han and Ekkad. *5 Schematics of Rib Turbulators*. 2013 (cit. on p. 129).